AD-A080 982 PENNSYLVANIA STATE UNIV UNIVERSITY PARK APPLIED RESE--ETC F/G 6/5
ADAPTIVE DYNAMIC RANGE COMPRESSION ALGORITHM FOR ECHOCARDIOGRAP--ETC(U)
MAY 79 E H LAM N00014-79-C-6043
UNCLASSIFIED ARL/PSU/TM-79-138 NL

1 OF 3
AD-
A080982

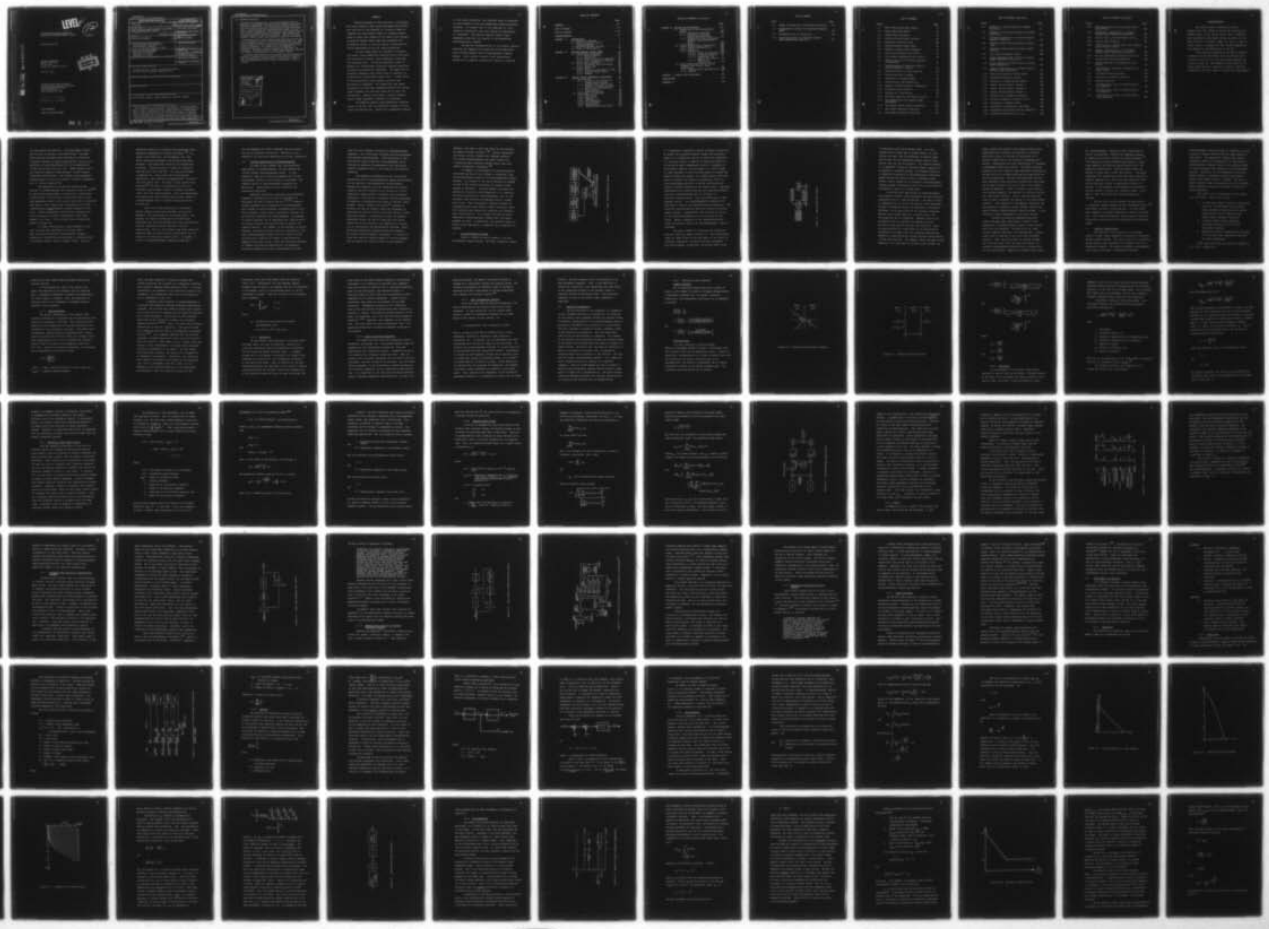

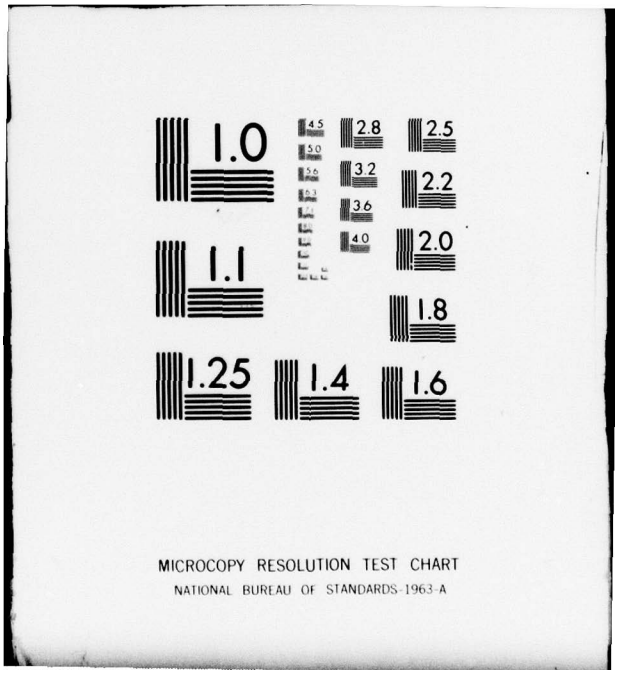
1.0
1.1
1.25
1.4
1.6
1.8
2.0
2.2
2.5
2.8
3.2
3.6
4.0
4.5
5.0
MICROCOPY RESOLUTION TEST CHART
NATIONAL BUREAU OF STANDARDS-1963-A

LEVEL II

12

B.S

ADAPTIVE DYNAMIC RANGE COMPRESSION ALGORITHM FOR ECHOCARDIOGRAPHIC IMAGING

Edward Hung Tat Lam

Technical Memorandum
File No. TM 79-138
May 24, 1979
Contract No. N00024-79-C-6043

Copy No. 5

The Pennsylvania State University
Institute for Science and Engineering
APPLIED RESEARCH LABORATORY
Post Office Box 30
State College, PA 16801

NAVY DEPARTMENT

NAVAL SEA SYSTEMS COMMAND

UNCLASSIFIED

SECURITY CLASSIFICATION OF THIS PAGE (When Data Entered)

REPORT DOCUMENTATION PAGE	READ INSTRUCTIONS BEFORE COMPLETING FORM
1. REPORT NUMBER: TM 79-138	2. GOVT ACCESSION NO. (9)
	3. RECIPIENT'S CATALOG NUMBER: Doctoral thesis
4. TITLE (and Subtitle): (6) ADAPTIVE DYNAMIC RANGE COMPRESSION ALGORITHM FOR ECHOCARDIOGRAPHIC IMAGING (14) ARL/PSU	5. TYPE OF REPORT & PERIOD COVERED: PhD Thesis, March 1980
	6. PERFORMING ORG. REPORT NUMBER: TM-79-138
7. AUTHOR(s): (10) Edward Hung Tat Lam	8. CONTRACT OR GRANT NUMBER(s): (15) N00024-79-C-6043
9. PERFORMING ORGANIZATION NAME AND ADDRESS: The Pennsylvania State University, Applied Research Laboratory, P. O. Box 30, State College, PA 16801	10. PROGRAM ELEMENT, PROJECT, TASK AREA & WORK UNIT NUMBERS: (11) 24 May 79
11. CONTROLLING OFFICE NAME AND ADDRESS: Naval Sea Systems Command, Department of the Navy, Washington, DC 20362	12. REPORT DATE: May 24, 1979 (12) 214
	13. NUMBER OF PAGES: 213 pages & figures
14. MONITORING AGENCY NAME & ADDRESS (if different from Controlling Office)	15. SECURITY CLASS. (of this report): Unclassified, Unlimited
	15a. DECLASSIFICATION/DOWNGRADING SCHEDULE

16. DISTRIBUTION STATEMENT (of this Report)

Approved for public release, distribution unlimited, per NSSC (Naval Sea Systems Command), 8/3/79

17. DISTRIBUTION STATEMENT (of the abstract entered in Block 20, if different from Report)

18. SUPPLEMENTARY NOTES

19. KEY WORDS (Continue on reverse side if necessary and identify by block number)

echocardiography, dynamic, range, compression, algorithm, imaging

20. ABSTRACT (Continue on reverse side if necessary and identify by block number)

Echocardiography is used routinely in cardiology. The typical dynamic range encountered spans about 90 dB. The objective of this research is to devise a means to compress this wide dynamic range to a narrower dynamic range for grey scale display or for digital data storage. An adaptive dynamic range algorithm to maximize the information content of the echo signal is developed and tested experimentally and also using simulations.

An echo signal model is developed to formulate the dynamic range compression algorithm and to facilitate the evaluation of dynamic range compression

DD FORM 1 JAN 73 1473 EDITION OF 1 NOV 65 IS OBSOLETE

391007

UNCLASSIFIED

SECURITY CLASSIFICATION OF THIS PAGE (When Data Entered)

20. ABSTRACT (Continued)

algorithms with simulated data. The echocardiographic signal is modeled as a nonstationary stochastic process consisting of specular and scatterer components. The separation of scatterer components from blood volume is important in establishing a significance signal level. A lower bound on this significance level based on acoustic wave divergence is suggested. The significant echo signal of specular and scatterer components possess wide dynamic range throughout the scanning volume due to their nonstationarity. Based on this model, a general adaptive dynamic range compression algorithm is developed.

The adaptive dynamic range compression algorithm relies on the fact that the stochastic process is of the slowly fluctuating type. Based on an independent estimate of local power statistics, the algorithm tends to normalize the echo signals so that they approximate pseudo-stationary processes. An integral part of the algorithm is a nonlinearity introduced so that only signals of significance are normalized. This general adaptive dynamic range compression algorithm also applied to multidimensional echocardiographic imaging.

Two specific implementations of this general adaptive algorithm are suggested for M-mode and three-dimensional sector-scanned snapshot mode echocardiographic imaging systems. Their ability to adapt to the nonstationary signals and to suppress insignificant signals is examined.

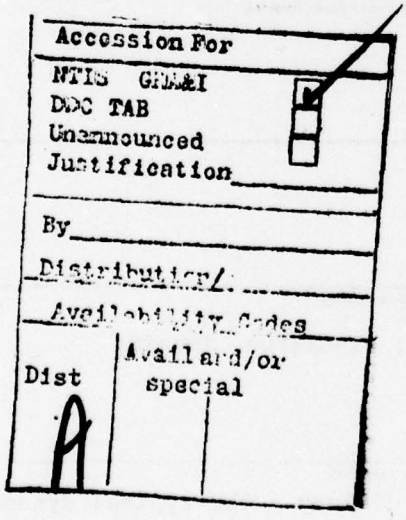

ABSTRACT

Echocardiography is used routinely in cardiology. The typical dynamic range encountered spans about 90 dB. The objective of this research is to devise a means to compress this wide dynamic range to a narrower dynamic range for grey scale display or for digital data storage. An adaptive dynamic range algorithm to maximize the information content of the echo signal is developed and tested experimentally and also using simulations.

An echo signal model is developed to formulate the dynamic range compression algorithm and to facilitate the evaluation of dynamic range compression algorithms with simulated data. The echocardiographic signal is modeled as a nonstationary stochastic process consisting of specular and scatterer components. The separation of scatterer components from blood volume is important in establishing a significance signal level. A lower bound on this significance level based on acoustic wave divergence is suggested. The significant echo signal of specular and scatterer components possess wide dynamic range throughout the scanning volume due to their non-stationarity. Based on this model, a general adaptive dynamic range compression algorithm is developed.

The adaptive dynamic range compression algorithm relies on the fact that the stochastic process is of the slowly fluctuating type. Based on an independent estimate

of local power statistics, the algorithm tends to normalize the echo signals so that they approximate pseudo-stationary processes. An integral part of the algorithm is a non-linearity introduced so that only signals of significance are normalized. This general adaptive dynamic range compression algorithm also applies to multidimensional echocardiographic imaging.

Two specific implementations of this general adaptive algorithm are suggested for M-mode and three-dimensional sector-scanned snapshot mode echocardiographic imaging systems. Their ability to adapt to the nonstationary signals and to suppress insignificant signals is examined.

TABLE OF CONTENTS

TABLE OF CONTENTS (continued)

LIST OF TABLES

LIST OF FIGURES

LIST OF FIGURES (continued)

LIST OF FIGURES (continued)

ACKNOWLEDGMENTS

The author wishes to express his sincere appreciation to Mr. Norman B. Miller for initiating the research topic, to Mr. Miller and Dr. John B. Lewis for their guidance and assistance during the course of this work, and to Dr. William S. Adams, Dr. John L. Brown, Jr., and Dr. Edsel G. Crenshaw for their helpful suggestions and comments on the presentation of the text.

This study was supported by the Applied Research Laboratory of The Pennsylvania State University under a contract with the U.S. Naval Sea Systems Command, and jointly by Grant No. 1R01 HL20872-01 RAD awarded by the Public Health Service, Department of Health, Education and Welfare, and their support is gratefully acknowledged.

CHAPTER I

INTRODUCTION

Echocardiography, a pulse-echo ultrasonic technique, is fast gaining favor as a diagnostic medical instrument in the evaluation and analysis of heart disease. It is comparatively low risk due to its nonionizing and non-invasive nature. Many echocardiographic systems and techniques have been developed since the initial use of ultrasound to ascertain the volume of the human heart in the 1950's. This thesis considers a specific problem encountered in echocardiography -- that of dynamic range compression. A general dynamic range compression technique applicable to multidimensional (which includes time) echocardiographic imaging systems is presented. The specific application of such a technique to a three-dimensional snapshot camera is emulated. This technique is evaluated with simulated echo data for a model presented here. Experimental data from volunteers are also presented for comparison with the model and evaluation of the dynamic range compression algorithm.

1.1 Historical Remarks

The utilization of pulse echo ultrasonic systems for cardiology started in the early 1950's. As in all ultrasonic instruments, the evolution was stimulated by the development of sonar during World War II. Firestone,[11]

in the early 1950's, started the use of pulse-echo ultrasound for nondestructive testing. Keidel[24] was one of the first investigators to use ultrasound to examine the heart. His technique was to transmit ultrasonic waves through the heart and record the effects of the ultrasound on the otherside of the chest. The purpose of his work was to try to determine cardiac volume.[10]

The true beginning of echocardiography did not start till Hertz and Elder[9] modified a commerical non-destructive testing ultrasonoscope in 1953. Preceding and during this period, ultrasonic diagnosis also flourished in other medical applications. One of the dominant figures in diagnostic ultrasound was D. H. Howry.[20] A period of investigation and interpretation of the echograms followed Hertz and Elder's first venture into echocardiography. The display utilized at that time was the A-mode display. The A-mode display presents echo strength versus range (actually time) data. Since the pulses were repeated, an additional dimension is time. Thus, the early echocardiographic imaging systems presented the echo information along two independent variables, range and time.

"Technical improvements followed with the development of the time-motion mode (TM mode) of display and simultaneous recording of the electrocardiogram."[27] This improvement in 1956 by Elder enables an operator to view the past history by displaying time and range with

the echo modulating intensity. This development enabled the clinician to quantify structural motion. Although other scanning techniques were developed for pulse-echo ultrasonic systems for medical applications, they are not applicable in cardiology because of the incompatability of fast motions and slow scan rate. These scanners, such as B mode and compound B mode scanners, usually produce transverse cross-sections. The TM mode echocardiographic imaging system is still the principal ultrasonic diagnostic tool in clinical applications.

The application of B mode and compound B mode scanners to echocardiography was achieved by King in 1970.[27] By using electrocardiograms to synchronize a conventional B mode scanner, King was able to accumulate echos at the same approximate phase of the cardiac cycle over a relatively long period. This "stop action" technique was the first two-dimensional pseudo-snapshot imaging technique of the heart. Various researchers utilized this technique with motion pictures to simulate cross-section versus time images of the heart. This technique was not adopted for general clinical use.

To image two-dimensional echocardiograms in real time, scanners were developed in the early 1970's. Real time scanners generate two-dimensional images by sequentially transmitting and receiving an ultrasonic beam at different angles, usually through a plane. This two

dimensions versus time technique was implemented using mechanical components by Griffith and Henry.[15] By using a motor oscillate, the transducer, real time sector scans were provided by the Griffith and Henry scanners. This particular system is now commercially available. Electronic means to sweep the ultrasonic beam spatially were used also. By using multielement transducers in a linear array and activating each sequentially, Bom, Roelandt and Hugenholtz[5] achieved a real time planar scan. By using a linear phased array, Thurstone[61] was able to electronically steer the ultrasonic beam through a sector to produce two-dimensional real time echocardiograms. Such three-dimensional (two spatial and time) scanners mark another advance in echocardiography which is rapidly being acquired for clinical use.

Each of the newer generations of echocardiographic imaging systems has advantages over its predecessors, and each system has its strong points. For example, the earliest A-mode pulse echo system has advantages over the most advanced real-time electronically steered, phased-array sector scanners in certain applications. That is, the A mode's high pulse repetition frequency (PRF) can detect atrial flutter, where the low frame rate of the sector scanner cannot. In summary, a variety of echocardiographic imaging systems exist

for the diagnosis of cardial disorders and each system has its own operating limitations. Selection of one depends on the particular application and other constraints.

1.2 Clinical Applications of Echocardiography

In order to gain insight into the engineering requirements of echocardiography, one must examine the clinical purpose echocardiography serves. In this subsection, some of the uses and proposed uses of echocardiography relevant to this thesis are discussed. The important points of echocardiographic diagnosis are pointed out. These points are then translated into engineering objectives.

Excellent information regarding echocardiographic diagnostic techniques can be found in monographs by Feigenbaum and also in Termini and Lee.[10,60] Numerous cardiac disorders can be diagnosed by echocardiography. Such diseases as mitral stenosis, prolapsed sintral valve, aortic stenosis, atrial tumors, pericardial effusion, etc. are routinely detected with echocardiograms. The process of cardiac diagnosis can be summarized into identification of cardiac structure and quantification of spatial and temporal features. For example, in the diagnosis of mitral stenosis, the anterior mitral leaflet is recorded on a TM-mode echocardiographic system; then the velocity of the anterior mitral leaflet (E-F slope) is quantified and compared with normal values. Here, the structural dynamics or temporal features are exploited for the diagnosis. Structural dimensions and their relationship with each

other are also important features for echocardiographic diagnosis. Left ventricular functions are often estimated with TM-mode echocardiograms. Good correlation of left ventricular stroke volume with cine-angiograms can be obtained by measuring one-dimensional left ventricular internal dimensional data at both systolic and diastolic instances.

The examples of assessing the left ventricular performance with an echocardiographic imaging system points out the need for a multidimensional echocardiogram. Perhaps more important than just assessing the ejection volume of the left ventricle is the ability of a multi-dimensional imaging system to quantify local myocardial hypokinesis. This ability to quantify ischemic dyssynergy is important in determining the extent of coronary artery disease. Miller, Lawther, and Zelis[39] proposed to evaluate the area of ischemic venticular dyssynergy by examining the regional motion of the heart within a three-coordinate system. A substitute to study the regional dyssynergy without the use of a high data rate motion capability can be achieved by the comparison of cardiac wall at end-systolic and end-diastolic instances. Other established methods of analyzing ventricular geometry are biplane ventriculographic techniques. "It should be noted that there are certain aspects of ventriculography over and beyond its invasive nature and the radiation

exposure, that make it less than ideal for the analysis of regional cardiac function."[39] Various researchers have found clinical evidence that compound scanning with M-mode echocardiography has higher sensitivity in detecting small regional abnormal motion than with biplane angiographic techniques.[39]

In summary, the development of echocardiographic techniques has been on the increase in dimensions, from the one-dimensional A-mode to the three-dimensional sector scanners. An increase to the fourth dimension is thought to help in the clinical evaluation of coronary artery disease in particular. Although display techniques are essentially limited to three dimensions, it is important that data acquisition be four-dimensional; that is, the ultrasonic scan should be accomplished within a single heart cycle. This is especially important because the intended patients might exhibit cardiac arrythmia, therefore rendering data acquisition intervals over different heart cycles invalid. It is toward this goal of multi-dimensional echocardiographic imaging that this thesis proposes to reach. In particular, the specific problem of dynamic range compression is examined and an algorithm is proposed.

1.3 Echocardiographic Systems

Figure 1.1 shows the basic elements in an echocardiographic imaging system. The basic components include

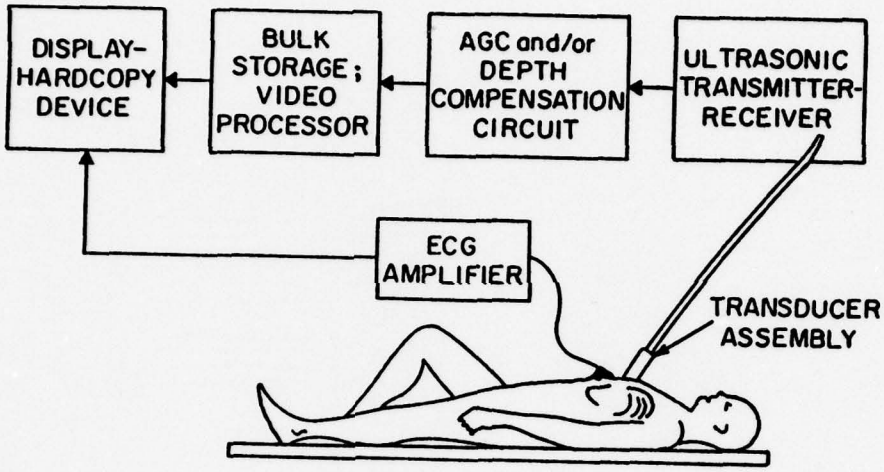

Figure 1.1 Basic Echocardiographic System

1) a transducer to generate a beam of ultrasonic energy and to convert the reflected acoustic energy into electrical signal, 2) a transmitter circuit to excite the transducer, 3) a receiver circuit to amplify the weak echo signal, 4) an AGC and/or depth compensation circuit to compress the wide dynamic range of the echo signal, 5) a bulk storage or video processor to store the echo signal or process the signal suitable for display, 6) a display and/or hard copy device to present the image to the physician, and 7) an electrocardiogram amplifier to provide synchronization and/or to provide reference to the cardiac cycle. Auxiliary subsystems such as positioning arm with associated display circuits or phonocardiogram may be included in a particular display system. Also, the system may be under computer control. All echocardiographic systems can be described in terms of the aforementioned configuration. This artificial characterization eases the analysis of various imaging systems. Investigation into the state of the art of the various subsystems is out of the scope of this thesis. Rather, components of the imaging system that affect the dynamic range of the echocardiographic image are discussed.

The basic elements of the pulse echo transmitter receiver system are shown in Figure 1.2. The large dynamic range (at least 90 dB) of the echo signal is the result of ultrasonic absorption, reflection and wave divergence. A grey scale display, in practice, can provide about 15 dB

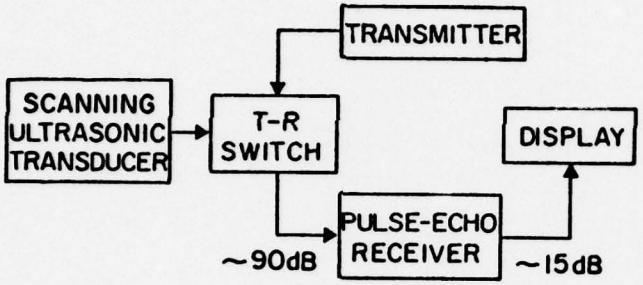

Figure 1.2 Basic Pulse Echo System

of discernable grey scale dynamic range. If a bulk storage such as video tape or digital memory, or color display are used, then the difference in dynamic range may be less; but the displayable dynamic range is much smaller than the raw echo signal's. For digital memories, it is important to keep the required dynamic range as low as possible to conserve storage. The storage constraint is especially pronounced for multidimensional echocardiography because the amount of data is extremely large. Without loss of generality for different echocardiographic imaging systems, the dynamic range of the raw echo must be compressed at least two to three times.

Since the early applications of echocardiography, the problem of dynamic range compression has been partially compensated for by a time-varying gain. The basis of such an implementation is that as the acoustic wave transverses through the scanning volume, the amplitude is attenuated. Therefore, by the application of the linearly increasing dB gain curve versus range (or in reality time), the echo amplitude can be normalized. Operator controls are provided so that the operator can optimize the gain profile for each patient and each look direction. Since the power profile for a ping might not be monotonically decreasing at a single rate, this technique required compromises at higher gains for certain sections and saturation in some other sections. For example, echos from heart valves, especially at a high angle of incidence might produce low

echos, whereas the posterior wall produces strong echos. Compromises must be made by the operator to sacrifice sensitivity within the atriums or ventricules or to sacrifice resolution at the anterior or posterior wall regions. Recognizing this need, Barnes et al.[4] proposed a programmable swept gain control. The basic operating principle for such a dynamic range compression technique is through the use of voltage-controlled gain amplifiers and wave form generators. The wave form generators can generate piecewise linear continuous voltage wave forms which can be used to control the gain (in dB) in the voltage-controlled amplifier. Thus, by dividing a ping interval into multiple segments, the operator can optimize the gain for a particular function. Also, a constant rejection level is used to suppress the display of low level signals ("grass"). This technique of multisgement sweep gain has been applied to commercial A-mode, TM-mode, B-mode, and spector-scanned echocardiographic imaging systems. It was hailed as a great improvement in grey scale imaging.

Although the manually programmed sweep gain control provides great improvement in dynamic range compression in echocardiographic imaging, manual adjustment still has drawbacks. The quality of the image is still operator dependent, and nonrepeatable. Considerable time is required to set up the gain parameters manually. Also, the gain profile is constant throughout the sector scan; thus, for some look angles, the problem of compromising saturation with low sensitivity or vice versa occurs. Adaptive or automatic gain control

for echocardiographic imaging has been investigated by various investigators. DeClercq and Maginess proposed an adaptive gain control system with analog approach.[7] "The operating prototype examines peak signals in eight-range segments, anticipating required gains from a progressively updated store. Isolated strong echoes are ignored to avoid loss of lower level detail." The system recognizes that optimal gain occurs over small spatial or temporal segments only, and by the power profile's correlation from ping to ping, an updated gain control is derived. At the present, seven seconds are required for the gain control to settle for a constant target. With a PRF of 1 KHz, that means seven thousand samples are required.

The use of an on-line computer for gain control in ultrasonic imaging systems has been implemented by Fry.[12] This system utilizes a time-gated mode. In other words, small segments are sampled repeatedly to derive its optimal gain. This "time-gated display" method requires long data acquisition intervals and is not applicable for echocardiography.

1.4 Scope of Investigation

The main goal of the thesis is to investigate adaptive dynamic range compression techniques in echocardiographic imaging systems. The state of the art in echocardiography dynamic range compression is inadequate for multi-dimensional imaging. The manually adjusted, multisegmented gain control contained in commercially available

echocardiographic imaging systems is inadequate for multi-dimensional imaging because there are rapid changes in look angles. The experimental adaptive gain control proposed by DeClercq and Maginess is not applicable to multidimensional imaging because of the unwieldy amount of analog components when adapted for three-dimensional scanning. Therefore, for multidimensional echocardiography imaging, an automated, adaptive gain-control scheme under computer control is needed. The use of a digital computer eases the implementation of the dynamic range compression technique and offers flexibility in system parameters.

The scope of this investigation can be divided into three areas. They are as follows:

1. An echo-signal model to provide a theoretical basis for the development of the dynamic range compression algorithm and to provide simulated data for the testing of the dynamic range compression algorithm.
2. A general dynamic range compression algorithm applicable to any scanning and display technique.
3. Examples of specific implementation technique of the dynamic range compression algorithm and their performances.

These three main areas are covered in Chapters II, III, and IV, respectively.

CHAPTER II

ECHOCARDIOGRAPHY SIGNAL MODEL

The purpose of this chapter is to present an echocardiographic signal model for the development and test of the dynamic range compression algorithm. It is not intended to model every acoustical phenomenon in the echocardiographic imaging process. Rather, a statistical approach is used to provide a reasonable signal power profile. Furthermore, the model is not acoustically validated in this study; as such, this model is based on published results from other researchers. For the development and test of the dynamic range compression, an accurate model of the echo returns from the scanning volume is not necessary, but rather appropriate power profiles are necessary.

Based on this simplified approach to modeling, the process is illustrated in Figure 2.1. The acoustic wave propagates through a medium. As it encounters reflectors, a portion of the energy is reflected, while the transmitted wave propagates further into the medium. The reflected wave propagates through the medium again, reaching the transducer, and subsequently is converted to an electrical signal. The next two subsections examine the first-order transmission and reflection processes. Subsection 2.3 presents a signal model with reference to parameters used by other researchers.

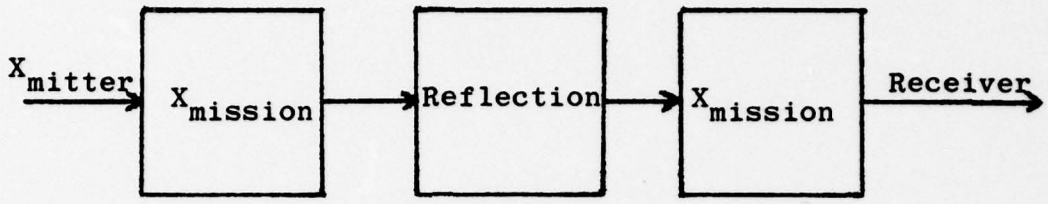

Figure 2.1 Signal Model Processes

2.1 Transmission Components

A single transducer is used as the transmitting and receiving element in the pulse mode echocardiographic imaging system. Transducers in use or proposed include unfocused or focused discs of piezoelectric material, a linear phased array, or two-dimensional phased arrays. Often a mechanical system and its associated synchronization electronics are used with such a transducer to form a scanning system. In the case of phased arrays, this task is done electronically. But, no matter how the scanning system is implemented--manually, mechanically, or electronically--the function of the transducer is to transmit a pulse of narrow beam acoustic energy into the scanning volume and to receive the echos produced by different anatomical structures. The generation and propagation of the acoustic wave in this inhomogeneous material is a complex process, but for practical applications, a

study of the first order effects provides sufficiently accurate results.

In this subsection, some of the factors that affect the amplitude of the acoustic wave are examined. Here, a transducer responding to pressure and operating in the linear region is assumed. Also, the mechanical to electrical gain of the transducer is assumed known but ignored in this discussion.

2.1.1 Beam Divergence

The spatial distribution of the acoustic wave intensity radiated by a transducer may be calculated by the application of Huygen's Principle. The intensity pattern applies to both transmitted and received functions of the transducer by the reciprocity principle. Since most echocardiographic imaging systems are designed with a narrow beam with sufficiently low side lobes, and we seek a first-order approximation only, we will consider the intensity pattern along the direction of propagation within the main lobe. Then, for an arbitrary transducer, the intensity can be expressed as a function of range,

$$I(r) \triangleq \frac{p_{max}^2(r)}{p_{max}^2(o)} \quad ,$$

where r = range, along the direction of main beam, and

$p_{max}(r)$ = temporal maximum pressure.

Since the same transducer is used for transmit and receive functions, the intensity of a completely reflected wave through a lossless medium should be $I^2(r)$. If we are interested in the pressure or the electrical output of the transducer, the attenuation effect due to the radiation from a transducer is just $I(r)$.

A commonly used transducer in echocardiography is a one-half-inch-diameter unfocused transducer operating at 2.25 MHz. The circular disc radiator permits easy analysis and is shown here as an example for echo signal attenuation due to beam divergence. The solution to the vibrating plane disc is well covered in acoustic and ultrasonic imaging literature.[40,68] Here, the steady state intensity distribution is used for simplicity. Much work on transient conditions has been done by investigators as reported by Wells.[70] It is commonly reported that the solution converges to steady state within three to six half-cycles. Since the region at close range is of no interest (skin and tissure) to the cardiologist, the steady state assumption involves no degradation to the model. For this steady state plane disc radiator, the beam can be considered to be composed of two regions. Classically, the transition point between the Fresnel (near) zone and the Fraunhofer (far) zone is considered to be a^2/λ, where a is the diameter of the radiating disc, and λ is the wavelength. But Fernauek's (Ref. 70) simulation shows that the

transition occurs about 25% closer than the classical result, a^2/λ. Nonetheless, the time maximum, spatial average along the beam in the Fresnel zone can be considered to be constant, while in the Fraunhofer zone, it can be considered to diverge. Then, for the case of the unfocused disc transducer:

$$I(r) = \begin{cases} 1 & r \leq r_o \\ \left(\frac{r_o}{r}\right)^2 & r > r_o \end{cases} ,$$

where

r_o = transition range between the Fresnel and Fraunhofer zone

= 0.75 a^2/λ or a^2/λ (see text).

2.1.2 Refraction

As the acoustic beam encounters an interface where two media meets, the beam is refracted. Section 2.2.1 covers the refraction angle and transmission coefficient for the single and double interface cases. In summary, because part of the energy is reflected, the acoustic wave undergoes an attenuation T, the transmission coefficient at that particular range. Also, to account for the beam refracted away from the look angle of the receiver, another attenuation should be included. Since this component due to the refraction angle will have to take into account the

total angle as the beam traverse through all the previous interfaces, it is difficult to calculate this component. Since the velocity of acoustic wave in biological materials does not vary drastically, the refraction angle is relatively small for most cases and the exclusion of this component is of no great consequence. Another term of attenuation that occurs at the boundary is wave mode conversion. "Mathematical analysis of the conditions which arise with oblique incidence where mode inversion is possible is tedious. The analysis becomes difficult if the media are anisotropic, as in the case with many biological materials."[70] Therefore, this component is not treated here. The total effect of these attenuations, then, is an impulsive differential attenuation component occurring at the boundary.

2.1.3 Other Attenuation Components

The reason that the attenuation components such as absorption, scattering, etc., are grouped together under one component is that experimental results bear much more significance than theoretical results. Absorption is due to the conversion of ultrasonic energy into heat. When the acoustic wave encounters obstacles that are smaller than the wavelength, the wave is said to be scattered. For the transmission component, we are interested in forward scattering; for reflection component, we are interested in back scattering. It is important to note that most biological materials exhibit frequency dispersive characteristics. As such, in a

pulse-echo system, the shape of the pulse envelope is changed as it transverses through the scanning volume. The attenuation parameters of different types of biological materials have been investigated by various researchers, and a summary can be found in Wells.[70]

2.1.4 Total Transmission Effects

As we have seen from the previous subsections, the total attenuation of the acoustic beam is due to many processes. In this subsection, we will combine these effects to model the transmission process for our model. Since we will sample the echo returns, let

$\alpha_i \triangleq$ differential total attenuation in dB's.

Then α_i is equal to the sum of attenuation due to beam divergence, refraction, absorption, mode conversion, scattering, etc. In general, one can approximate the total attenuation as a function of range for any scan angle. To simulate the actual processes involved, it is more practical to use measured data than theoretical results. Furthermore, to account for the dispersion effects as the acoustic pulse is transmitted through the scanning volume, one can modify the pulse shape as a function of range. Since essentially no research data are available for dispersion, the property of acoustic pulse transmission is ignored in this simple model. Also, because of the complexity of the attenuation processes involved, it is impossible to account for all these

factors. The only component that is accountable is the beam divergence component. Thus, if one uses this to account for attenuation, this establishes the lower bound on the attenuation effects as the acoustic pulse is traversed through the scanning volume. This particular component is used in the dynamic range compression algorithm.

2.2 Reflection Components

The echo received at the transducer is a summation of many phenomena governed by a complex set of conditions as the acoustic wave propagates through the scanning volume. A conceptual understanding of how echocardiography works is obtained by considering the reflection of a uniform plane wave off a boundary of different acoustic impedance normal to the direction of propagation. But this simplified model of the acoustic process is inadequate. For example, as the acoustic wave transverses through the scanning volume, it encounters many surfaces where the angle of incidence is highly oblique. By Snell's Law, the angle of reflection is equal to the angle of incidence; then, no specularly reflected signal will be present at the receiver. But this does not render echocardiography useless. As in radar and sonar, backscattering off a surface is an important component. What the cardiologists are able to observe on existing echocardiographic imaging systems contains a high amount of signal due to backscattering. The major acoustic reflection phenomena examined here includes reflection due to interfaces and reflection due to backscattering.

2.2.1 Reflection from Interfaces

Single Interface

For a transverse uniform plane wave incident at angle θ_i with respect to normal on boundary between medium 1 and medium 2 (Figure 2.2), the angles, reflection coefficient, and transmission coefficient can be expressed as follows:

$$\frac{\sin \theta_1}{\sin \theta_2} = \frac{V_1}{V_2} \quad ,$$

$$R = \left| \frac{p_{1r}}{p_{1i}} \right| = \left| \frac{\rho_1 v_1 \cos\theta_2 - \rho_2 v_2 \cos\theta_1}{\rho_1 v_1 \cos\theta_2 + \rho_2 v_2 \cos\theta_1} \right|$$

and

$$T = \left| \frac{p_{2t}}{p_{1i}} \right| = \left| \frac{2\rho_1 v_2 \cos\theta_1}{\rho_1 v_1 \cos\theta_2 + \rho_2 v_2 \cos\theta_1} \right| \quad .$$

Multiple Layer

If a thin (relative to pulse envelope) medium is interposed between two media, interference from the reflection from the two boundaries results. Figure 2.3 shows such a configuration for a normal incidence plane wave. For simplicity, the oblique incidence case is not discussed here; the effect of interference due to medium thickness is similar to the normal incidence case. The reflection and coefficients are as follows:

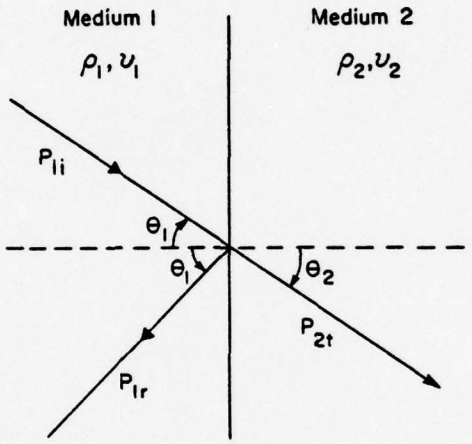

Figure 2.2 Reflection From Single Interface

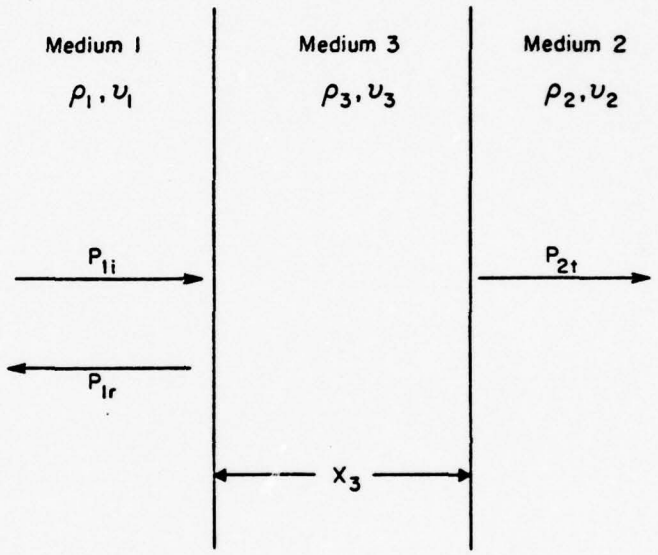

Figure 2.3 Reflection From Thin Layer

$$R = \left| \frac{p_{1r}}{p_{1i}} \right| = \left[1 - \frac{}{(r_{2/1}+1)^2 \cos^2 \frac{wx_3}{\sqrt{3}} + (r_{3/1}+r_{2/3})^2 \cdot} \right.$$

$$\left. \frac{4r_{2/1}}{\cdot \sin^2 (\frac{wx_3}{\sqrt{3}})} \right]^{1/2}$$

and

$$T = \left| \frac{p_{2t}}{p_{1i}} \right| = \left[\frac{}{(r_{2/1}+1)^2 \cos^2 \frac{wx_3}{\sqrt{3}} + (r_{3/1}+r_{2/3})^2 \cdot} \right.$$

$$\left. \frac{4(r_{2/1})^2}{\cdot \sin^2 \frac{wx_3}{\sqrt{3}}} \right]^{1/2}$$

where

$$r_{2/1} = \frac{\rho_2 v_2}{\rho_1 v_1} \quad ,$$

$$r_{3/1} = \frac{\rho_3 v_3}{\rho_1 v_1}$$

and

$$r_{2/3} = \frac{\rho_2 v_2}{\rho_3 v_3} \quad .$$

2.2.2 Scattering

In this subsection, we consider targets whose dimension is smaller than the wavelength. Although targets of the order of the wavelength are usually present in biological terms, the effect of these scatterers is angle

dependent, much like the small scatterer under discussion. Although different physical phenomena govern the two cases, generality is not lost for the signal model. For scatterers much larger than the wavelength, this is just a specular component discussed under reflection from boundaries.

According to Rayleigh's scattering theory, each individual scatterer can be described by differential scattering cross-section,

$$\sigma_d = \frac{1}{9}\left(\frac{2\pi}{\lambda}\right)^4 a^6\left[\frac{K_e - K}{K} + \frac{3\rho_e - 3\rho}{2\rho_e + \rho}\cos\theta\right]^2 ,$$

where

λ = wavelength,

a = scatterer radius ($<<\lambda$) ,

K = adiabatic compressibility of embedding medium,

K_e = adiabatic compressibility of scatterer,

ρ = density of medium

ρ_e = density of scatterer, and

θ = angle of incidence.

Note that σ_d is proportional to the fourth power of frequency. This fact is confirmed by Shung, et al.[57]

For forward scattering, one component of the attenuation effect, $\theta=\pi$, and therefore:

$$\sigma_d\Big|_{\theta=\pi} = \frac{1}{9}\left(\frac{2\pi}{\lambda}\right)^4 a^6\left[\frac{K_e-K}{K} - \frac{3\rho_e-3\rho}{2\rho_e+\rho}\right]^2 .$$

And for backscattering, $\theta=0$,

$$\sigma_d\Big|_{\theta=0} = \frac{1}{9}\left(\frac{2\pi}{\lambda}\right)^4 a^6\left[\frac{K_e-K}{K} + \frac{3\rho_e-3\rho}{2\rho_e+\rho}\right]^2 .$$

Then if such scatterers are contained in a volume, one must consider the total reflection from all of the scatterers. Furthermore, if a scatterer moves with velocity v along the acoustic beam direction in a medium with velocity of sound equal to c, then this scatterer introduces a Doppler shift, $w_i = 2\frac{v}{c} w_o$, to the carrier frequency, w_o. Then to characterize this scattering volume, one can use the average scatterer cross-section,

$$\sigma(r,f) = \sum_i \overline{\sigma_i^2} ,$$

where the summation is over all scatterers for which

$$r_i = r$$

and

$$w_i = 2\pi f .$$

For tissue structures, the velocity of the scatterer is relatively slow, then one can approximate this as dispersive in time only, or

$$\sigma(r,f) = \delta(f)\sigma(r) \ .$$

For blood cells, where the individual scatterer velocities are significant, the average scatterer cross-section is both dispersive in time and frequency.

Furthermore scatterers can be classified into two types, random and lattice. For randomly located scatterers, the scattering function is independent of the incident beam. But for scattering from a lattice structure, Bragg diffraction occurs. Consider adjacent scatterers to be distance d apart. By Huygen's principle, the path length from the reflection of two adjacent scatterers is then different by $d \sin\theta$. Obviously constructive and destructive interference can occur depending on the difference in path length. Then for scatterers with a lattice structure, the scattering cross-section depends on the angle of incidence.

Shung, et al.[57] reported that blood at low hematocrits (percentage packed-cell volume occupied by blood cells below 8%), "the red blood cells behave as incoherent, randomly-distributed scattering centers;" and "at high hematocrits (greater than 58% or so), the blood resembles a perfect crystalline" which must be accounted for.

Hill[19] reasoned that "if one considers the known histology of two human tissues, skeletal muscle and liver parenchyma, one finds that they consist of fibers and lobules, respectively, whose boundaries are, in each case, defined by connective tissue structures... The structures

thus may constitute arrays which, in practice, exhibit an appreciable degree of short range order... By assuming reasonable values for the parameters describing such arrays, one may construct computational models for them. He found supporting evidence to support such a Bragg diffraction theory with data for skeletal muscle.

In summary, scattering is a complex process with very few experimental results where many parameters are unknown. If we consider the effect of the scatterers at one point and at a single angle, we can assume that it is a Rayleigh process. But the parameter is a difficult to predict function of many factors. Also, frequency dispersion introduces a time-varying filter property to the pulse envelope. Dispersion is unimportant to our signal model because the effect is greatest for blood cells, which are of little interest in an echocardiographic image.

2.3 Signal Model

The preceding sections discussed some of the mechanisms which affect the echo returns in echocardiography. Since echocardiographic imaging requires information throughout the scanning volume to generate an image, we are concerned with phenomena taking place throughout the scanning volume. This particular aspect of echocardiographic imaging is dissimilar to radar or sonar analysis. In the latter, the volume of interest spans only a small part of the scanning volume. Even for the case of multiple

targets, for example, aircraft in formation, the problem is mathematically tractable because of the target similarity and of the propagation medium. In echocardiography, the process is much more complicated because of the medium and of the continuum of highly dissimilar targets. Therefore, a simplified signal model is presented here for simulating the power level profile rather than the acoustic processes involved.

2.3.1 Reflection from a Small Volume

From the preceding subsections, we see that the received signals are composed of returns from distinct fixed targets, such as boundaries of acoustic impedance mismatch and from point targets, such as random or structured scatterers. Then, without lost of generality, we can model the echo as a sum of a specular and a scatterer component. (If only the specular component is present, one can set the scatterer component to zero, or vice versa.) In Section 2.2.1, we saw that the reflection from the interface between two media is highly angular dependent. There are probably more oblique angles of incidence than occurrences of normal incidence. (Consider a sphere or ellipsoid, for instance; from any scanning angle, there are more highly oblique angles of incidence than those close to normal incidence.) Also, for irregular interface surfaces, such as the endocardium, there are different angles to incidence within the beam width. Therefore, there is probably a preponderance of scatterer returns rather than specular returns.

For simplicity in this discussion, let us ignore the time delay involved. That is if pulse p(t) is transmitted at t=0, the echo from a target distance x away will be received as $p(t-2x/v_H)$, where v_H is the harmonic velocity and is equal to $x\left[\int_0^x \frac{1}{v(y)}dy\right]^{-1}$. Then, ignoring the delay, a general received signal from a single target and/or small scatterer volume,

$$r(t) = \alpha p(t)\cos[w_c t + \phi_p(t) + \delta]$$

$$+ \beta p(t)\cos[w_c t + \phi_p(t) + \theta],$$

$$0 \leq t \leq T .$$

where:

$r(t)$ = echo signal received at the transducer,

$p(t)$ = transmitted pulse envelope,

$\phi_p(t)$ = phase of transmitted pulse,

w_c = carrier frequency,

α = amplitude of the specular component,

δ = phase of the specular component,

β = amplitude of the scatterer component, and

θ = phase of the scatterer component.

Since echocardiography pulse echo systems are not phase modulated, $\phi_p(t)=0$. In this case, α and δ are assumed to be known. Without loss of generality, we can let $\delta=0$.

Decomposing r(t) into the quadrature terms,[62]

$$r(t) = a_1(t)[p(t)\cos w_c t] + a_2(t)[p(t)\sin w_c t],$$

where a_1 and a_2 are independent Gaussian random variables with

$$E(a_1) = \alpha ,$$

$$E(a_2) = 0 ,$$

and

$$Var(a_1) = Var(a_2) = \sigma^2 .$$

Then, at the output of the detector, the envelope is

$$s(t) = \sqrt{a_1^2 + a_2^2}\; p(t) .$$

The probability density function for s(t) is Rician,

$$p_s(s) = \frac{s}{\sigma^2} e^{-\frac{(s^2+\alpha)}{2\sigma^2}} I_o\left(\frac{s\alpha}{\sigma^2}\right) U(s),$$

where $I_o(x)$ = Bessel function of the first kind.

Actually, the above describes three basic situations: reflection from a boundary, reflection from a heterogeneous tissue volume, and reflection from a blood volume. Conceptually, we desired to identify each of the three situations and to estimate the parameters involved. The parameters for the different situations are from different underlying populations. For the reflection from a boundary,

α = reflection coefficient (normalized transmit pulse)

and

σ^2 = backscatter component of the boundary surface.

For the reflection from heterogeneous tissue volume,

$\alpha = 0$

and

σ^2 = backscatter component of the tissue volume.

For the reflection from blood volume,

$\alpha = 0$

and

σ^2 = backscatterer component from blood cells.

Or, from the detection viewpoint, there are two hypothesis: H_1, specular component present; and H_o, only scatterer component present. The H_o hypothesis can be further broken

down for high and low σ^2; the latter with a high probability of being a volume of blood only.

2.3.2 Complete Signal Model

If we are to consider the total echo return as the acoustic wave traverses through the scanning volume, we have to modify the aforementioned small volume model. This can be accomplished by first assuming the pulse envelope to be sufficiently short in duration compared with the sampling time. Then, the sampled envelope signal for a target volume at distance x_j is

$$s(i) = \sqrt{a_o^2(j) + a_1^2(j)} \quad \delta(i-j) ,$$

where

$s(i)$ = echo detector output at the i^{th} sampling time,

$a_{0,1}(j)$ = quadrature components due to reflection from target volume at x_j, and processes statistically properties as in Subsection 2.3.1,

$\delta(i-j)$ = Kronecker delta

$$= \begin{cases} 1 & i=j \\ 0 & i \neq j \end{cases}$$

and

j = sample delay corresponding to distance x_j $\left(= \frac{2x_j}{\Delta t V_H}\right.$, where Δt = sampling interval) .

Suppose we introduce a pulse function $p(t) \neq 0$ for $t \; \Delta t$, and with pulse samples, $p(K)=p(tK)$, for $k=0,1,\ldots,K$, then the quadrature components will have to be modified to

$$\sum_{k=i-K}^{i} p(i-k)a_{o,1}(k) \quad ,$$

or, since $p(k)=0$ for $k>K$,

$$\sum_{k=i-K}^{i} p(i-K)a_{o,1}(K) \quad ,$$

Now, if we introduce the total attenuation, we have to introduce a multiplier, m(k), where

$$m(k) = \prod_{\ell=0}^{k} \alpha_{\ell} \quad ,$$

and

α_{ℓ} = total attenuation per sample distance.

Then the detector output becomes

$$s(i) = \sqrt{\left[\sum_{k=i-K}^{i} m(k)a_{o}(k)p(i-k)\right]^2 + \left[\sum_{k=i-K}^{i} m(k)a_{1}(k)p(i-k)\right]^2} \quad .$$

Figure 2.4 shows a block diagram of the signal model. Note that the process is still an envelope of the quadrature terms,

$$s = \sqrt{b_o^2 + b_1^2} \quad .$$

But now with the introduction of the pulse envelope and total attenuation terms, the quadrature terms become

$$b_{o,1}(i) = \sum_{k=i-K}^{i} m(k) a_{o,1}(k) p(i-k) \quad .$$

Since $a_{o,1}$ is a normal process, then $b_{o,1}$ remains a normal process, but means and variances change to the following:

$$E\{b_{o,1}\} = \sum_{k=i-K}^{i} m(k) p(i-k) E\{a_{o,1}(k)\}$$

and

$$\sigma^2\{b_{o,1}\} = \sum_{k=i-K}^{i} \sigma^2\{m(k) p(i-k) a_{o,1}(k)\}$$

$$+ 2 \sum_{k=i-K}^{i} \sum_{\substack{\ell=i-K \\ k \neq \ell}}^{i} Cor\{m(k) p(i-k) a_{o,1}(k),$$

$$m(\ell) p(i-\ell) a_{o,1}(\ell)\} \quad .$$

Note that even if $a_{o,1}(k)$ are uncorrelated in range, with the introduction of m, p, the modified quadrature terms will be correlated in range. For each sample, though, it still has a Rician distribution. The variance for such a

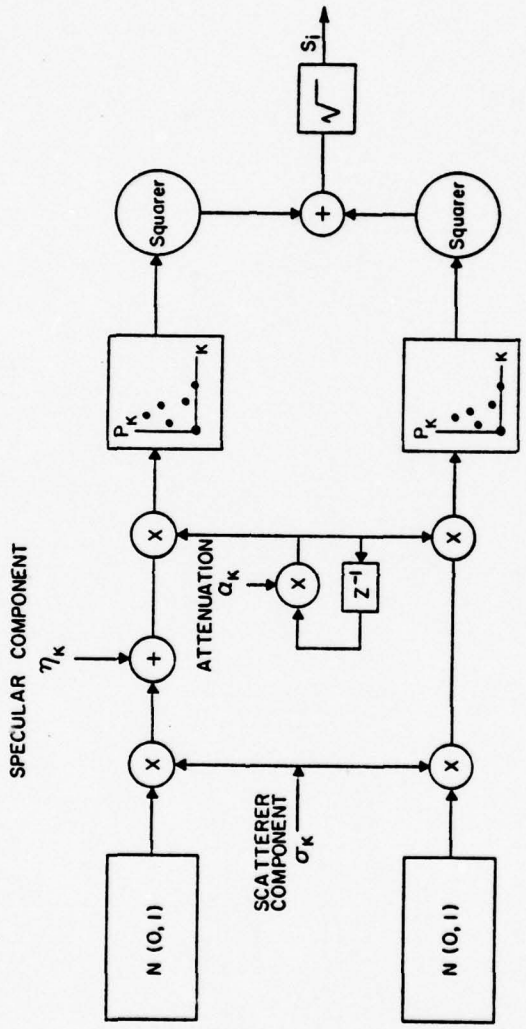

Figure 2.4 Echocardiography Signal Model

sample is now increased due to the correlated nonstationary process. It appears that if we wish to estimate $\sqrt{a_o^2+a_1^2}$, we would desire to make the process stationary. Choosing p(t) short is one step toward avoiding correlation induced by the ensonification. This limits the available power, especially in medical applications where peak power must be constrained. Pulse compression techniques such as those utilized in radar might be considered here, but the complexity and expense preclude the feasibility of such systems at that time. The other approach to making the processes stationary then is to compensate for m. Anyway, it is necessary to compress the dynamic range of the signal into the limited dynamic range of a real processor. The effect of eliminating m then is equivalent to using an even illumination function, as if the transducer is directly in front of each target. It seems reasonable to estimate m and divide by the estimate. Since m is a complicated process whose effects show up within the signal information itself, a direct estimation is infeasible. The dyanmic range compression algorithm to be presented contains a multiplier, which is proportional to the received power. Over small volume, this represents a rough estimate of m and $\sigma_{a_{o,1}}$. Therefore, it tends to normalize the signal power level throughout the scan volume.

2.3.3 Example

In Subsection 2.3.2, a model of the complete echo return along a scan direction was presented. In this

subsection, examples of how the parameters for the model can be obtained are given. As mentioned earlier, the acoustic reflection and propagation processes are immensely complex, the method only serves to estimate power profiles rather than a complete acoustic model. Therefore, simplifications were made where the power profile is not severely affected.

Figure 2.5 shows a typical single scan in echo-cardiography. The region of interest spans from the anterior epicardium to the posterier chest wall.

In the chest wall, the ultrasound is mainly scattered by the muscular tissue. Actually, a complicated phenomenon occurs in this near zone. Reverberation is another possibility. Also, the sternum and ribs tend to contribute dislocation from the ideal case also. Very little experimental work has been done in this area. Since this region is of no interest, the simple model of just scattering is sufficient.

As the ultrasonic beam traverses through the scanning volume, it encounters tissues and fluids of different acoustical impedance. The reflection coefficient and transmission can be calculated at these interfaces from their characteristic impedances and angle of incidence. Since the transducer serves as the transmitter and the receiver, only the reflected component in the direction of incidence should be considered. This can be estimated by multiplying by the transducer's directivity function; thus, the specular component can be estimated. At the same time,

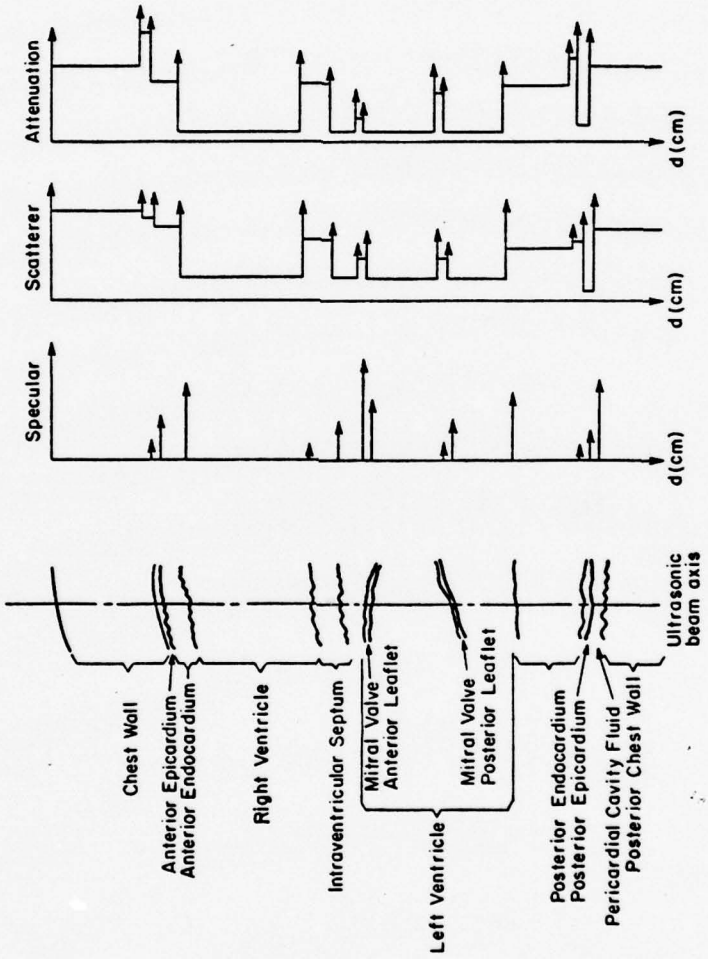

Figure 2.5 Example of Signal Model Parameter

the transmission coefficient on the return trip can be calculated. The two transmission coefficients can then be combined with the attenuation component for that medium to form the total attenuation parameter. The attenuation and scatterer component parameters at the different ranges can be set according to the value for the medium. The scatterer component at the interfaces has to be changed to account for scattering off the surface. Since an overall power profile is desired, it is not necessary to adjust the scatterer component according to the angle of incidence. An example of parameters is illustrated in Figure 2.5.

The velocity, absorption, attenuation parameters and characteristic impedances have been investigated by many researchers and is well summarized in Wells.[68] For echocardiography, a transducer frequency of 2.25 MHz is normally used. For this frequency, the parameters are summarized in Table 2.1.

Table 2.1 Ranges of Parameters in Biological Materials

	Density, ρ ($g\ ml^{-1}$)	Velocity, c (ms^{-1})	Characteristic Impedance, z ($10^6 Kg\ m^{-2} s^{-1}$)	Attenuation, α ($-dB\ m^{-1}$)	Scattering, σ (-dB)
Blood	1.06	1530	1.62	0.2	74
Soft Tissue	1.04 - 1.06	1500 - 1610	1.62 - 1.68	0.9 - 3.4	50 - 70
Muscle	1.07	1550 - 1640	1.65 - 1.74	3.4 - 5.0	

CHAPTER III

DYNAMIC RANGE COMPRESSION TECHNIQUES

The object of the section is to develop a general dynamic range compression algorithm applicable to any of the scanning and display techniques. Although the hardware implications of various echocardiographic imaging systems are drastically different from each other, the basic pulse echo technique is common to all. The receiver turns on for a period of time before the transmitter can be activated again. This ping-by-ping or line-by-line approach is common to all of the scanning display methods. Only the transducer orientation and display format are different. In this section, the organization of echo signal for various systems is defined. Based on the statistical echo signal model suggested in Chapter II, a general dynamic range compression algorithm for echocardiographic imaging systems is proposed. Basic implementation and feasibility of the general algorithm are examined.

3.1 Introduction

Although application of dynamic range compression techniques to echocardiographic imaging has been limited as shown in Section 1.3, a wealth of information on automatic gain control and dynamic range compression in the radio, radar, sonar, and data transmission area exists. Also, the

process of compressing the dynamic range of an echocardiogram is an image processing technique. Therefore, relevant investigation in this area exists. There are special features and objectives where these well-explored off-line computer techniques cannot be applied to echocardiographic image processing directly, but these results have a significant impact on the algorithm proposed here.

3.1.1 Automatic Gain Control in Communication Systems

Automatic gain controls (AGC) are used extensively in receiver circuits to minimize gross variation on signal power levels. The most common purpose of an AGC system is to suppress low-frequency variation in signal strength without disturbing the higher frequency signal components. Numerous AGC configurations have been designed to accomplish this goal. For simplicity, AGC systems can be considered to be one of three different types: feedback, feedforward and instantaneous types. Various configurations of AGC circuits were adopted for use in echocardiography. Since these circuits are generally used to suppress low frequency power level variation, they essentially process in one dimension only. Therefore, these AGC systems must be modified to some extent to accommodate multidimensional imaging.

A commonly used AGC system in echocardiography is the implementation of instantaneous automatic gain control (IAGC) with logarithmic amplifiers. These IAGC's might or might not be used with sweep gains. The difference is that

their compression ratios are different. The dominant appeal of such logarithmic amplifiers in the echo receiver chain is that a human responds to logarithmic levels visually. This definitely serves as a matching transformer between the electrical signal with the human visual response system. But if the signal is stored in some kind of bulk storage, for example, a digital memory, then the question of matching to the recording medium arises. The logarithmic compression to match the human response can always be incorporated into the display system, and the signal should then be matched to the recording medium. In terms of quantization, if digital memory is used, logarithmic compression has tremendous appeal. Signals quantized uniformily after logarithmic amplification provide constant percentage error. This uniform percentage error property is valid for any signal distribution. But for human distribution, logarithmic quantization is not optimal in the least square error sense. Also, for echocardiographic imaging applications, the logarithmic compression ratio must be set over the whole scanning volume; thus for local neighborhoods with fairly constant power profiles, the compression ratio cannot be set optimally in order to satisfy the global requirement. Therefore, IAGC's are inadequate for echocardiography dynamic range compression.

Radio type feedback automatic gain controls are used in some echocardiography instruments.[34] Figure 3.1 illustrates such an AGC system. DeClercq[7] summarized

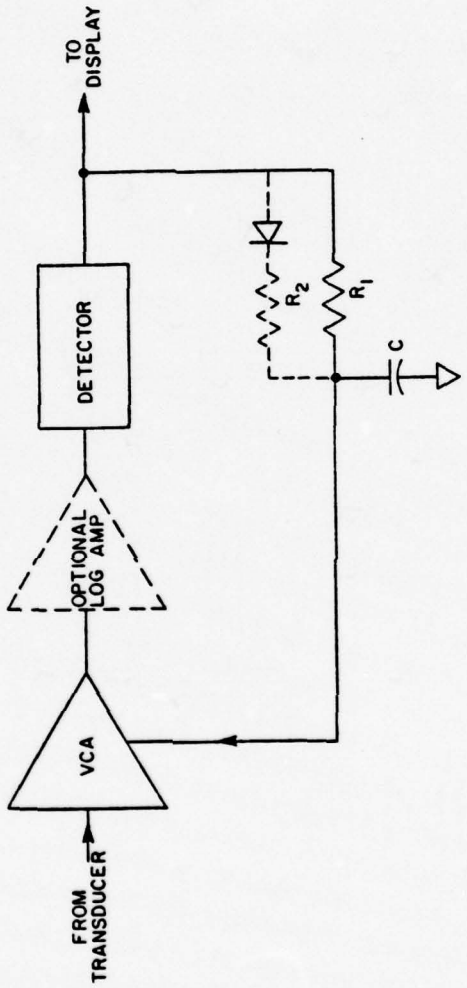

Figure 3.1 Radio Type Feedback Gain Control

the gain control's inadequacy as follows:

> "[However,] this method is basically inappropriate to the type of signal in ultrasonic pulse echo systems. Conventional radio and television signals are modulated onto a continuous carrier. Detection provides an average output readily extracted with the simple filters indicated. Ultrasound signals are discontinuous with periods of zero return over which the best that can be achieved is gain increase until the noise output rises. When the next distinct echo occurs, receiver gain can start to adjust. If adjustment is fast enough to follow the fastest pulses the system becomes unstable. Longer response times permit transitory overloads and the final gain value reached depends on the duration as well as the amplitude of the echo."

DeClercq further suggested that a dual channel feed-forward configuration such as Figure 3.2 can overcome, to some extent, the limitations in the feedback configuration. "This arrangement still suffers from the basic limitation that it acts with only local knowledge of the signal statistic."[7] Based on this configuration, DeClercq and Maginess developed the adaptive gain control for dynamic ultrasound imaging.

In summary, radio type automatic gain controls are inadequate for multidimensional imaging limitations in taking advantage of the spatial and the temporal correlations which exists in multidimensional images.

3.1.2 Adaptive Gain Control for Dynamic Ultrasound Imaging

DeClercq and Maginess[7] disclosed an adaptive gain control for dynamic ultrasound imaging. A schematic for such a system is shown in Figure 3.3. "The operating

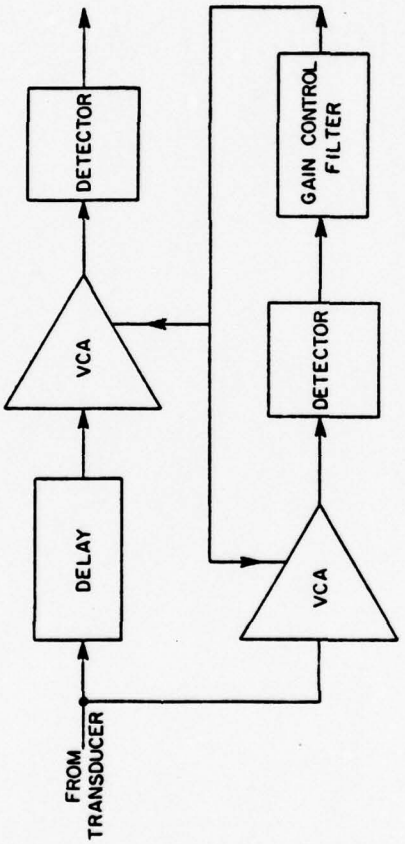

Figure 3.2 Dual Channel Feedforward Gain Control

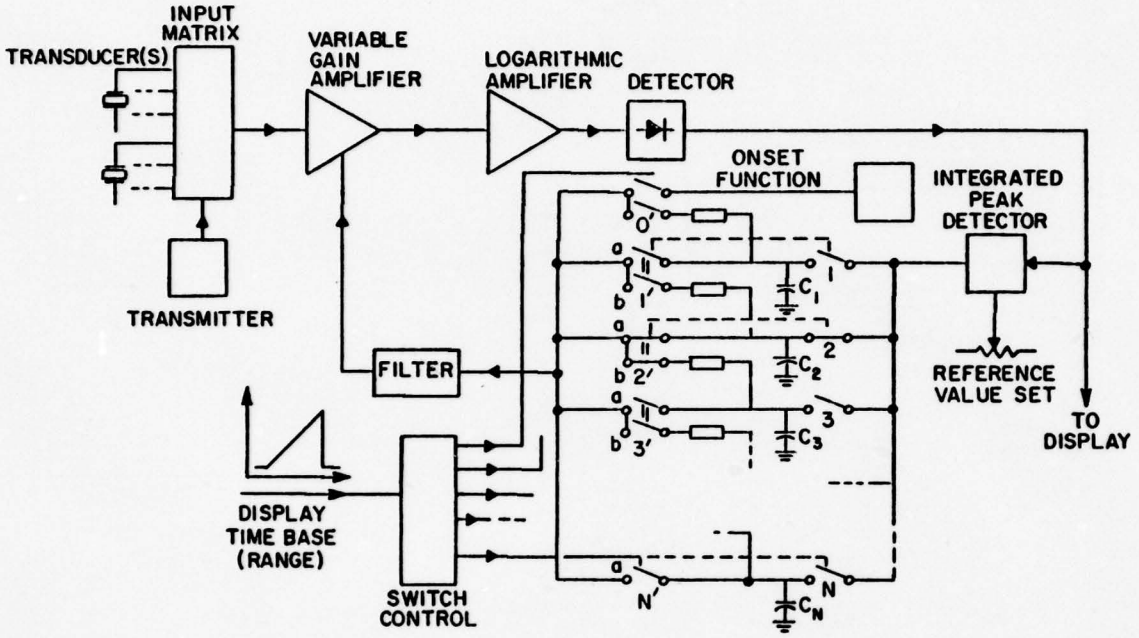

Figure 3.3 Adaptive Gain Control System (DeClercq and Maginess[7])

prototype examines peak signals in eight-range segments, anticipating required gains from a progressively updated store. Isolated strong echoes are ignored to avoid loss of lower level detail."[7] This feedforward adaptive gain control utilizing temporal (if manually scanned, spatial also) correlation of a power profile has been tried on an M-mode echo cardiographic imaging system. It was shown that a satisfactory gain profile was reached in seven seconds for a constant target. Apparently, this is satisfactory if M-mode images are desired.

This analog technique is an automated adaptation of sweep gain control, which has clinically shown its grey scale capability. The long settling time or learning period precludes real time or fast scanning at wide look angles. Its adaptability shows its main advantage in adjusting to different patients. Due to its long settling time, this technique is inadequate for multidimensional echocardiographic imaging.

Other practical considerations hamper this technique in multidimensional imaging. For example, for sector scanning, if different gain profiles are used for small scanning angles, then banks of capacitors are required for memory. An extension to three or four dimensions will definitely be uneconomical to implement. The large number of "memory" capacitors required is further increased if the number of segments is increased to 16, which is commercially available in manually adjusted sweep gain echocardiographic systems.

The problem of the large amount of analog memory required can be solved by the use of digital memory and the use of digital computer. This increases the flexibility of the control scheme. The use of a digital computer permits statistical techniques rather than a "heuristic" implementation in the analog system. Also, the traditional constant rejection level can be implemented in the same fashion. These value-added features form the basis of the dynamic range compression algorithm presented in this thesis.

3.1.3 Statistical Techniques for Gain Control

A gain control problem similar to that in echocardiographic imaging systems exists in communication and radar receivers. The statistical aspects of gain control in such applications is well explored in the literature.[47-51] The most applicable situation can be found in a paper by Rappaport.[49] The problem of optimum AGC in an incoherent receiver is explored.

> "A Bayesian learning algorithm for statistically optimum adaptive gain control (AGC) is derived in which the receiver gain is adjusted during the learning process so that the average cost of excluding the received signal from the receiver's dynamic range is minimized. Application of the approach to the frequently occurring situation of Raleigh-distributed signals of unknown strength yields a recursive algorithm that can be easily implemented."[49]

Although these techniques form a good statistical basis for a statistically optimum gain control to minimize exclusive cost, it lacks applicability to echocardiography in certain aspects. In echocardiographic images, the "clutter" consists of scatterer returns from blood, and any signal above the clutter level is of interest to the operator. Therefore, the lower limit should be set by the clutter level rather than by considering the exclusion cost as suggested in the algorithm. An improvement which eliminates the learning nature of the algorithm can be accomplished by using a separate power level estimation channel. These statistical techniques must be modified for echocardiographic imaging applications.

3.1.4 Image Processing

The dynamic range compression problem in multi-dimensional echocardiography can be considered as an image processing problem. Consider any two dimensional-plane of the multidimensional echocardiographic image (for example, the M-mode or the B-mode images). The object is to improve the grey scale assignment of such an image. This is also equivalent to produce an even illumination function. This problem and other associated image processing techniques have been investigated generally and specifically for echo-cardiography.

Various investigators have implemented echocardio-graphic image processing techniques incorporating a digital computer. Ballard, Waag and Angel [3] use two-dimensional Fourier Transform techniques to enhance echocardiographic

images by high and low pass filtering. Waag and Gramiak[66] use digital linear filtering to distinguish and separate signal, noise, and clutter components in an augmentation of M-mode scanning. Other image processing techniques besides amplitude manipulation have been investigated also. McSherry and Keller,[36] for example, incorporate by means of a digital computer an inverse filter for deconvolving the effects of the ultrasonic beam width. Digital interpolation in both time and distance simultaneously have been used in an attempt to eliminate artifacts, to diminish the effects of drop-out with unfavorable angles of reflection, and to facilitate data expansion.[35,63-67] Although these techniques show promise, all of the data have been digitized from commercial echocardiographic units or through video-tape recorders. The dynamic range of their data has been compressed by sweep gain and rejection circuits. The digitizers quantize the data to eight bits, equivalent to 48 dB. Therefore, even though these techniques show promise in compressing the 48 dB data to the display level of about 24 dB,they are not applicable in real time dynamic range compression where the raw echocardiographic signal must be compressed to display dynamic range.

Techniques for general image processing have implications in the echocardiography dynamic range compression problem. "Andrews, Hall and others[1,17-18] have produced enhanced imagery by a histogram equalization process for which the histogram of the enhanced image is

forced to be uniform."[46] To minimize the effects of nonuniform illumination, Oppenheim, Schaffer and Stockham[44] suggest the use of homomorphic filter with a high pass function. These two techniques have applications in echocardiographic image processing, but they are post-processing techniques. Again, a wide dynamic range image data must be quantized for computer processing, thus the methods cannot be utilized for echocardiographic dynamic range compression.

3.2 Development of Algorithm

It is desired to develop a general dynamic range compression algorithm applicable to multidimensional echocardiographic imaging. The algorithm should be implemented in or near real time under computer control. It should be capable of compressing the echo level dynamic range (~90 dB) to a display level dynamic range (~15 dB) or to a storage level dynamic range (example, 48 dB). The latter permits flexibility for post-processing; but the same algorithm can be applied again to reduce the dynamic range to display level. Without loss of generality, a grey scale display is considered because color assignment is arbitrary and can be considered a post-processing technique.

3.2.1 Objectives

The objectives of producing a grey scale echocardiographic image can be summarized as follows:

MINIMIZE:

A. Effects of attenuation, absorption, divergence, etc. In other words, provide a constant illumination function.

B. Clutter. Extraneous returns such as back-scattering from a blood volume should be eliminated from the display.

C. Artifacts due to the AGC algorithm. The algorithm should not generate false structures.

D. Saturation. Although saturation at isolated locations does not degrade the image full brightness over a local neighborhood it tends to degrade resolution.

MAXIMIZE:

E. Detection of structures at high angles of incidence. Cardiac structures such as values leaflets are of great interest, but they usually are at high incidence angles to the ultrasonic beam. Elimination of this "wash-out" effect is highly desirable.

F. Use of dynamic range of display. Full dynamic range of the display unit should be utilized over a local neighborhood.

3.2.2 Definitions

Although there are many types of scanning and display methods in echocardiographic imaging, dynamic range compression or signal processing problems are common to all. The

difference between these different types lies in the geometry and time-frame organization. It is intended in this subsection to unify the difference scanning and display methods so that the general dynamic range compression algorithm is common to all but the actual implementation method varies.

The objective of echocardiography is to visualize a solid and its motions. Thus, echocardiographic imaging systems are organized.so that one or more of the four cardinal dimensions, the three geometric dimensions plus time, can be viewed alone with the echo amplitude. For example, for M-mode devices, range and time are the independent variables and the echo amplitudes is a function of these two variables. Perhaps at this stage, the variables range and time should be clarified. Range is actually a time function, since it is proportional to the product of sound, velocity and time. For echocardiography, the maximum range of interest is usually about fifteen centimeters with the corresponding maximum time equal to about two-hundred microseconds. Since the cardiac structure moves with a much slower period, this is essentially a snapshot of a line of tissues. The time variable as defined here refers to the next group of transmit-and-receive cycles, or the neat frame. With these definitions for the geometric and temporal dependencies, one can combine all the different types of scanning and display methods and define the received echoes or other variables as in Table 3.1.

Table 3.1 Independent Variables for Different Scanning Modes

Mode	Continuous	Discrete
M mode	(r, t_ℓ)	(r_i, t_ℓ) or (i, ℓ)
Sector Scan Snap Shot	(r, θ)	(r_i, θ_j) or (i, j)
Real Time Sector Scan	(r, θ, t_ℓ)	(r_i, θ_j, t_ℓ) or (i, j, ℓ)
3D Snap Shot	(r, θ, Φ)	(r_i, θ_j, Φ_k) or (i, j, k)
3D Real Time	$(r, \theta, \Phi, t_\ell)$	$(r_i, \theta_j, \Phi_k, t_\ell)$ or (i, j, k, ℓ)

Where = r = range

θ = transducer beam angle within sector plane

Φ = transducer sector angle

t_i = time frame

The difference for different scanning and display methods is illustrated in Figure 3.4. The data acquisition intervals are illustrated in the figure. Times for display can be concurrent with the data acquisition interval or bulk storage can be used and then the image displayed at the end of each frame. Without loss of generality, the independent variable defined on Table 3.1 apply to each of these scanning methods and $(\cdot)$ denotes these independent variables depending on the method used.

The echo signal and other variables are defined as follows:

$s(\cdot)$ = received echo amplitude,

$v(\cdot)$ = dynamic range compressed video,

$v_q(\cdot)[q = 1,2,\ldots,Q]$ = quantized $v(\cdot)$
or discrete grey or color level assignments,

$g(\cdot)$ = gain level,

$b(\cdot)$ = bias level,

I = number of echo amplitude samples per ping,

J = number of pings per sector,

K = number of sectors per frame,

L = number of frames,

$M = IxJxKxL$ = total number of echo amplitudes, and

s_p = set of all possible subset of data points
$= \{\underset{\sim}{s}_{p1}, \underset{\sim}{s}_{p2}, \ldots, \underset{\sim}{s}_{pm}\}$,

where

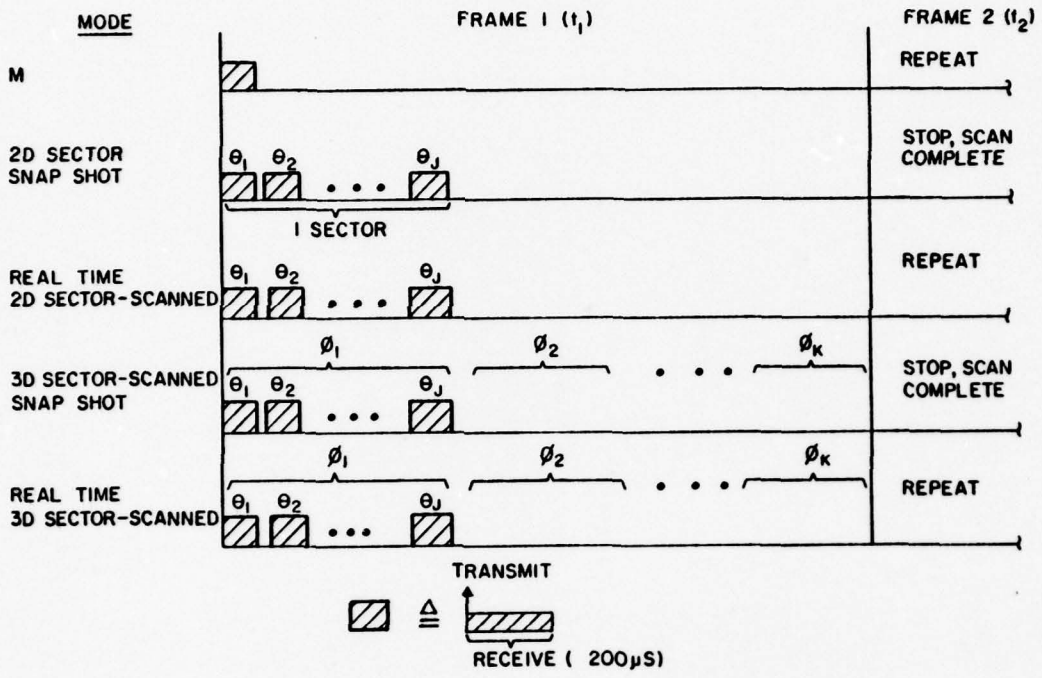

Figure 3.4 Timing Diagram for Different Modes of Echocardiographic Imaging

s_{pm} = all possible subsets of data points with m points in subset,

p = index for subset = 1,2,...,P, and

m = number of points in subset = 1,2,...,M .

Therefore, if there are M data points,

$$P = \sum_{m=1}^{M} \binom{M}{m} .$$

3.2.3 Approach

The objective of determining volumes of similar biological material and ascertaining their attributes has a direct theoretical solution. If one takes all combinations of the received echo amplitude samples and uses them to test the hypothesis of samples from a certain population, then one solves the problem of clustering samples from the same biological material and estimating its parameters. This method will lead directly to a likelihood ratio test:

$$\Lambda(\underset{\sim}{s}_p) \underset{\bar{H}}{\overset{H}{\gtrless}} \eta \quad ,$$

where

H = hypothesis that these group of echoes belong to similar material,

$\bar{H}$ = negative of H, and

η = threshold value.

Since there are $P = \sum_{m=1}^{m} \binom{M}{m}$ combinations of s_p and M = IxJxKxL, this approach is impractical; P is an astronomical number. Even if we limit the above combinations to sets that make geometrical sense (neighborhood echo amplitudes have a high probability of coming from similar materials), the number of combinations is still tremendous.

A practical approach is to treat each individual return separately. This has tremendous practical appeal because of reduced calculation requirements and has less dependency on the a priori probability distributions.

The objective of processing a single point, for the purpose of bistable (bilevel), grey level or color displays, or even for coding for subsequent retrieval, can be summarized as M-ary detection. In other words, we want to assign that particular point to one of the M hypotheses representing a specific material. Again this technique leads to the well-known Bayes or Neyman-Person criterion. Alternatively, this M-hypotheses can be expressed in terms of choosing the maximum a posteriori probability. Without loss of generality, if a continuum of grey level is sought, then one desires an MAP (Maximum A Posteriori) estimate.

As mentioned in earlier sections, the specular and scatterer parameters vary drastically. Since these underlying parameters are unknowns and at any point different probability density functions can occur, it is difficult to implement the aforementioned techniques.

Then, it is desired to implement a robust algorithm with similar signal processing approaches.

Without loss of generality, this estimation or M-ary detection problem can be stated as assigning the received echo $s(\cdot)$ to $[0,1]$. If discrete levels are desired, such as bilevel displays, computer memory or color display, the resultant assignment is further processed with a quantizer.

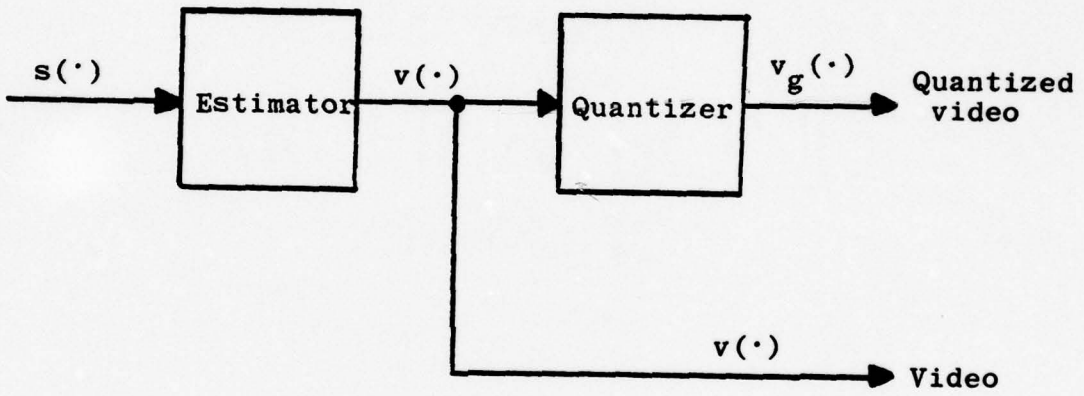

where:

$s(\cdot) \in R^+$ (positive real numbers),

$v(\cdot) \in [0,1]$, and

$v_q(\cdot) \in \{V_o, V_1, \ldots, V_Q\}$.

If video $v(\cdot)$ is used for grey level display, then without loss of generality, let 0 be dark and 1 be the brightest level. Let V_o be dark and V_Q be bright also. This is not the only way to assign the symbols, especially for color displays. It is beneficial to have an interactive system where an operator can dynamically change the color assignments to optimize the interpretation. An obvious assignment for color display is to let red represent blood. This grey level>color assignment problem is not essential to the dynamic range compression algorithm in question.

Now we can delineate the approach as an estimator which has the form:

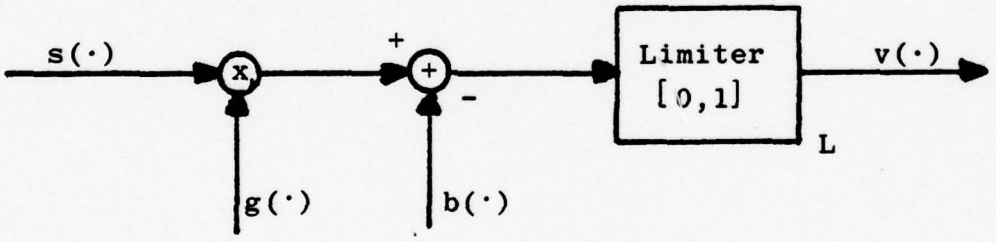

or

$$v(\cdot) = [g(\cdot)\, s(\cdot) - b(\cdot)]_L$$

where $[\ ]_L$ symbolizes the limiter operation.

Since $s(\cdot) \in R^+$, the magnitude of the received echo, the effect of the bias level $b(\cdot)$ is to assign $s(\cdot) \in [0, \frac{b(\cdot)}{g(\cdot)}]$ to the symbol 0. The effect of $g(\cdot)$ is to assign $s(\cdot) \in [\frac{b(\cdot)}{g(\cdot)}, \frac{b(\cdot)+1}{g(\cdot)}]$ to (0,1). For $s(\cdot) > \{\frac{b(\cdot)+1}{g(\cdot)}\}$, the symbol

1 is assigned. This corresponds to the dark and saturation levels of display systems.

To repeat, we want to assign the point value $s(\cdot)$ to a specific symbol to represent a certain type of biological material. This simple processing structure will accomplish this goal. What remains is to choose the bias parameter $b(\cdot)$ and the gain parameter $g(\cdot)$. These parameters, of course, will be related to the underlying probability distributions.

3.2.4 Bias Parameter

The bias parameter, $b(\cdot)$, is used to group low level echo returns in one common symbol. For grey level displays, this should be the dark level. For a color display, perhaps red is appropriate. In echocardiography, these low level returns are generally from a volume of blood cells. This fact might not be true for other medical ultrasonic applications such as obstetrical abdominal scans for expectant mothers, where the lowest returns will probably be from water. But nontheless these low levels represent returns from one particular material and are of no interest for medical diagnosis. In radar, these returns are generally called clutter, where one possible source might be returns from the surface of the ocean. Then, this bias level should be a function of a scatterer parameter similar to that from blood cells.

As mentioned in Section 2.3.1, the echo from a volume of blood has a Rayleigh distribution. Furthermore,

we saw that in Section 2.3.2, the scattering parameter varies spatially and temporarily due to attenuation, wave divergence, etc. Since these parameters are unknowns and we seek a robust algorithm, this bias parameter will be derived from the data itself. In echocardiography, failure to detect a structure (especially valves in a volume of blood) are "costlier" than false alarms. This is especially true for an image because the probability of false alarms over a small neighborhood is highly unlikely and thus if a false alarm occurs, it appears at an isolated point and the human interpeter can easily recognize its insignificance. This couples nicely with the proposed algorithm since this helps in eliminating some of the effects of acoustic energy attenuation.

The following is an examination of the characteristics of the bias parameters under different signal parameters. Let

and P_M = probability of missing a significant structure

P_F = probability of false alarm (or displaying blood volume).

The significant structure can either be a distinct specular component or a backscattering from tissue layers. Without loss of generality, the probability density function for either case (H_1) is

$$p_{s/H_1}(s/H_1) = \frac{s}{\sigma_1^2} \exp\left[-\frac{(s^2+\eta_1^2)}{2\sigma_1^2}\right] I_o\left(\frac{s\eta_1}{\sigma_1^2}\right),$$

and for backscattering from the blood volume (H_1),

$$p_{s/H_o}(s/H_o) = \frac{s}{\sigma_o^2} \exp\left[-\frac{s^2}{2\sigma_o^2}\right] \quad U(s) \quad .$$

Since the bias parameter, $b(\cdot)=b$, operates on each single point, s, the probabilities P_M and P_F can be expressed as follows:

$$P_M = \int_o^b p_{s/H_1}(s/H_1)\,ds$$

and

$$P_F = \int_b^\infty p_{s/H_o}(s/H_o)\,ds \quad .$$

Solving for P_F,

$$P_F = \int_b^\infty \frac{s}{\sigma_o^2} e^{-\frac{s^2}{2\sigma_o^2}} \quad ds$$

$$= 1 - e^{-\frac{s^2}{2\sigma_o^2}}\Big|_b^\infty$$

$$= e^{-\frac{b^2}{2\sigma_o^2}}$$

One can fix the probability of false alarm P_F by choosing the threshold b proportional to σ_o. In this algorithm, σ_o will be estimated. Let

$$b = K\sigma_o ,$$

then

$$P_F = e^{-\frac{k^2}{2}} .$$

Since an estimate of σ_o will be used in the algorithm, it is important to examine the sensitivity of P_F.

$$\frac{dP_F}{dk} = -Ke^{-\frac{k^2}{2}} .$$

Figures 3.5 and 3.6 show P_F vs. k and $\frac{dP_F}{dk}$ vs. k, respectively. As shown on the graphs, if K>1, one can choose K to give relatively good performance. But this performance is in terms of false alarms only, it is important to know k affects missed targets. Since the specular or scatterer components from tissues and interfaces vary widely, P_M cannot be specified explicitly. We will examine how P_M changes as the parameter changes. Recall that for a significant target, we have:

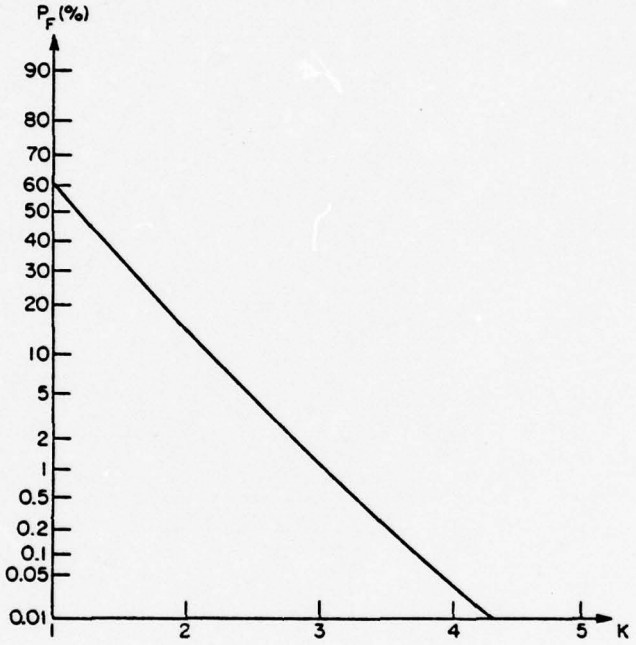

Figure 3.5 False Alarm Rate vs. Bias Constant

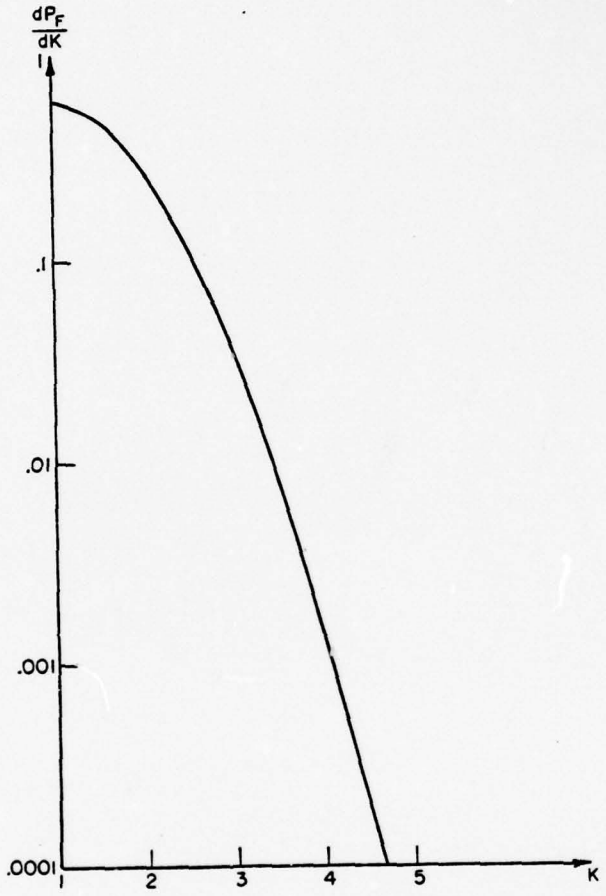

Figure 3.6 False Alarm Rate of Change

$$p_{s/H_1}(s/H_1) = \frac{s}{\sigma_1^2} e^{-\frac{(s^2+\eta_1^2)}{2\sigma_1^2}} I_o(\frac{s\eta}{\sigma_1^2}) U(s).$$

Since this is a point-by-point detection problem and the threshold value is b, the probability of a missed target, is:

$$P_M = \int_o^b p_{s/H_1}(s/H_1)ds$$

$$= 1 - \int_b^\infty p_{s/H_1}(s/H_1)ds$$

$$= 1 - \int_b^\infty \frac{s}{\sigma_1} e^{-\frac{(s^2+\eta_1^2)}{2\sigma_1^2}} I_o(\frac{s\eta_1}{\sigma_1^2}) ds .$$

The integral cannot be evaluated analytically. The normalized function was tabulated by Marcum in terms of a function commonly called Marcum's Q function:

$$Q(\alpha,\beta) \triangleq \int_\beta^\infty Z \exp(-\frac{z^2+\alpha^2}{2}) I_o(\alpha z)dz .$$

Therefore, P_M can be expressed as

$$P_M = 1 - Q(\frac{\eta_1}{\sigma_1^2}, b) .$$

If

$$b = K\sigma_o \ ,$$

then

$$P_M = 1 - Q(\frac{1}{\sigma_1^2} \ , \ K\sigma_o) \ ,$$

which can be expressed as

$$P_M = 1 - Q(\frac{1}{\sigma_1^2} \ , \ \sigma_o\sqrt{-2 \ \ell n \ P_F} \ ) \ .$$

Let

$$\gamma = \frac{\sigma_1^2}{\sigma_o^2} \quad \text{and} \quad \xi = \frac{1}{\sigma_1^2} \ .$$

Figure 3.7 shows P_M for various normalized values of γ and ξ.

Within the scanning volume, there is always a region of blood. Therefore, one can estimate σ_o at that particular region. Recall that due to attenuation, beam divergence and other effects, σ_o will not be constant throughout the scanning volume. One must compensate for this effect if $b=K\sigma_o$ is to be used throughout the whole volume. Since the attenuation effects cannot be estimated, it is logical to compensate for the beam divergence. This

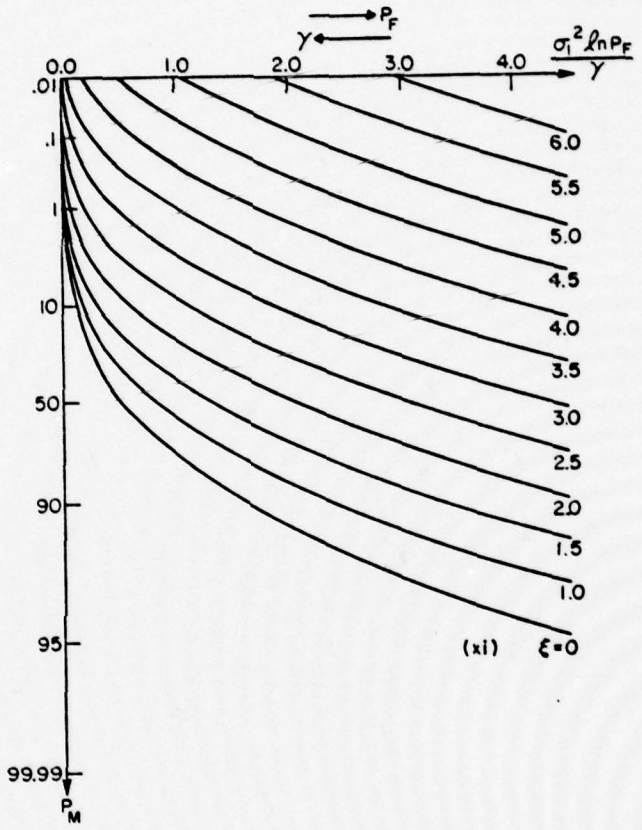

Figure 3.7 Probability of Missed Target

has an effect of using a lowered threshold; but this is desirable because of reasons mentioned earlier.

Estimation of σ_o depends on implementation techniques. For example, real-time processing will force an analog approach rather than the digital approach used for nonreal-time processing. Also, the optimization of hardware will dictate the estimation technique. Since echo signals from this volume of blood has a Rayleigh distribution, the estimate can be the sample mean or from second order statistics, which follows from,

$$E\{s/H_o\} = \sqrt{\frac{\pi}{2}}\ \sigma_o$$

and

$$E\{s^2/H_o\} = 2\sigma_o^2 \quad .$$

For calculating $g(\cdot)$, we need the higher order statistics, therefore, from the hardware standpoint, it is better to estimate σ_o with a mean square value. Since the blood scattering occur over a volume (spatial and/or temporal) the estimate can best be formed over the whole volume depending on the dimensionality of the scan. The large number of samples needed to make the estimates tends to decrease the error (proportional to $\frac{1}{\sqrt{N}}$). For computer approach, a running estimate over the entire volume and a comparison to stored values of the minimum will be used. The "box car" estimate, $\hat{\sigma}_o$, can be expressed as

$$\hat{\sigma}_o = \left[\frac{1}{2} \frac{1}{N_I N_J N_K N_L} \sum_{w=i-\frac{N_I}{2}}^{i+\frac{N_I}{2}} \sum_{x=j-\frac{N_I}{2}}^{j+\frac{N_J}{2}} \sum_{y=k-\frac{N_J}{2}}^{k+\frac{N_K}{2}} \sum_{z=l-\frac{N_L}{2}}^{l+\frac{N_L}{2}} \cdot s^2(w,x,y,z) \right]^{1/2},$$

where N_I, N_J, N_K, N_L denote the number of samples over the respective dimensions, i, j, k, l. Obviously the total number of samples is equal to $N_I x N_J x N_K x N_L$. For practical purposes, and in the case of snapshots, the ℓ-axis, or time, is not used, and $N_I = N_J = N_K$ since no obvious advantage can result if one particular axis is favored. A trade-off in using a larger volume is between computation time and the geometric dimensions of the heart chamber. A good reliable estimate can be calculated. For real time application applications, averaging over range can be accomplished by utilizing an analog filter; this will enable a lower sampling rate for this channel for the purpose of computing b and g. Figure 3.8 illustrates such a scheme. Here, the computer or digital filter is used to store adjacent lines and to compute $\hat{\sigma}_o$ over the other dimensions. Now, the minimum value of σ_o can be found for an estimate of σ_o for blood. This value is valid at that particular volume only, and as shown in Section 2.3.2, we see that σ_o is a spatial and temporal function due to the beam divergence, attenuation, etc. An example of the bias

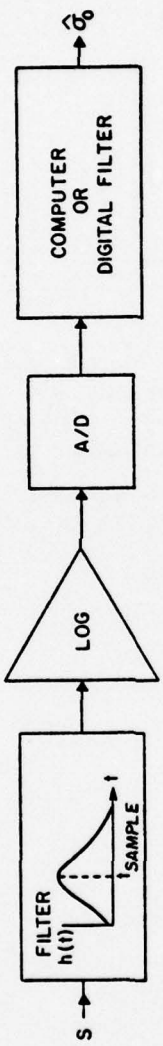

Figure 3.8 Analog Filter Aided Estimation

value adjusted for the beam divergence is illustrated in Figure 3.9.

3.2.5 Gain Parameter

The effect of the bias parameter, as described previously, is to assign all low level returns from blood to one symbol. On the other hand, the gain parameter has two major effects. Analogous to the bias parameter, the gain parameter tends to assign all "high" returns from specular reflectors to a common symbol. Also, depending on the instantaneous gain value, the gain parameter can be used to assign a specific code. In other words, besides the saturation effects, the gain parameter couples with the quantization scheme.

The major objective of the gain parameter is to maximize the information content of the dynamic range-compressed image. This is similar to a source coding problem. Due to the subjective nature of a fidelity criterion for images, a classical source coding criterion approach is not taken here. Another reason for not using the source coding approach is the highly nonstationary nature of the echo returns. First, we will decide which approach should be taken if *a priori* statistical information is available for the volume scanned.

As described in the previous section, the statistical model of the ultrasonically scanned volume consists of Rayleigh distributions due to scatterers and Rician distributions due to specular reflectors. Then, setting the

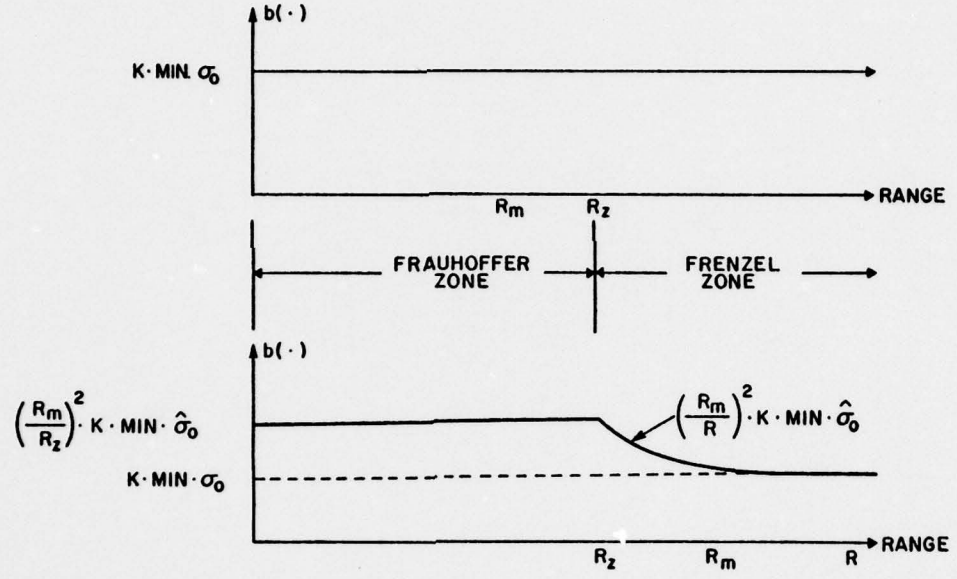

Figure 3.9 Example of Beam Divergence Compensation

gain parameter involves normalizing the distribution so that a satisfactory maximum value will be equal to the saturation level of the encoder, for example, an analog-to-digital converter. Then, if we consider that α percent of high level echo returns can be grouped under one symbol, the saturation level, one easily can evaluate the gain parameter at each point. We consider only a Rician distribution only for the following discussion (Rayleigh distribution is just a special case). The probability of the echo signal being higher than a value s_m is

$$P_{s>s_M} = \int_{s_M}^{\infty} p_s(s)\,ds$$
$$= Q\left(\frac{\eta_o}{\sigma_o^2},\ s_M\right) \quad ,$$

where Q is the Marcum's Q function. Clearly,

$$s_M = f(\alpha,\ \eta_o,\ \sigma_o^2)\ ,$$

where η_o and σ_o^2 are from the normalized distribution function. Now, for an arbitrary point in the scanning volume with η and σ^2, the saturation level, s_M, is:

$$s_m = f(\alpha,\ \eta,\ \sigma^2)\ .$$

The gain parameter can be found easily as

$$g = s_M / s_m \ .$$

Using this gain parameter, the echo returns from significant reflectors, either specular or scatter components, tend to form a stationary process. The exception occurs at regions of blood scatterers. With the application of the bias parameter, the blood regions will have zero intensity. Therefore, the total effect is that the significant cardiac structures are evenly illuminated by the acoustic wave.

Besides the unavailability of the a priori statistics other problems are present in implementing this gain parameter. For abrupt changes such as from endocardium to blood volume, the gain tends to switch from a low value to a high setting. In practical hardware implementation, this abrupt change will tend to generate an artifact, a false return. A more gradual change in gain can combat this problem. Low pass filtering and using continuous gain profiles are ways to implement this gradual change in gain profile. Besides the need for a priori statistics, to implement this scheme, one must also know where the blood volume occurs. This does not offer a practical implementation method which can be applied to the whole scanning volume. But all is not lost since the information from the bias parameter offers a clue to the location of blood volume; then, the gain parameter can be set with the bias parameter as one of the dependent variables. These points are taken into account in the algorithm proposed.

The gain parameter can be calculated with the following steps:

1. Use the "box car" $\hat{\sigma}_n$ estimate from the bias parameter calculation. This saves computational requirements.
2. Based on the ratio $\hat{\sigma}_o/\hat{\sigma}_{o,min.}$, where $\hat{\sigma}_{o,min}$ denotes min.$(\hat{\sigma}_o)$ over the scanning volume, form a multiplier k from a nonlinear function, f_{NL}.
3. Form the multiplier $g = s_{max}/k\hat{\sigma}_o$, where s_{max} is the saturation level.

The nonlinear function, f_{NL} is such that

$$f_{NL}(\hat{\sigma}_o/\hat{\sigma}_{o,min} = 1) = k_1$$

and

$$f_{NL}(\hat{\sigma}_o/\hat{\sigma}_{o,min} \rightarrow \infty) = k_\infty ,$$

with $k_o > k_\infty$. For example, a piecewise linear function illustrated in Figure 3.10 is effective.

k_∞ is chosen such that the saturation effect is satisfactory. An estimate of what k_∞ should be will be covered later in this subsection. If k_o is chosen greater than k_∞, the effect is such that the resultant brightness level of the display is reduced for certain regions where

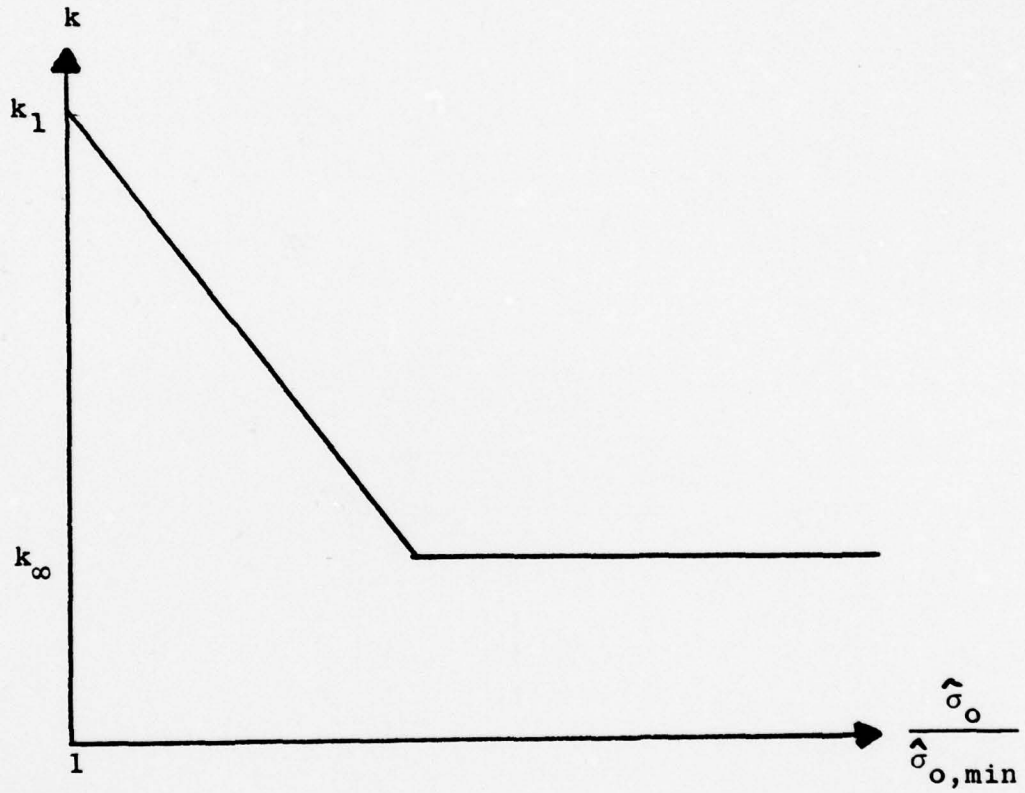

Figure 3.10 Piecewise Linear Function

$\hat{\sigma}_o \approx \hat{\sigma}_{o,min}$. The regions where this will occur are within the blood volume itself since $\hat{\sigma}_o \approx \hat{\sigma}_{o,min}$. In that case, there are two reasons why $k_o < k_\infty$. First, $\hat{\sigma}_o$ will be on the low side at the isolated structure due to "box car" averaging. The second reason is that this isolated structure occurs in a volume of darkness, that is, blood. In order to reduce artifacts, the brightness level should be subdued. Of course, k_o should be operator interactive. This does not change the adaptive nature of the algorithm; it merely gives the operator a choice for visualizing isolated structures better at the possible expense of increased artifacts.

Another way to interpret this algorithm is to consider σ_o as a root mean square power estimate. Normalization using this power estimate is a common practice. The nonlinearity is introduced to reduce brightness somewhat in the blood region.

The question remains on how this algorithm works. A statistical analysis of how this receiver behaves is presented here. A simplification is used to illustrate the receiver behavior that is, only a scattering component is considered. The analysis applies since, over a local volume, the actual distribution function is a conglomerate of different Rayleigh and Rician distributions, and thus, the "sharper" distribution is "broadened", as discussed previously.

Let us consider a small volume where the distribution is Rayleigh, or the returns are mainly from a heterogeneous

and/or layered region. Also, σ_o for this region is much greater than $\sigma_{o,min}$ for the scanning volume. Then, the gain parameter:

$$g = \frac{s_{max}}{k_\infty \hat{\sigma}_o} \quad .$$

Then, the echo returns in this region that exceed the saturation level are such that

$$gs > s_{max}$$

or

$$s \frac{s_{max}}{k_\infty \hat{\sigma}_o} > s_{max} \ ,$$

or

$$s > k_\infty \hat{\sigma}_o \quad .$$

Since

$$p_s(s) = \frac{s}{\sigma_o^2} e^{-\frac{s^2}{2\sigma_o^2}} \ ,$$

the probability or portion of the echo in the saturation level is:

AD-A080 982 PENNSYLVANIA STATE UNIV UNIVERSITY PARK APPLIED RESE--ETC F/G 6/5
ADAPTIVE DYNAMIC RANGE COMPRESSION ALGORITHM FOR ECHOCARDIOGRAP--ETC(U)
MAY 79 E H LAM N00014-79-C-6043
UNCLASSIFIED ARL/PSU/TM-79-138 NL

2 OF 3
AD-
A080982

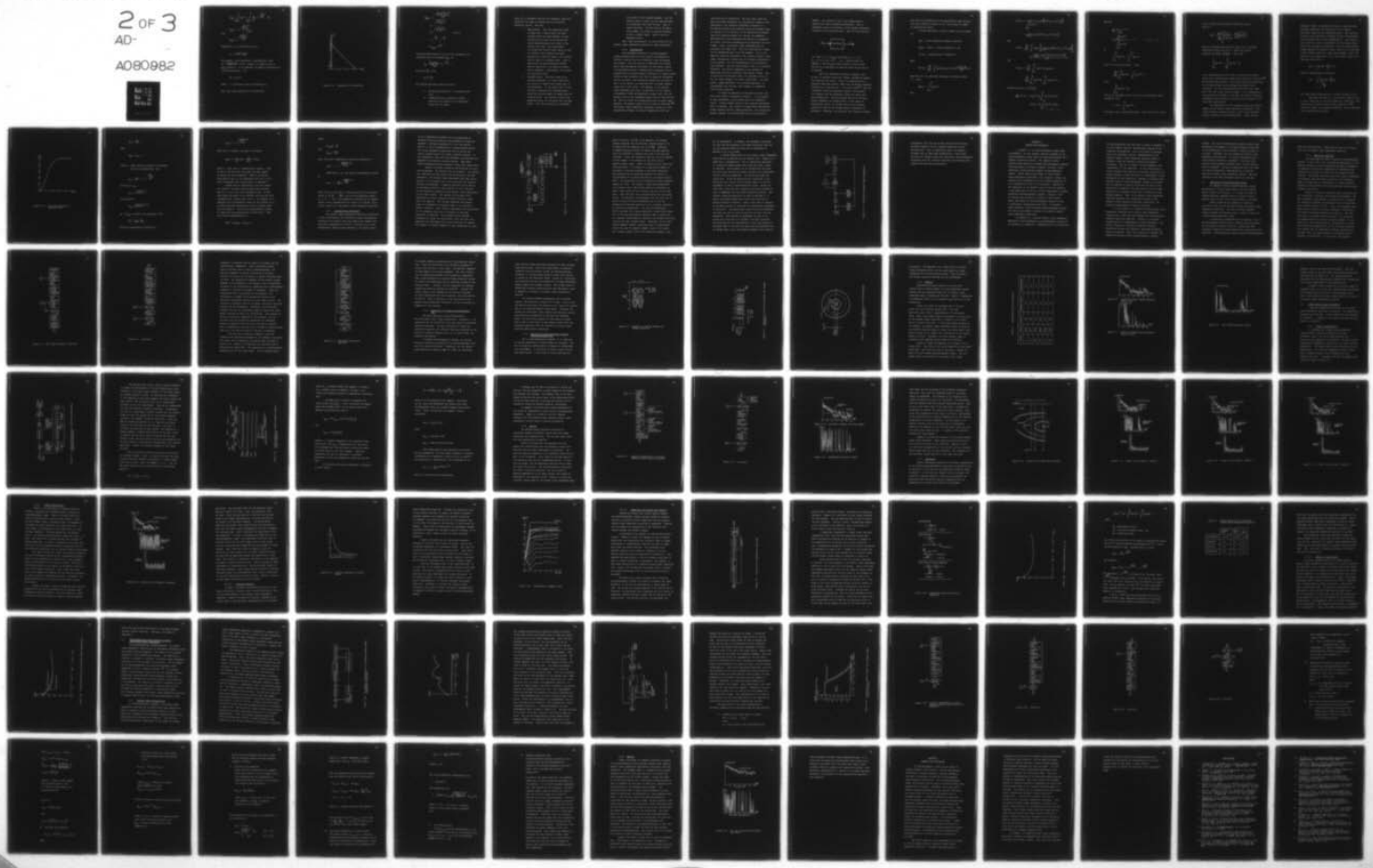

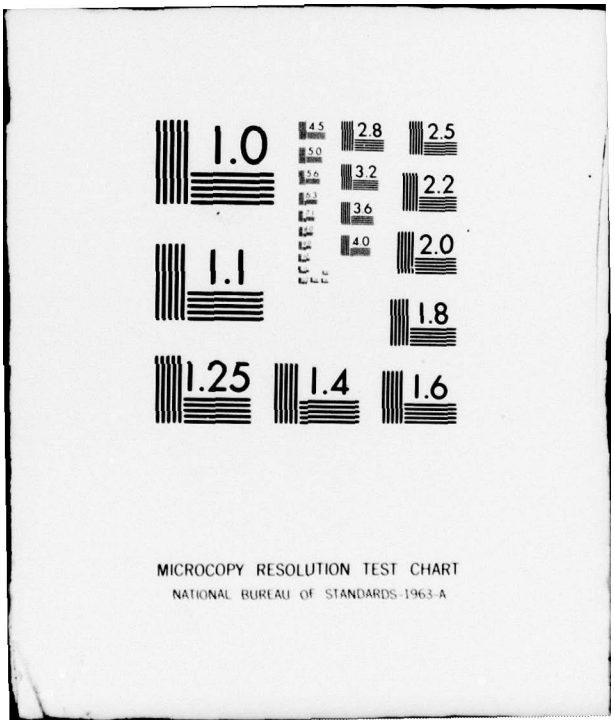
1.0
1.1
1.25
1.4
1.6
1.8
2.0
2.2
2.5
2.8
3.2
3.6
4.0
4.5
5.0
5.6
MICROCOPY RESOLUTION TEST CHART
NATIONAL BUREAU OF STANDARDS-1963-A

$$P_{SAT} = \int_{k_\infty \hat{\sigma}_o}^{\infty} p_s(s) = \int_{k_\infty \hat{\sigma}_o}^{\infty} \frac{s}{\sigma_o^2} e^{-\frac{s^2}{2\sigma_o^2}} ds,$$

$$P_{SAT} = - e^{-\frac{s^2}{2\sigma_o^2}} \Bigg|_{k_\infty \hat{\sigma}_o}^{\infty}$$

and

$$P_{SAT} = e^{-\frac{(k_\infty \hat{\sigma}_o)^2}{2\sigma_o^2}} .$$

Suppose $\hat{\sigma}_o = \sigma_o$, and solving for k_∞:

$$k_\infty = \sqrt{-2 \ln \rho_{SAT}} .$$

For example, if 5% saturation is satisfactory, then $k_\infty = \sqrt{-2 \ln(.05)} = 2.45$. Figure 3.11 shows a plot of P_{SAT} versus k_∞. It is important to examine the effects of σ_o estimation error. Let

$$\hat{\sigma}_o = \sigma_o(1+\gamma),$$

where γ = fractional error is estimating σ_o.

Then, the actual probability of saturation,

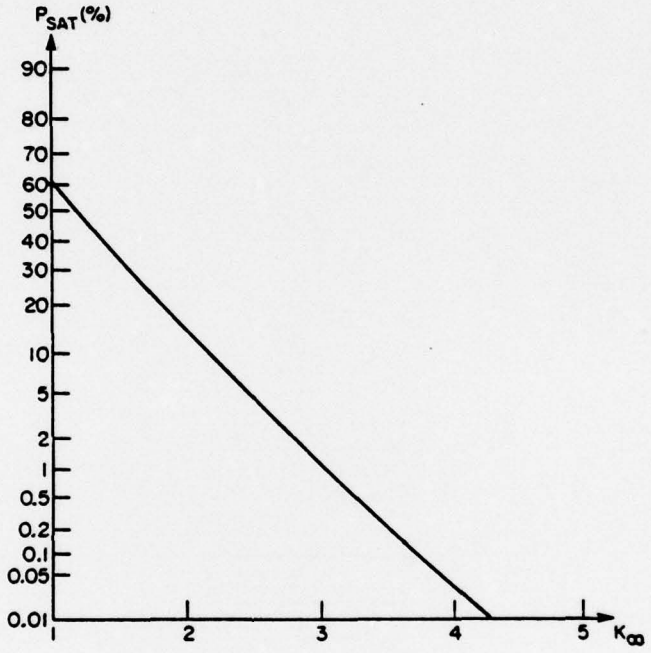

Figure 3.11 Probability of Saturation

$$\hat{P}_{SAT} = e^{-\frac{(k_\infty \sigma_o)^2 (1+\gamma)^2}{2\sigma_o^2}}$$

$$= e^{-\frac{k_\infty^2 (1+\gamma)^2}{2}}$$

$$= e^{-\frac{k_\infty^2 (1+2\gamma)}{2}}$$

$$\simeq e^{-\frac{k^2}{2}} \quad \text{for } \gamma<1$$

$$= e^{-\frac{k^2}{2}} e^{-k_\infty^2 \gamma}$$

$$\simeq P_{SAT}\, e^{-k_\infty^2 \gamma} \quad .$$

The percentage deviation of the actual probability of saturation from the designed P_{SAT} is:

$$\Delta_p = \frac{\hat{P}_{SAT} - P_{SAT}}{P_{SAT}} \simeq e^{-k_\infty^2 \gamma} - 1 \quad .$$

For small $k_\infty^2 \gamma$, then,

$$\Delta_p \simeq -k_\infty^2 \gamma \quad .$$

Two implications come from this result;

1) Δ_p deviates greatly as γ increases since $k_\infty > 1$,
2) Underestimating σ_o implies a greater portion of the signal in the saturation level and vice versa.

Since $\hat{\sigma}_o$ is estimated from box car averaging, there are basically two types of regions which will give $\hat{\sigma}_o$ estimation errors. They are:

1. Edge effects. When the averaging volume is taken over a region where the endocardium meets the blood chamber, an overestimation will occur on the blood side and an underestimation will occur on the cardiac wall side. The overestimate will cause the initial blood region to take on a darker value, whereas the underestimate will cause the edge of the cardiac wall to take on a brighter value. This is essentially an edge enhancement effect. This is equivalent to an additive differential component. Fortunately, this occurs as a positive effect.
2. Isolated points. This can either be an isolated reflector in a blood volume such as a valve or a small fluid volume such as the epicardian. In the former case, we see that $\hat{\sigma}_o$ is definitely an underestimation since the box care region is larger than the isolated point. As a matter of fact, this estimation error will be worse than the edge effect. With the nonlinearity introduced,

this effect can be reduced somewhat. But the overall effect is that, for the isolated point, the brightness level will be high. This is highly desirable. For the case of the small fluid region, the effect is exactly opposite: we have a darker region. Again, this is a desirable result.

Then, from this analysis, an extra benefit of the dynamic range compression algorithm is image enhancement.

3.2.6 Quantization

This discussion pertains to echocardiographic imaging systems where the echo returns are sampled and stored by digital means for subsequent image processing and viewing. This can further be separated into systems where image processing techniques are used before coding into brightness levels or pseudo-color assignments and to systems where the digital memory performs as an image storage medium or scan converter only with no numerical processing of the echo data. The difference between the two cases is that, in the former, the quantizer has a narrower dynamic range than in the latter. For example, if the dynamic range compressed echo data, as described in this chapter, is sampled at 2 MHz and quantized to eight bits, then the dynamic range of the compressed signal must be less than 48 dB. This can easily be accomplished since for small range segments, the dynamic range is of the order of 30-50 dB.[69] The dynamic range compression algorithm, acting as a local normalization scheme, can easily compress the 50-70 dB

variation due to attenuation. For this case, where the data is further processed, the quantization scheme is well described in the literature mentioned in Section 3.1. For practical grey scale displays, where the dynamic range is limited to 15 to 20 dB's, or for pseudo-color displays where the colors available are limited, the immediate quantization of the compressed data should be "optimized." Of course, the actual processing can be separated into two stages. First, the dynamic range compressed data is quantized into eight bits. Then the "quantization" scheme can be implemented again with the computer. But if the eight-bit data are available in the computer already, other image "enhancement" schemes such as histogram equalization can be applied. But the disadvantage is the processing time required. For real-time systems, this is not feasible. Therefore, this section addresses to the problem of quantizing directly to display level dynamic ranges. Bear in mind that the resultant code, the quantized value, is not the video voltage, but rather a grey level. In other words, a gamma amplifier, or an antilog amplifier, is incorporated into the grey level display to compensate human visual responses.

In order to optimize the quantization scheme, one must first choose a reasonable criterion. If the purpose is data processing, a mean square cost is a reasonable choice. Another common choice is that constant percentage error is desired. This leads to a logarithmic quantization scheme commonly used for image processing. For echocardiographic imaging, this scheme might not be statistically

optimal. As a matter of fact, such images usually improve with local histogram equalization. Then, a reasonable choice of criterion is the average information contained in the quantized data. Then for the quantizer,

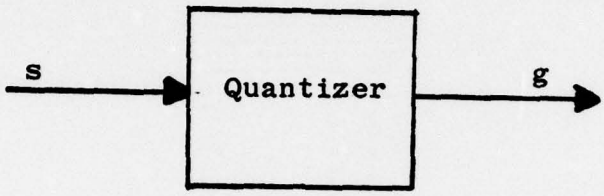

let input s, $s \in (0, s_{MAX})$ and output q, $q = i$ if $d_{i-1} \leq s < d_i$ for $i=0,1,\ldots,N-1$. Usually $N=2^B$; for example, a 16-level grey scale display, N=16 and B=4. The set of values $\{d_i\}$ are decision levels which have to be decided.

With the information theoretic approach, then we want to maximize the mutual average information between the input and the output. This is an application of a discrete memoryless channel (DMC) with the source alphabets extended to an infinite set. It is well known[13] that for a symmetric discrete memoryless channel, full-channel, full capacity can be obtained by using the inputs with equal probability. By partitioning the set of infinite source alphabets into subsets equal to the number of quantization levels, it follows that the full-channel capacity is used or the average mutual information is maximized. Therefore, the decision level should be chosen

such that the probability of the quantization input falling into that interval is equal to 1/N, the inverse of number of quantization levels.

A direct derivation of such a result are as follows: Let

$p_S(s)$ = input probability density function,

$P_Q(q_n) = P(q=n)$ = output probability, and

$I(s,q_n)$ = average mutual information.

Then,

$$I(s,q_n) = \sum_{n=1}^{N} \int_{-\infty}^{\infty} P_Q(q_n) p_{S\ Q}(s\ q_n) \log \frac{p_{S\ Q}(s\ q_k)}{p(s)}\ ds.$$

Note that, if s is quantized according to decision levels dn , then:

$$P_Q(q_n) = \int_{d_{n-1}}^{d_n} p_S(t)dt$$

and

$$p(s/q_n) = \frac{1}{\int_{d_{n-1}}^{d_n} p_s(t)dt}\, p_S(s)\left\{U(s-d_{n-1})-U(s-d_n)\right\}$$

$$= \frac{1}{P_Q(q_n)}\, p_S(s)\left\{U(s-d_{n-1})-U(s-d_n)\right\}.$$

Now,

$$I(s/q_n) = \sum_{n=1}^{N} \int_{-\infty}^{\infty} P_Q(q_n)\left[\frac{1}{P_Q(q_n)} p_S(s)\left\{U(s-d_{n-1})-U(s-d_n)\right\}\right] \cdot \log \frac{\frac{1}{P_Q(q_n)}\, p_S(s)\left\{U(s-d_{n-1})-U(s-d_n)\right\}}{p_S(s)}\, ds$$

and

$$I(s,q_n) = -\sum_{n=1}^{N} \int_{d_{n-1}}^{d_n} p_S(s)\log P_Q(q_n)\, ds$$

$$= \sum_{n=1}^{N} \int_{d_{n-1}}^{d_n} p_S(s)\log \int_{d_{n-1}}^{d_n} p_S(t)dt\, ds\ .$$

Maximizing $I(s,q_n)$ over $\{d_n\}$,

$$\frac{\partial}{\partial d_n} I(s,q_n) = -p_S(d_n)\log \int_{d_{n-1}}^{d_n} p_S(t)dt + p_S(d_i) + p_S(d_n)\ \log \int_{d_{n-1}}^{d_n} p_S(t)dt - p_S(d_i)\ ,$$

$$i = 1,2,\ldots,N\ .$$

Setting

$$\frac{\partial}{\partial d_n} I(s,q_n) = 0 \ ,$$

$$\log \frac{\int_{d_n}^{d_{n+1}} p_S(t)dt}{\int_{d_{n-1}}^{d_n} p_S(t)dt} = 0 \qquad i = 1,2,\ldots,N \ .$$

Or

$$\int_{d_{n-1}}^{d_n} p_S(t)dt = \int_{d_n}^{d_{n+1}} p_S(t)dt \ ,$$

which is the desired result. Since

$$\sum_{n=1}^{N} \int_{d_{n-1}}^{d_N} p_S(t)dt = \int_{-\infty}^{\infty} p_S(t)dt = 1 \ ,$$

then,

$$\int_{d_{n-1}}^{d_n} p_S(t)dt = \frac{1}{N} \ .$$

One way to implement this is to use an instantaneous transformation, T(s):

$$w = T(s) = \int_{-\infty}^{s} p_S(t)dt \ ,$$

and feed w into a uniform quantizer. Note that w$\in$[0,1] since

it is a cumulative distribution function, and for $w \epsilon [0,1)]$:

$$p_w(\omega) = \frac{p_S(s=T^{-1}(\omega))}{\left|\frac{d}{ds}\int_{-\infty}^{T^{-1}(\omega)} p_S(t)dt\right|} = \frac{p_S(s=T^{-1}(\omega))}{p_S(s=T^{-1}(\omega))} \quad .$$

Then, the transformation maps the input into a uniformly distributed output over $[0,1]$. Since the uniform quantizer has $\{d_n\} = \{0, \frac{1}{N}, \frac{2}{N}, \ldots, 1\}$, then:

$$\int_{d_{n-1}}^{d_n} p_S(t)dt = \int_{\frac{n-1}{N}}^{\frac{n}{N}} p_w(t)dt = \frac{1}{N} \quad .$$

It is interesting that this result is the same as quantization with a minimum mean square error distortion criterion.[46] The results were derived in this case avoiding the definition of an output symbol and the average mean square error criterion. For the transformation of raw data into image data, this has a more intuitive appeal. As a consequence of this quantization scheme, if the data are used for numerical processing, the quantization scheme is still optimal in the least mean square sense.

For application of this maximum entropy quantization scheme to this dynamic range compression algorithm, a nonlinear amplifier should be used in front of the analog-to-digital converter (a uniform quantizer). Since the gain

parameter "tends" to normalize the data, a time-invariant nonlinear amplifier will suffice due to the pseudo-stationary nature of the compressed signal. The nonlinear function can be derived by assuming the input distribution to be Rayleigh (over a small neighborhood). One reason is that there is a lack of information for the Rician distribution due to specular reflectors. With the normalization scheme applied, the specular return tends to be at the high levels (bright levels for a grey scale display); thus, the quality of the image itself is not sacrificed. Then, for a Rayleigh distribution:

$$p_S(s) = \frac{s}{\sigma_o^2} \exp\left[-\frac{s^2}{\sigma_o^2}\right] U(s) \quad .$$

Then the transformation desired is:

$$T(s) = \int_o^s \frac{t}{\sigma_o^2} \exp\left[-\frac{s^2}{\sigma_o^2}\right] dt$$

$$= 1 - e^{-\frac{s^2}{\sigma_o^2}} \quad .$$

The input-output characteristic is shown in Figure 3.12.

Now since the input to a "real world" amplifier has a limit, which was in the last subsection called S_{max}, this should be set slightly above the d_{N-1} decision level. Since the output is uniformly distributed, and the quantizer has uniform decision levels:

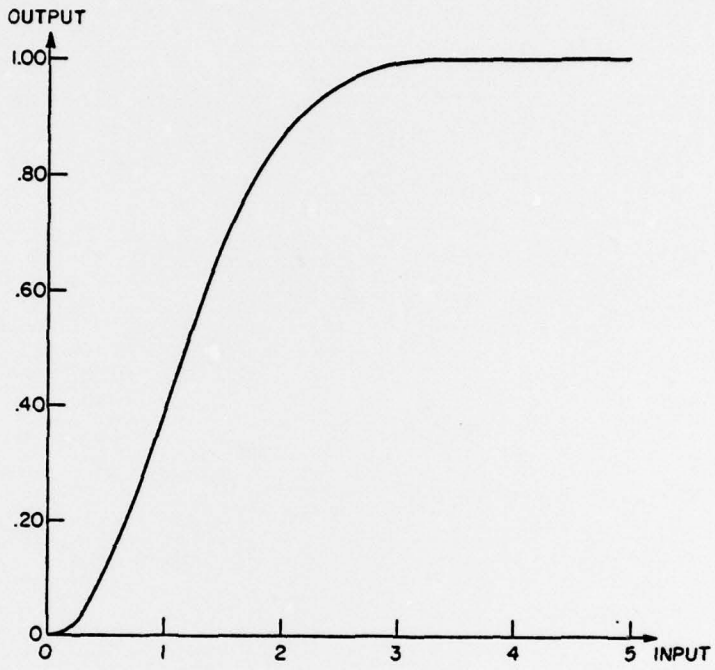

Figure 3.12 Nonlinear Amplifier I/O Characteristics

$$d_{N-1} = \frac{N-1}{N} \quad .$$

Then

$$S_{max} = t_{N-1} + \Delta \ ,$$

where Δ = small quantity choose by the designer and has no significance, and:

$$d_{N-1} = \frac{N-1}{N} = 1 - e^{-\frac{t_{N-1}^2}{2\sigma_o^2}} \quad .$$

Solving for t_{N-1},

$$t_{N-1} = \sqrt{2\sigma_o^2 \, \ell n \ N} \ ,$$

and therefore,

$$S_{max} = \sqrt{2\sigma_o^2 \, \ell n \ N + \Delta} \quad .$$

Or if S_{max} is fixed by the equipment, then:

$$2\sigma_o^2 = \frac{1}{\ell n \, N} \ S_{max}^2 \ .$$

Then, the transformation required is:

$$T_1(s) = 1 - e^{-\left(\frac{n\,N}{s^2_{max}}\right)s^2} \quad .$$

Note that, in reality, the $p_S(s)$ is actually

$$p_S(s) = K \frac{s}{\sigma_o^2} \exp\left[-\frac{s^2}{2\sigma_o^2}\right] U(s-b) \quad ,$$

where b = bias, and K = normalization constant. This is due to the fact that the signal has been biased to remove the blood component. Since b is usually much smaller than σ_o, the assumption that b=0 is of no great consequence and is much easier to implement.

Another note of importance is that one symbol, say symbol 0, has been used for blood level already. That is, if s=0, then this represents blood. If $s \neq 0$, that means the signal is of interest, and this should be represented by a symbol other than 0. For example, if a quantizer has N quantization levels on the interval [0,1], we should consider quantizing s into N-1 symbols other than the symbol 0. This can be accomplished by adding an offset and by multiplying by a scale factor. Then, this second transformation is:

$$T_2(s) = K_{offset} + K_{mult}\, s,$$

where

$$K_{offset} = \frac{1}{N}$$

and

$$K_{mult} = \frac{N-1}{N} .$$

Also, the first transformation should be modified to:

$$T_1(s) = 1 - e^{-\frac{\ell n(N-1)}{s^2_{max}} s^2} .$$

Combining T_1, T_2, the overall transformation should be:

$$T(s) = 1 - \frac{N-1}{N} e^{-\frac{\ell nN-1}{s^2_{max}} s^2} .$$

Then, if T(s) is fed into a uniform quantizer with decision levels $(0, \frac{1}{N}, \frac{2}{N}, \ldots, \frac{N-1}{N})$, and with corresponding symbols (0, 1, 2,..., N-1), the probability distribution of symbols around a local neighborhood will tend to be uniform, which is the intention of the dynamic range compression algorithm.

3.2.7 Implementation Techniques

The dynamic range compression algorithm is basically a local normalization and information content optimization technique with inherent real-time application capabilities. The actual implementation of such a technique to an echocardiographic imaging system depends on the system itself.

It is a feedforward processor with its advantages of possible infinite system gain and avoidance of stability problems. Although conceptually it is a two-channel device, it can be implemented as a single-channel device with a gain parameter acquisition scan to derive the control signals rather than using a separate channel. In this subsection, some real time processor architectures are suggested for different scanning systems. Some basic timing considerations are examined to show their feasibility.

Figure 3.13 shows a possible configuration for real-time processing. The receiver has two channels: one channel for video data and one channel for deriving gain and bias parameters. The dynamic range-compressed video data can go directly to the display unit or the quantizer for computer storage or processing. A separate detector can be used in the processor channel so that fidelity of the video data can be improved by detection after dynamic range compression on the video channel. The log-amp and low-pass filter combination is used to derive the power statistic within scan line segments. The low-amp compresses the dynamic range to accommodate the dynamic range to the analog-to-digital converter. Here, optimal compression and quantization is not necessary since only an estimate of the power statistics is required. The low-pass filter provides averaging over range (or equivalently time) and thus, the sampling rate requirement for the A/D converter is reduced. For example, if sixteen segments of gain parameters are used,

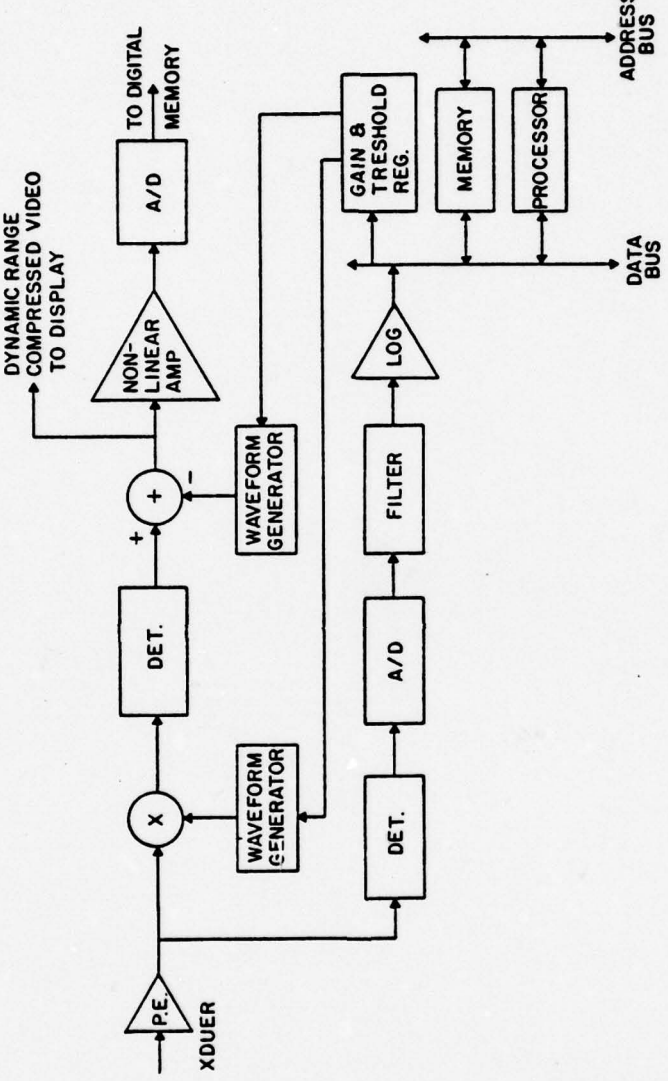

Figure 3.13 Two-Channel Real-Time Dynamic Range Compression

which clinically is shown to be adequate, the sixteen samples required over the 200 nSec. maximum range of 15 cm means that the sampling rate is 80 KHz. Therefore, a separate channel without the higher cost MHz sampling rate A/D converter is feasible with just a low cost A/D converter. Since the conversion time for the A/D converter is much longer, it is possible to use more bits to improve dynamic range. After the power statistic data has been digitized, it is stored in an appropriate memory or registers to provide averaging in the other dimensions. The processor can be dedicated hardware for speed or a microprocessor for economy depending on the speed requirements. The processing can be accomplished between segments samples or lines. For example, M mode echocardiographic units usually have a PRF (pulse repetition frequency) of about 1 KHz, since the data interval per line is only 200 nSec., about 800 μSec. are available before the next pulse occurs. An economical microprocessor can use this time to derive the gain and bias parameters and to load the registers for waveform generation with no severe constraint on software considerations. But for multidimensional sector scanners, the timing requirement is much more severe. Due to the high data density required, PRF is usually set at a maximum, which means no available time between receiving time and the next transmit pulse. Therefore, for the same sixteen-segment example, processing must be accomplished within the time for segment samples, which is 12.5 μSec. For a simple digital filter with dedicated hardware, this

can be synthesized. In summary, the processor calculates the gain and bias parameter with power statistics from the i_{th} and previous frames and this set of parameters is applied to the $i+1_{th}$ frame.

A similar application of this dynamic range compression algorithm can be applied with one channel only. Figure 3.14 shows such a configuration. This is especially applicable to a snap shot camera system since only one frame of data is required. The procedure can be divided into two scans. The first scan acquires the power statistics for calculating the gain and bias parameters. The second scan does the actual scan. Since the physicians are interested in one particular time instant of the cardiac phase, an electrocardiogram is used to synchronize both scans. During the first scan, zero bias and a norminal multiplier waveform is used to compensate for the gross attenuation effects. The optional logarithm amplifier can then be switched in to ensure the dynamic range falls within the range of the analog-to-digital converter. Again, since only an estimate of the power profile is required, the logarithmic compression is sufficient. The applied gain profile and the compressed echo data can then be used to calculate the gain and bias parameters. This new set of parameters is used in the second scan along with the "optimal" nonlinear amplifier. One advantage of this configuration is that the method and constants used to calculate the gain and bias parameters can be changed easily with the software package of the computer.

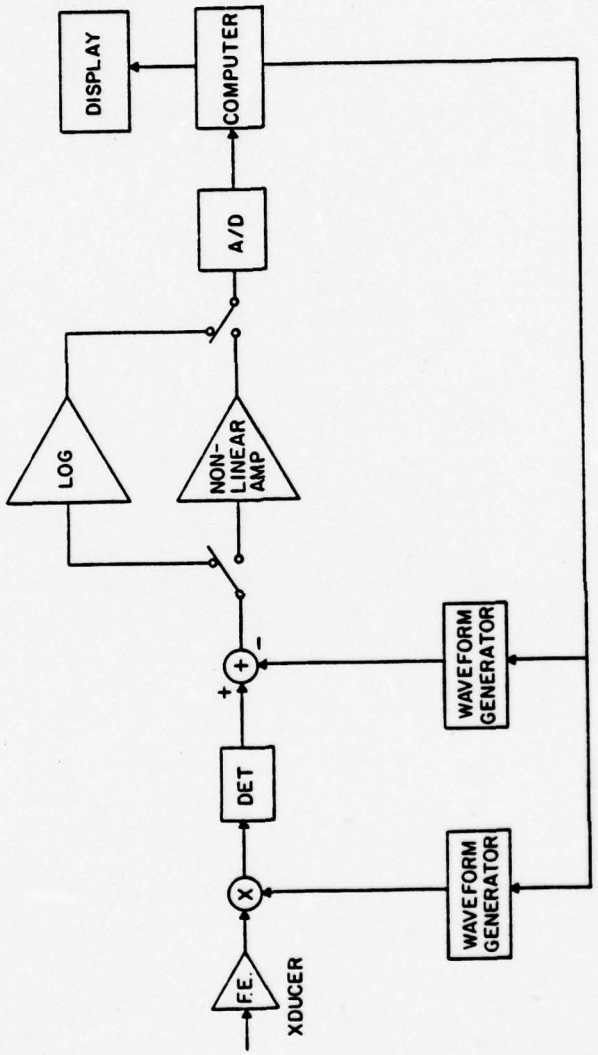

Figure 3.14 One-Channel Dynamic Range Compression

Furthermore, with the use of zero bias and with the gain parameter applied, the full dynamic range data can be reconstructed. This is especially useful for research purposes such as beam width deconvolution. This reconstructed full dynamic range data definitely offers processing advantages over the currently used data with arbitrary and unknown bias and time varying gains.

CHAPTER IV

RESULTS AND DISCUSSION

In Chapter II, an echocardiographic signal model is presented. In this chapter, specific examples of the echocardiographic signal model are described together with computer simulation results. The computer results simulate power profiles of M-mode echocardiographic signals (from stationary and dynamic targets), and also, three-dimensional sector-scanned snapshot echocardiographic signals. These results were needed to check dynamic range compression algorithms in two respects. First, the signals should correspond to fairly complex geometries to be a representative test of the algorithm. (Because of the complexity of the geometry and the need for dynamics, it was impractical to set up in-vitro experiments to gather repeatable echocardiographic signals.) Second, it was not economically feasible to record the wide dynamic range, high speed raw echocardiographic signals to form a sufficiently comprehensive data base. To overcome these obstacles, these simulated echocardiographic signals are used in the chapter to examine the adaptive dynamic range compression algorithms.

In Chapter III, a general dynamic range compression applicable to multidimensional echocardiographic imaging of any dimension is presented. Implementation of the algorithm

for one-dimensional real echo data is shown in Appendix A. In this chapter, specific implementation methods of the algorithm are presented. Due to the nature of hardware and of the economics involved, implementation of the adaptive dynamic range compression algorithm takes on different forms for different scanning and display techniques. This is, of course, at some expense to the "performance" of the algorithm. At this stage where no viable automatic gain control is available, especially for sector scanners, a small sacrifice in "performance" is not detrimental to the objectives. Besides, no objective performance index for echocardiographic images is available. One who operates an imaging system must be aware of the system and its behavior, and must realize that the image generated is a signature rather than a facsimile of the cardiac geometry. Then, if the dynamic range compression algorithm maximizes the information conveyed to the operator without serious untractable distortions, the algorithm accomplishes its design objectives.

In this chapter, an economical M-mode dynamic range compression technique and a dynamic range compression technique for a real-time three-dimensional sector-scanned snapshot camera are presented. Economy in the M-mode implementation is accomplished by hybrid processing. The analog integration, and digital sampling technique eliminates the need for high-cost, high-speed analog-to-digital converters. Thus, this technique is feasible for augmenting existing M-mode echocardiographic imaging

systems. For the three-dimensional snapshot camera under exploratory development at the Applied Research Laboratory at The Pennsylvania State University, digital storage is utilized. Therefore, the main problem of concern is the processing time required. To minimize processing time, a table look-up technique is proposed. An initial scan acquires the parameters necessary and a variable look-up table is computed. During the diagnostic scan, the table can then be dynamically interrogated and a resultant equivalent dynamic range compression applied. Some discussions of how these techniques behave are included.

4.1 Simulation of Echocardiography Signal

To represent typical echocardiographic signals encountered in clinical applications, the echo signals should include the following: 1) a region of blood, 2) isolated specular component within the blood volume to simulate heart valves, and 3) varied angles of incidence.

These attributes are necessary to check-out saturation, wash out and transient effects of dynamic range compression algorithms. The last two items represent typical problems the operator faces in order to adjust for a usable echocardiographic image.

An algorithm is presented here to generate a set of echocardiographic signals given a specific scanning method are the specific cardiac structure. M-mode data from stationary targets and moving targets are simulated with the algorithm. Three-dimensional sector-scanned echocardiographic

data are also presented. These data are used in the evaluation of the dynamic range compression algorithm.

4.1.1 Simulation Algorithm

Two algorithms are used to simulate echocardiographic signals. First, given a set of geometric descriptions of the cardiac structure, with the associated biological parameters, the specular and scatterer components and attenuation are obtained as a function of range for each transmit/receive interval. The second algorithm takes these sets of parameters and simulates the echo signal received at the transducer. These two algorithms are implemented in a single computer program for both M-mode and three-dimensional sector-scanned snapshot simulations.

Figure 4.1 shows the algorithm used to generate the set of specular, scatterer and attenuation parameters. The set of geometric descriptions is integral with the program for simplicity although the description can be entered for each transmit/receive interval. First, the biological parameters such as velocity of sound, impedance, attenuation, and surface scattering parameters are read in. For each scan angle, or transmit/receive interval, the boundaries are computed where the cardiac structure changes. At the beginning of the receive interval, the specular, scatterer and attenuation parameters are set for the whole interval. This assumes that all subsequent biological materials are the same; then, the range counter is incremented until a boundary is encountered. At this point, the specular

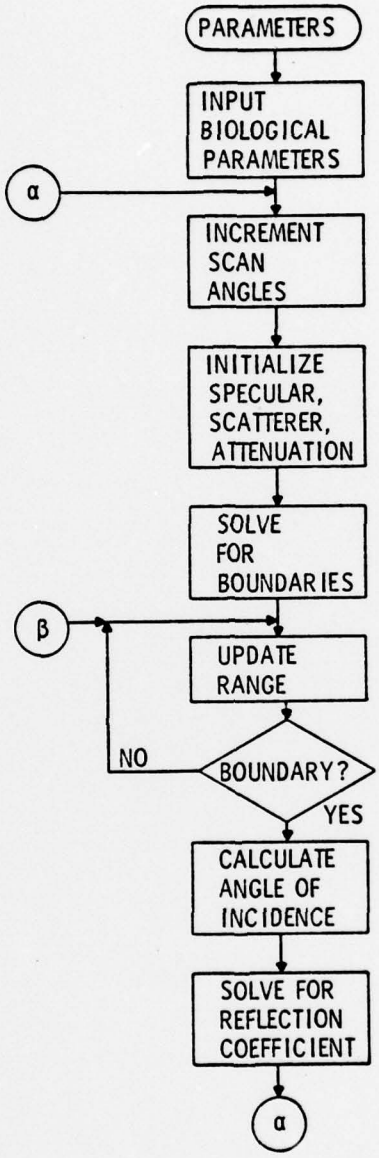

Figure 4.1 Echo Signal Parameter Algorithm

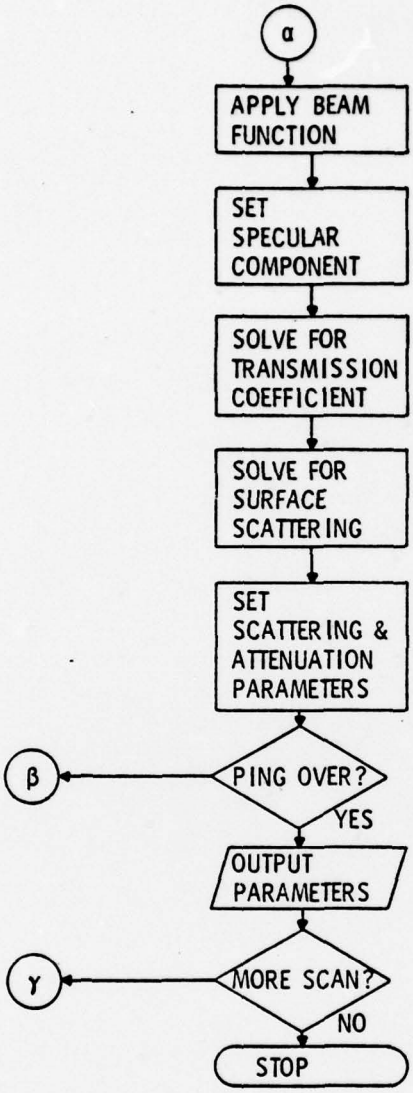

Figure 4.1 Continued

component is computed from the angle of incidence and the characteristic impedances. Since a relatively narrow beam of acoustic wave is used in echocardiography, the specular component is further multiplied by the beam function to account for the amount of energy reflected along the beam. The backscatter component of the acoustic energy depends on the roughness of the surface; this is calculated according to the characteristic impedances and a predetermined parameter to indicate the degree of roughness. Since the transmitted wave is attenuated by the boundary, this contribution is added to the attenuation factor of the particular biological material for that range interval. The attenuation parameter used in the signal simulation algorithm reflects two way propagation therefore, the attenuation parameter set for all subsequent ranges is double the incremental attenuation factor for the material. This process of setting the specular component at the boundary, and the scatterer and the attenuation parameters for subsequent ranges is repeated until the end of the receive interval. This is repeated for the next ping in M-mode or sector-scanned mode until the time or volume of interest is completed.

With this set of specular component, scatterer component and attenuation parameters, the program can generate echo signal data according to the signal model proposed in Section 2.3. Figure 4.2 illustrates the algorithm used to generate echo signal data. The algorithm is a straightforward implementation of the signal model. At each sampled range,

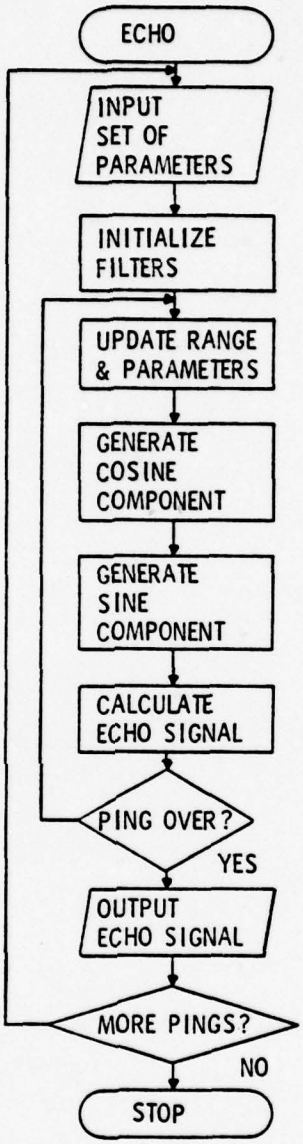

Figure 4.2 Echo Signal Generation Algorithm

two random numbers are generated for the quadrature components. Both are multiplied by the scatterer component to reflect the variance at that range. The specular component is then added to the cosine component. The total attenuation is updated and applied to the quadrature components. Then, these components are passed through different filters to reflect the pulse shape and the band-pass process of the receiver chain. Finally, the two components are squared, summed and rooted to simulate the detector. Although the actual acoustic wave propagation and receiver processes are more complicated than this algorithm, the power profile is similar. This is important in the evaluation of the dynamic range compression algorithm, and this simulation is adequate for this purpose.

4.1.2 Simulation of M-Mode Echocardiographic Data

The above simulation algorithm determines the echo signal from a ping-to-ping basis. Therefore, it is applicable for the simulation of an echo signal for different scanning techniques. The only difference in using the simulation algorithm for different scanning techniques is the spatial or temporal sampling rate, or, in other words, the geometric description.

In M-mode echocardiographic imaging, the cardiac structural velocity encountered in an echocardiographic scan can be as high as 250 mm/sec. Therefore, for the typical pulse repetition frequency (PRF) of 1 KHz, the simulation

model should include structural movements of about 0.25 mm from ping to ping. Since this rapid motion is generally caused by aortic or mitral valves, an isolated specular reflector in a blood volume having at least this velocity is chosen for the simulation model. Figure 4.3 illustrates the structure used for this simulation of M-mode echocardiographic signal with dynamic targets. The 50 mSec burst of M-mode data contains velocities more than 250 mm/sec, which is adequate to evaluate the dynamic range compressions behavior.

To simulate M-mode cardiography with stationary targets, the structure in Figure 4.4 is used. This is just the special case where the targets are all normal the acoustic beam in the previous dynamic M-mode model. Although, the targets are stationary, which implies the specular, scatter and attenuation parameters are the same for different pings, the actual echo signals for each ping can differ. This is due to the nature of the random process which the algorithm simulates, and this reflects the actual signal received under similar conditions.

4.1.3 Simulation of Sector-Scanned Snapshot Echocardiographic Data

For a three-dimensional snapshot, it is important to include reflectors at various angles of incidence. The set of concentric spheres shown in Figure 4.5 accomplishes this requirement. It simulates the sector scanner as the look angle varies. A thin layer of fluid simulates the

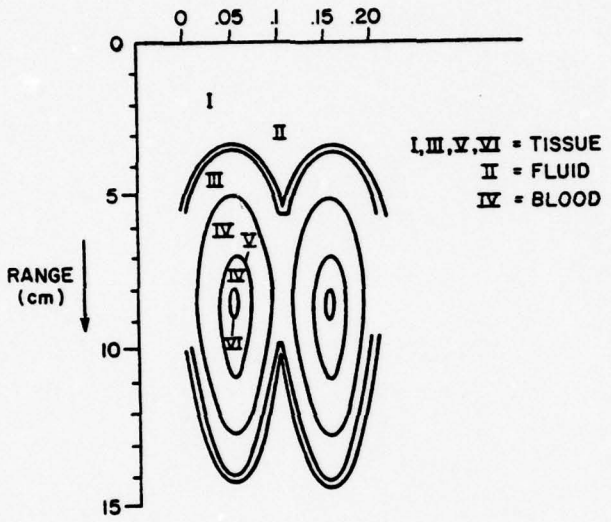

Figure 4.3 Schematic of Moving Targets for M-Mode Simulation

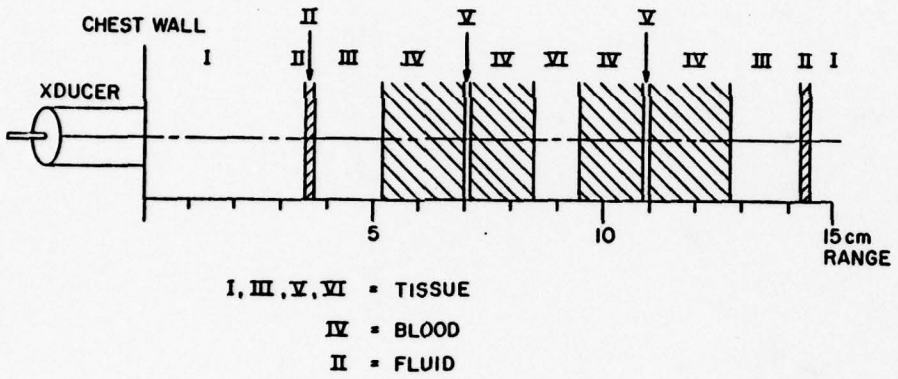

Figure 4.4 Schematic of Stationary Targets for M-Mode Simulation

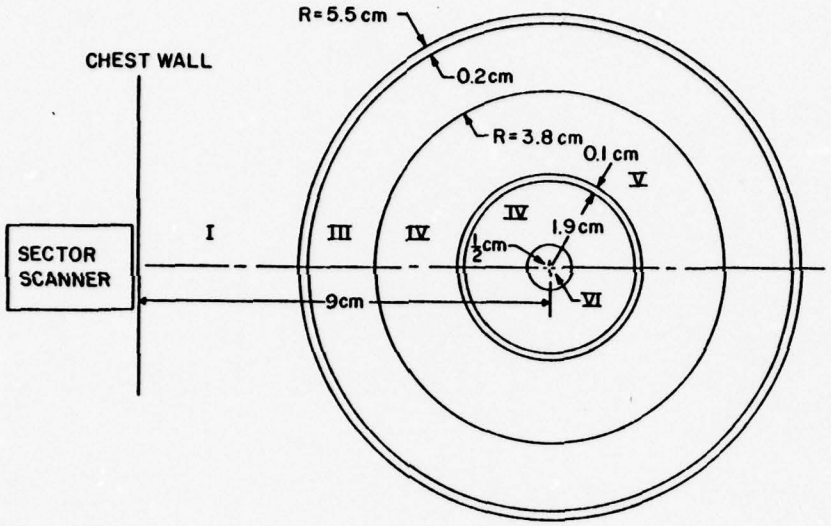

Figure 4.5 Concentric Spheres for 3-D Sector-Scanned Snapshot Simulation

pericardium. The spherical thin tissue within the blood volume simulates valves, and the inner sphere of tissue represents the intraventricular septum. With this model, the various cardiac structures are well represented.

4.1.4 Results

Selected echo signal results at various time instants and at various angles for three-dimensional sector-scanned mode are presented along with the dynamic range compressed image in subsequent sections. Table 4.1 summarizes the parameters used for the biological materials for all the simulations.

Figure 4.6 shows the log magnitude of the echo signal for the stationary target case. Note that particular ping, there is approximately a 75 dB dynamic range. Here, the dynamic range is considered to be the ratio of the highest signal amplitude of interest to the signal level of return from blood. If the blood signal returns are of interest, the dynamic range increases another 10 dB or so. At different scanning angles or times, the blood signal level might be lower due to higher total attenuation in the region before the blood. Therefore, the total dynamic range is consistent with reported values (about 90 to 100 dB).

Figure 4.7 shows the same data as in Figure 4.6 in linear scale. The first 2.5 cm is not shown due to the higher magnitudes. Note that the scale is arbitrary. Figure 4.8 shows an actual A-mode echocardiographic signal. The low signal level in the first 2.5 cm is due to the "long"

Table 4.1 Parameters Used for Simulation

REGION	MATERIAL	VELOCITY ms^{-1}	IMPEDANCE, $10^6 KgM^{-2}S^{-1}$	ATTENUATION $-dBM^{-1}$
I	TISSUE	1600	1.70	4.5
II	FLUID	1540	1.60	0.2
III	TISSUE	1575	1.68	3.6
IV	BLOOD	1530	1.62	0.2
V	TISSUE	1590	1.70	3.5
VI	TISSUE	1630	1.69	3.0

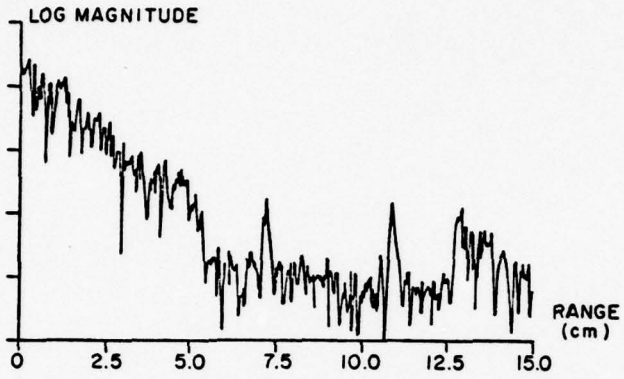

Figure 4.6 Simulated M-Mode Echocardiographic Signal (Log)

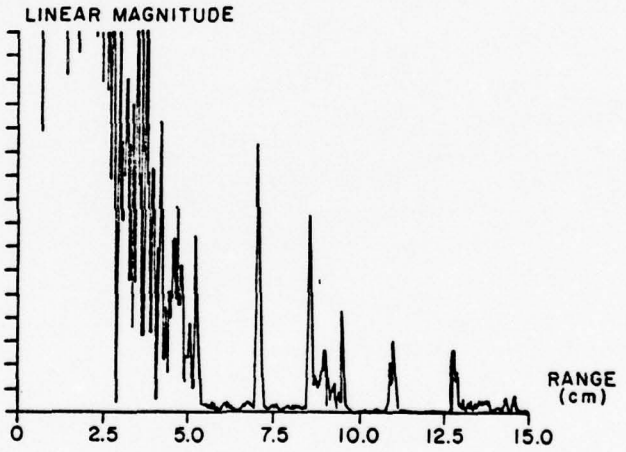

Figure 4.7 Simulated M-Mode Echocardiographic Signal (Linear)

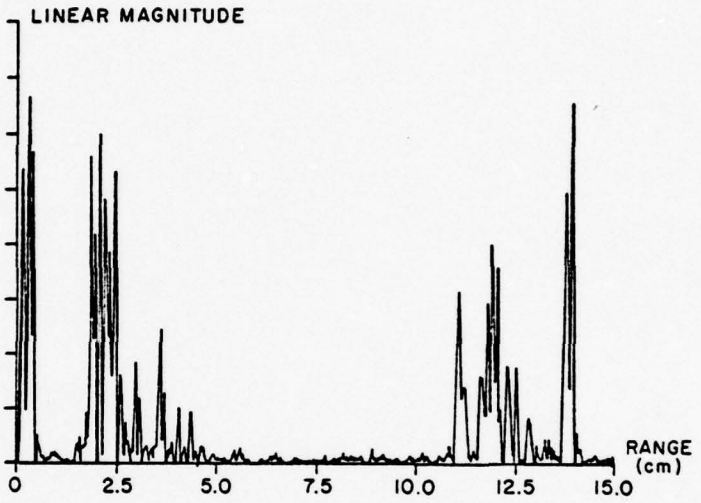

Figure 4.8 Real Echocardiographic Signal

recovery time of that particular amplifier. Note the similar nature of the data after this recovery period with the simulation in Figure 4.6. The isolated specular reflectors and the back-scattered signals from tissues have very similar appearances in the simulated data.

Although a direct prediction of the echo signal is attempted here, it is clear that simulated data are similar in the power profile to actual echocardiographic data. Thus, the simulated data forms a good basis for the test of the dynamic range compression algorithm.

4.2 M-Mode Dynamic Range Compression

A low-cost implementation method for the dynamic range compression algorithm is presented. The algorithm is simulated and evaluated. Various aspects of the algorithm are examined. A comparison with manual techniques of gain control is presented.

4.2.1 M-Mode Implementation

In implementing an M-mode echocardiographic imaging system. Digital processing is not most economical; hence, the use of digitized echo data to derive the gain parameter is unfeasible. The dual channel configuration suggested in Section 3.2.7 is ideal for this application. The present analog video circuits require no modification. The time gain compensation (TGC) circuit, often a separate module, can be replaced with the adaptive gain unit. A schematic for such an adaptive gain control is shown in Figure 4.9.

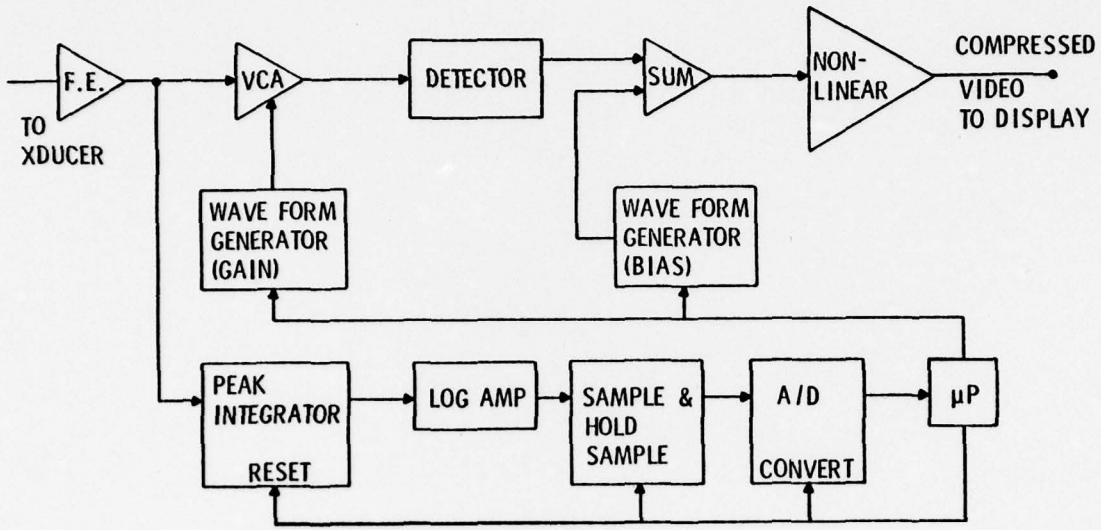

Figure 4.9 M-Mode Implementation of Adaptive Dynamic Range Compression Algorithm

The adaptive gain circuit uses an analog integrator to reduce the requirements on the gain channel data rates. Instead of a root mean square estimate of the signal power, an average estimate is used. By resetting the integrator at the beginning of each gain segment and using a sample and hold circuit, the conversion rate for the signal power estimate is only 12.5 μsec/sample. This can be accomplished with low cost analog-to-digital converters. Furthermore, the use of a logarithmic converter ensures that the dynamic range is within the capability of the analog-to-digital converter, for example, 48 dB for eight-bits. Since the PRF for M-mode cardiography is at 1 KHz and the receive interval for each ping is about 200 μsec., 800 μsec. is available for deriving the gain needed. For simplicity, a sixteen segment, constant gain profile can be used. Thus, in between the end of the receive interval and the next transmit times, the gain profile and the bias parameters for the next ping can be derived and transmitted to the waveform generators. Figure 4.10 shows an example of the timing involved.

The calculations involved in deriving the new gain are extremely simple. First, in order to utilize the ping-to-ping structural geometric correlation, a simple digital filter can be used. Then, for segment i, i=1,...,16, the new power statistic can be derived from the new average sample by

$$ix_n = A\ iX_{n-1} + B\ iU_n\ ,$$

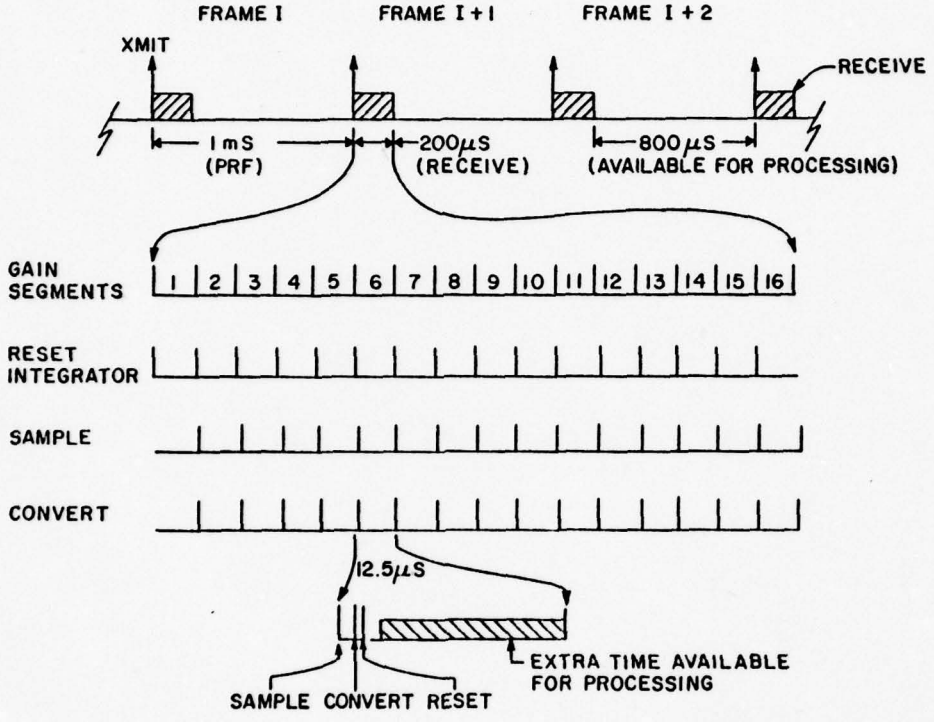

Figure 4.10 Timing Example for M-Mode Adaptive Dynamic Range Compression

where iX_n = average estimate for segment i at ping n, iU_n = average value for segment i at ping n, and A and B are constants chosen for appropriate correlation time.

A minimum value is chosen to represent the blood volume, $\min_i \{iX_n\}$. This, along with the segment where the minimum occurs, can be used to derive the maximum and minimum bias levels:

$$b_{max} = K[(i_{min}-.5)/5]^2 \min\{iX_n\}$$

and

$$b_{min} = K \min_i \{iX_n\} ,$$

where K = a constant depending on the tolerable false alarm level, and i_{min} = segment where min iX_n occurs. It is assumed that the near-filed to far-field transition zone occurs in the fifth segment. These two parameters can then be transmitted to waveform generators to form the suppression levels for the next ping.

To calculate the new gain parameter a multiplier is first formed:

$$iC = \max \left\{ K_\infty,\ K_o - m \left(\frac{iX_n}{\min_i iX_n} - 1 \right) \right\} ,$$

where iC is the multiplier for segment i, and where K_∞, K_o, and m are determined from target miss rates and brightness level for isolated targets (see Section 4.2.5). Then, the new gain for segment i can be calculated:

$$ig_{n+1} = S_{sat} / iC \cdot iX_n ,$$

where

ig_{n+1} = new gain, and

S_{sat} = signal saturation level.

After normalization and suppression by the gain and bias parameters, the echo signal undergoes a nonlinear transformation as expressed in Section 4.2.6 to equalize the distribution. Specifically, the transformation is:

$$T(s) = 1 - \frac{N-1}{N} e^{-\ell n(N-1) \cdot s^2} ,$$

where N = 16 for four-bit quantization.

Although only 5σ μSec are available to derive the new gain and bias parameters, careful design of the hardware can overcome this problem. For example, BiU_n can be performed by setting the correct gain in the analog amplifiers; and the division involved in setting the new gain can be avoided by coding the waveform generator accordingly.

In summary, this particular M-mode implementation can easily be implemented by using low-cost microprocessor components. Figure 4.11 shows an off-line computer simulation of the purposed M-mode adaptive dynamic range compression circuits used to evaluate performance.

4.2.2 Results

The dynamic-range-compressed echo-data for stationary targets and dynamic targets from the M-mode simulations are presented here. The raw echo signal data are also presented for comparison.

Figure 4.12 shows the log magnitude raw echo signal data versus range from the stationary target case. Note that the raw signal amplitudes are arbitrary. The absolute amplitude depends on the transmitted power and the gain of the transducer. Also, shown on the same graph are the saturation and the bias (suppression) levels. As seen from the graph, both the saturation and bias levels track the signal fairly well. The isolated specular reflectors are shown to be quite saturated. But this causes no apparent degradation of the image because they should be displayed at the brightest levels. Figure 4.13 shows the intensity versus range of the dynamic range compressed image.

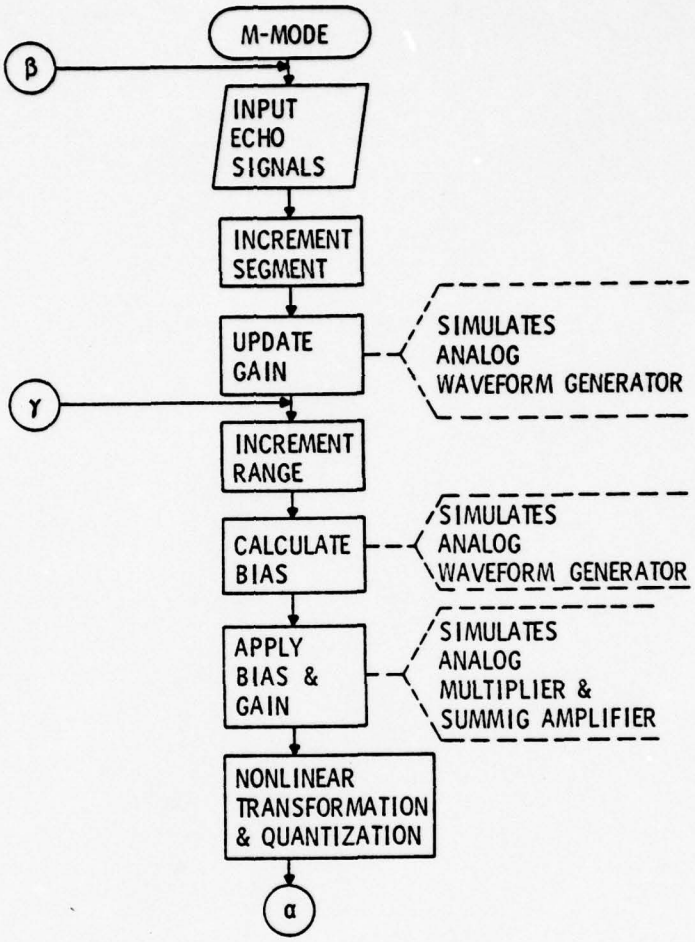

Figure 4.11 Computer Implementation of M-Mode Adaptive Dynamic Range Compression

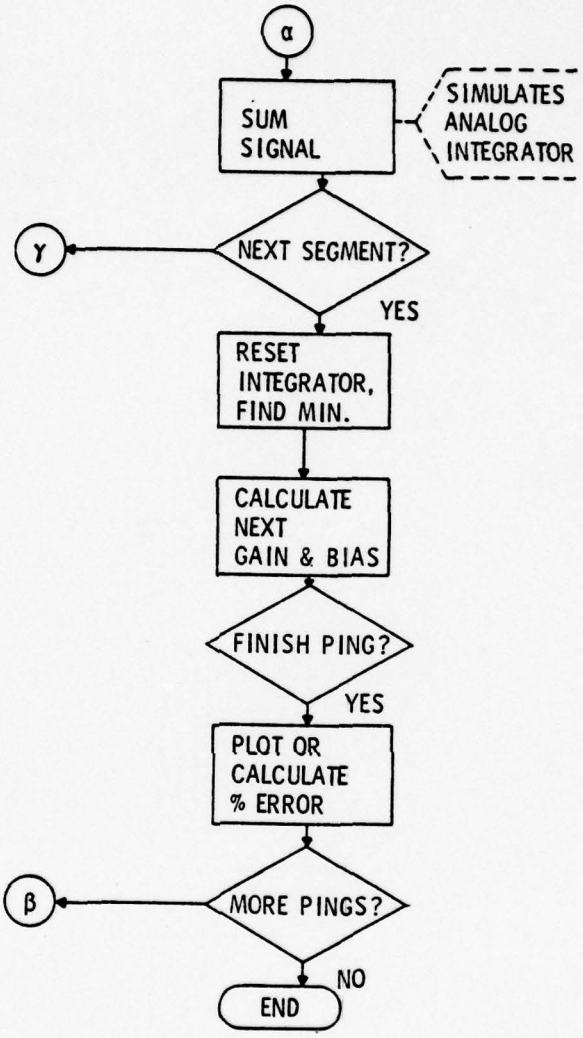

Figure 4.11 Continued

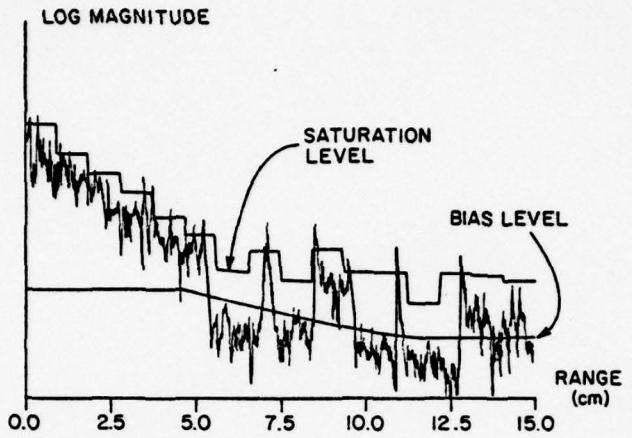

Figure 4.12 Stationary Targets, Raw Echo Signal

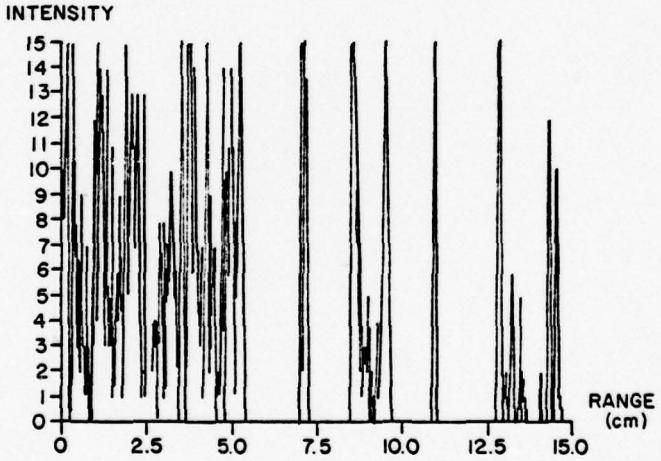

Figure 4.13 Compressed Stationary Targets

Also shown are the locations of the different biological materials. Note that the brightness level in the blood region is suppressed. The boundary of the different biological materials can easily be identified. The boundaries near the maximum range have reduced brightness levels. This is due to the lower limit on the bias level. Although the brightness is reduced, the signal still gets through. Also, since this represents the far side of the heart, performance of the algorithm is not severely degraded due to the relative unimportance in cardiac diagnosis. If this region is of special interest, such as the detection of pericardial effusion, the operator can set the bias level lower just for this particular operation only. In general, the algorithm produces the image desired.

Figure 4.14 shows the schematic of the M-mode dynamic target image simulated. Three pings are selected from this set to show the result of the algorithm. Figures 4.15 to 4.17 show the log magnitude of the raw data and the intensity versus range data for the three examples. The component for the stationary target applies to this image data also.

4.2.3 Discussion

Several performance aspects of the M-mode implementation of the dynamic-range-compression algorithm are presented here. In Section 4.2.2, we see that the algorithm yields the image we desired. In this section, aspects such as intensity distribution, transient behavior, effects of quantization on power-statistic estimation and gain commands as well as compression with manual gain control are discussed.

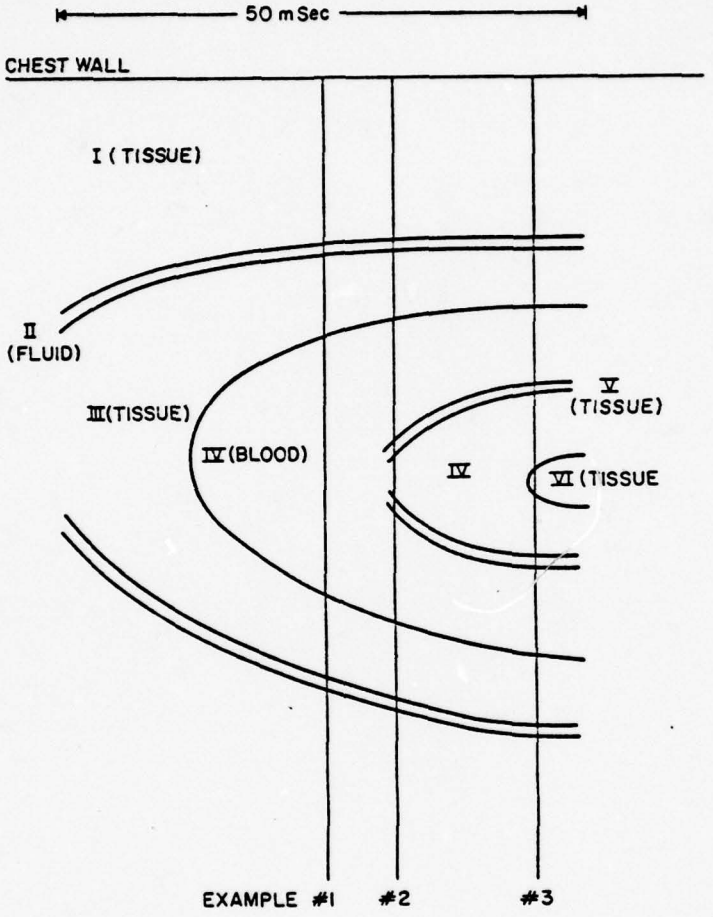

Figure 4.14 Schematic of M-Mode Moving Targets

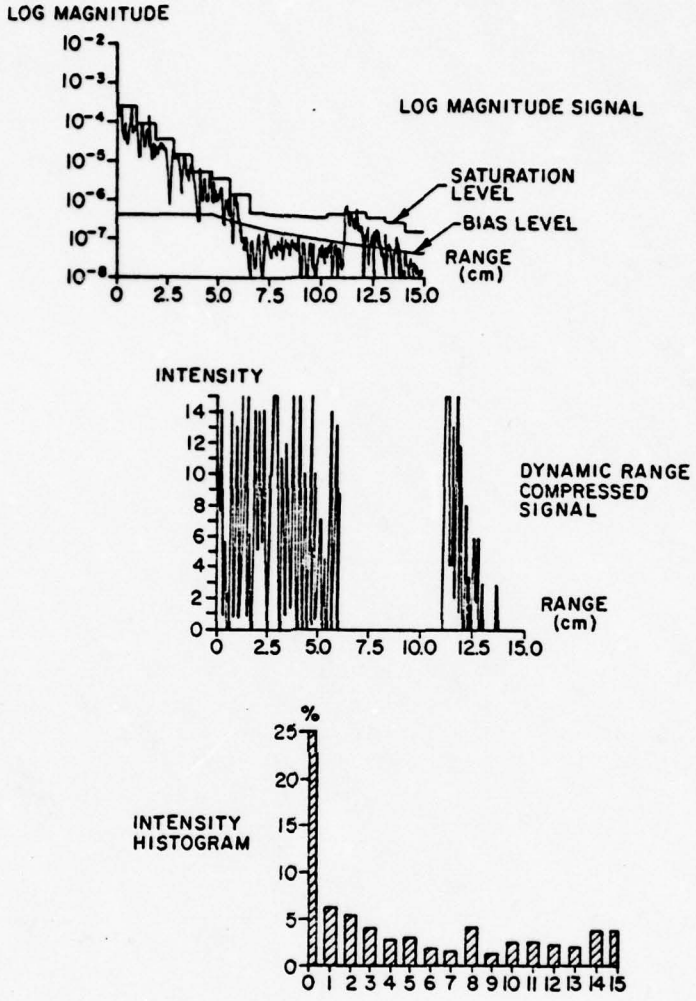

Figure 4.15 M-Mode, Moving Targets, Example 1

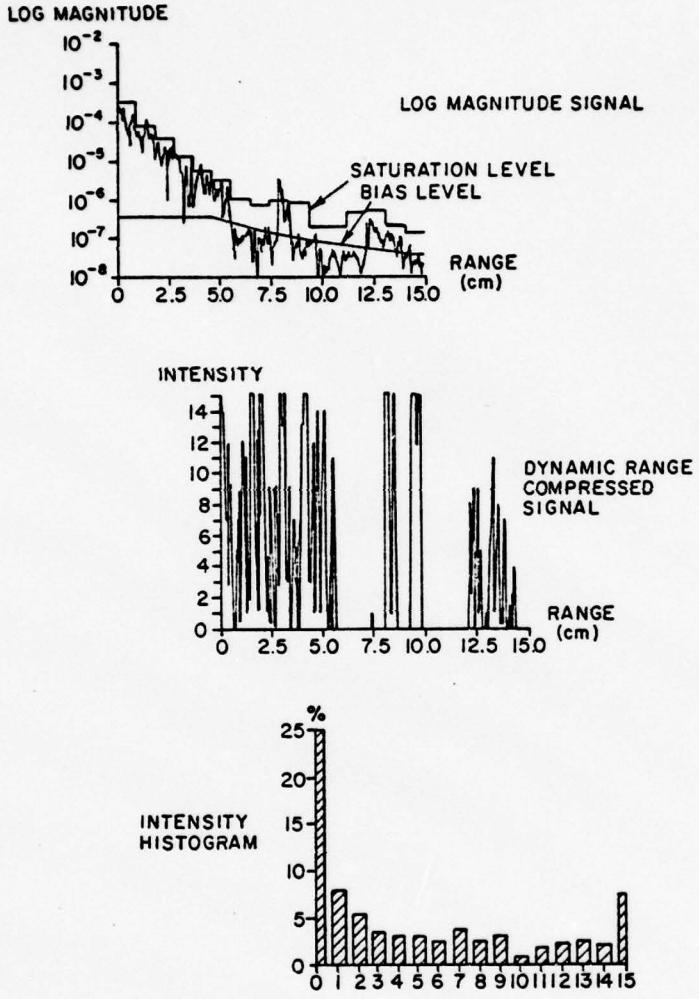

Figure 4.16 M-Mode, Moving Targets, Example 2

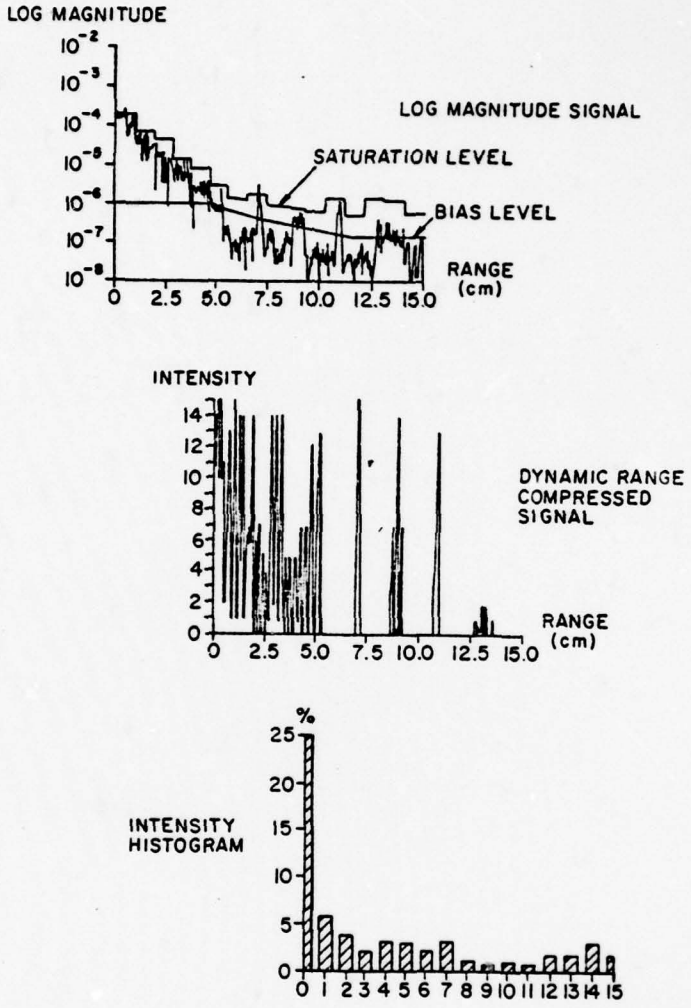

Figure 4.17 M-Mode, Moving Targets, Example 3

4.2.3.1 Symbol Distribution

Ideally, the distribution of symbols should be uniform to maximize the information and to enhance the echocardiographic image. There are factors which will cause the distribution to deviate from uniform. First, the null symbol, used to represent blood, is dependent on the amount of blood volume for that particular scan. In other words, the percentage of the symbol zero in a scan is image dependent. The same applies for the maximum symbol. If enough isolated specular reflection occurs in a scan, then there will be proportionately more signals of maximum amplitude. In order to investigate the symbol distribution, the bias parameter should be neglected and the scan should be relatively free of isolated specular reflectors.

The other factors that affect the symbol distribution are due to estimation errors and the implementation method. Since the gain parameters are applied for a small segment, namely, one-sixteenth of the receive interval, then due to the nonstationarity of the signal, an estimation error will occur on the signal statistics. Also, since all points within this segment are applied with the same gain parameter, all points cannot be normalized correctly. Therefore, the symbol distribution will deviate from the ideal uniform distribution.

Figure 4.18 shows a typical M-mode scan with the gain parameter but not the bias parameter of the dynamic range compression algorithm applied. This ping contains a region of blood and tissue but does not contain isolated specular

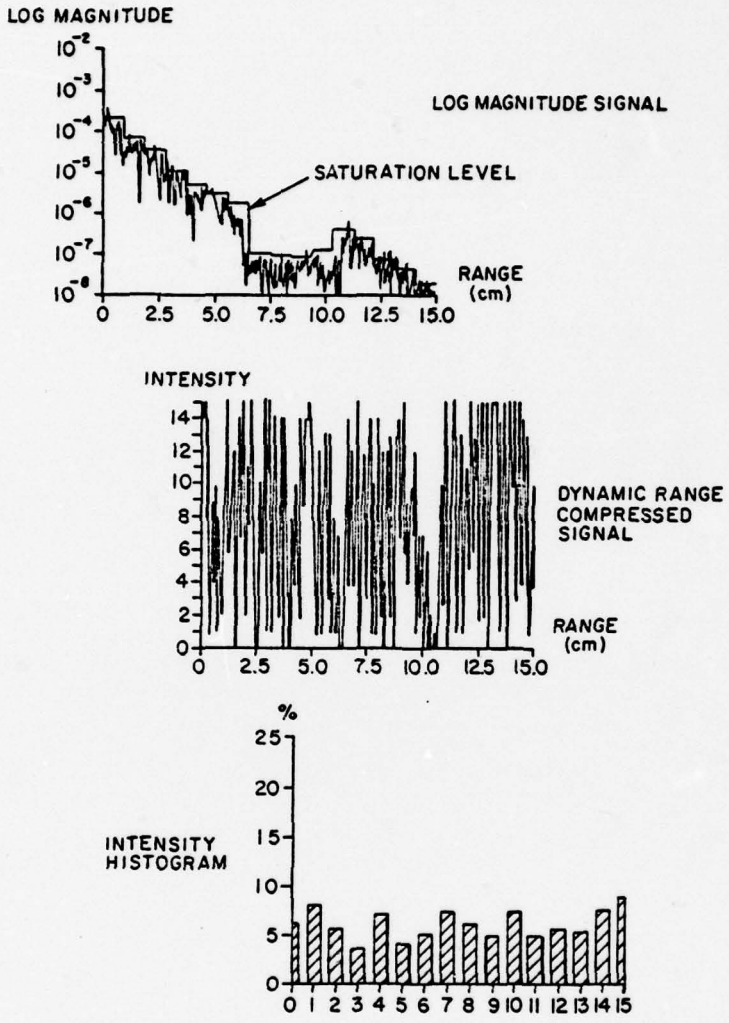

Figure 4.18 Distribution of Symbols (Intensity)

reflectors. The top graph shows the log magnitude signal data as a function of range. Also, the saturation level is shown. Since the gain profile is derived from the past pings in the M-mode implementation, the gains derived are not perfect, but obviously adequate. The middle graph shows the echo signal after adaptive gain and quantization. Note that the signal appears homogeneous and noisy throughout the scanning range. This illustrates the importance of the bias parameter. In order to automatically apply gain to the echocardiographic image, the suppression level must also be coupled so that the low level signal from a blood volume will not be automatically magnified and thus render the image useless. Also, note that since the segment transition points do not occur exactly at the signal transition points, the high and low magnitude regions are separated by a dark band. This results in additional information to the operator to signify a power transition point. This is similar to edge enhancement by differentiation. The bottom graph shows the resultant histogram. Even though the gain profile is derived from past pings, the histograms are still fairly uniform due to the high correlation from ping to ping. Clearly, a fairly uniform symbol distribution can be achieved.

4.2.3.2 Transient Behavior

In order to increase the estimation accuracy in the power statistics, a digital filter is used from ping to ping for the same segments in the dynamic range compression algorithm. Figure 4.19 shows the transient response of the filter used in this particular implementation of the dynamic

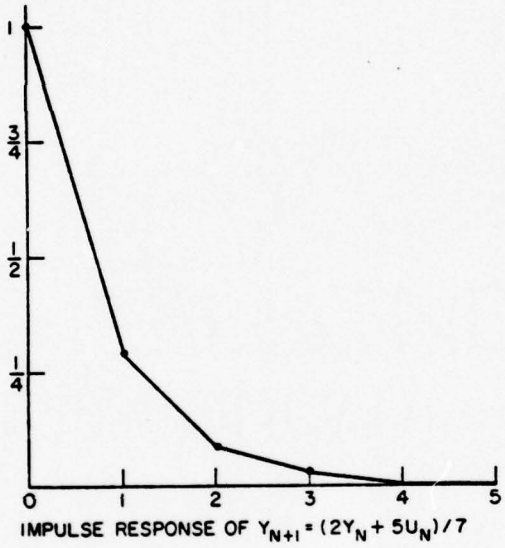

Figure 4.19 Transient Response of Digital Filter

range compression algorithm. Although the correlation time of the cardiac structure is longer, the shorter transient response speeds up the response to transient conditions. For example, with structure velocity of 0.25 mm/ping, then it will take 3.75 pings for the structure to move across the segment. Since there are essentially 25 independent samples available per segment for the power statistic estimate, it is sufficient to use a faster filter for better transient response.

Figure 4.20 shows how the sixteen gain segments converge to the final valve within two pings. This is for the M-mode simulation of a stationary target. Note that the variation after the third ping is quite small. Some variation can be attributed to the fluctuation of the signal itself; a stationary target means constant specular, scatterer and attenuation parameters only, but not a constant signal.

From the convergence rate of the algorithm shown, it is clear that it can handle rapid signal variations from ping to ping. This digital implementation for frame to frame operation has clear advantages over analog techniques. If the operator wishes, to change the filter constant in this digital implementation, it involves changing three memory words only. Therefore, to utilize the inherent signal correlation from frame to frame, the digital implementation is adequate to derive an adaptive gain for echocardiographic imaging.

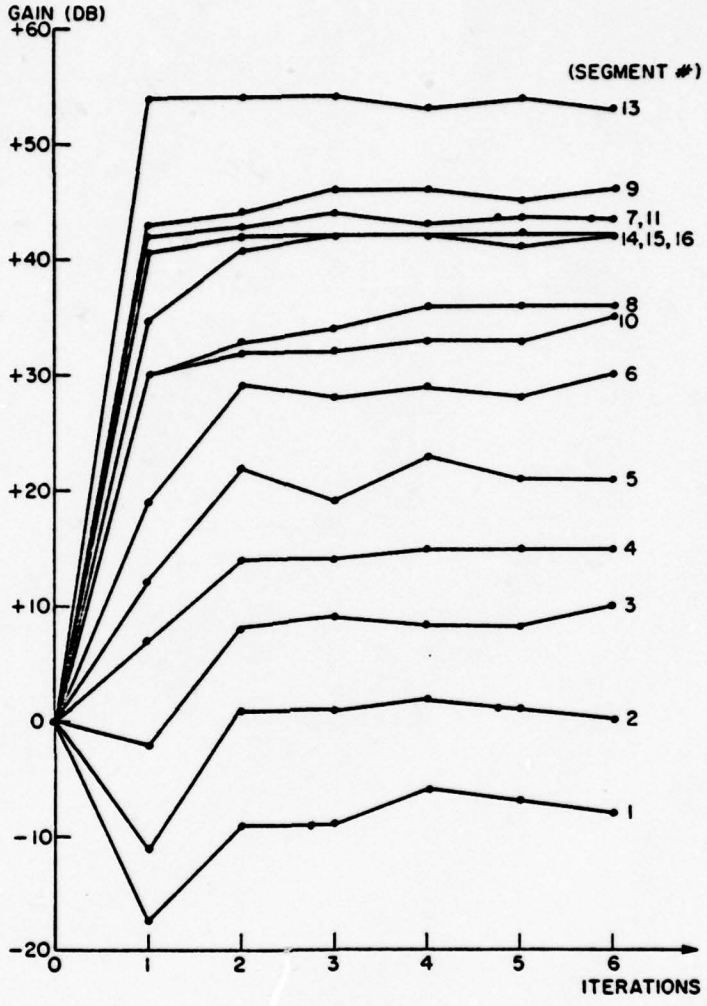

Figure 4.20 Convergence of Segment Gains

4.2.3.3 Comparison with Manual Gain Control

Because the manual gain control used in present day echocardiographic imaging systems depends on operator control, an objective direct comparison with the adaptive dynamic range compression algorithm is impossible. However, one can compare the adaptability of the different gain control systems with dynamic targets.

A percentage error approach is used here for several reasons. Fidelity criteria for images are hard to define objectively and consistently for different types of images. Furthermore, a transformation from raw echo data to image data cannot be readily defined. The percentage error approach applies if one wishes to reconstruct the full dynamic range echo data by applying the inverse gain. This approach has applications if the full dynamic range data is used in further processing or enhancement, for example, in beam width deconvolution or compound scanned image reconstruction. Figure 4.21 illustrates the process used to evaluate the average percentage error for the various gain control processes.

The manual gain control methods used in existing echocardiographic systems are constant throughout the image. Therefore, it can only be optimized for a single image or ping. The actual gain applied depends on the operator skill. Therefore, the percentage error presented here only serves as comparison between stationary target and the effects of the target motion. For the gain control, the parameters are

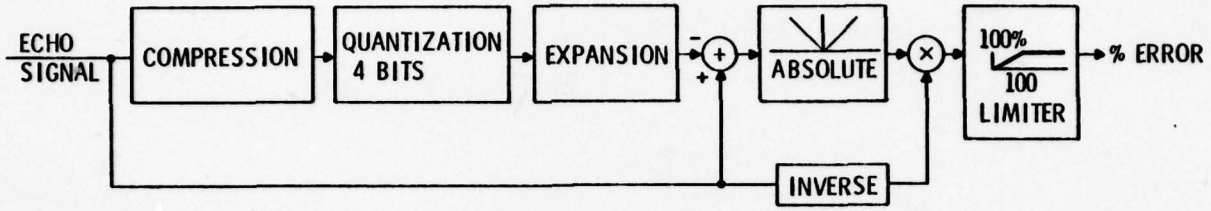

Figure 4.21 Evaluation of Compression Algorithms

derived from a stationary target, consistant with operating procedure. Figure 4.6 illustrates the echo signal selected for this purpose. The log magnitude data is used to derive the gain parameter. Usually, a static log magnitude display is not available to the operator; thus, this serves as a better guide in deriving the gain controls.

A logarithmic compression, a single slope time gain compensation (TGC) and slope and logarithmic manual gain control methods are selected as the baseline to compare to the adaptability of the dynamic gain control algorithm. Their corresponding schematics and the gain control parameters are presented in Figure 4.22. A summary of the average percentage errors for the three methods for the constant target and the dynamic target cases are presented in Table 4.2.

Since reconstruction of the full dynamic range data is desired, the bias parameter in the dynamic range compression algorithm is set to zero for this purpose. Figure 4.23 shows the average percentage errors for the adaptive dynamic range compression algorithm for various values of the parameter K_{∞}. Note that the errors reach a minimum for some value of K_{∞} and is relatively insensitive around the minimum value. The shape of the curve is expected because the error consists of three terms: quantization error, saturation error and low level exclusion error. Although the latter two are manifestations of quantization, they are highly dependent on the probability density of the signal. Since the low level error has a percentage error of 100% and the saturation error is fairly high, we can assume the form of the total error to be

LOG COMPRESSION:

$$y = \frac{1}{4.5} \text{LOG } 10^8 x \; ; \quad y \in [0,1]$$

SINGLE SLOPE GAIN:

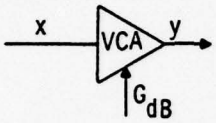

$$G_{dB} = 120 - 50 \max \left[0, 1 - \frac{r}{6.2}\right]$$

r = RANGE (in cm)

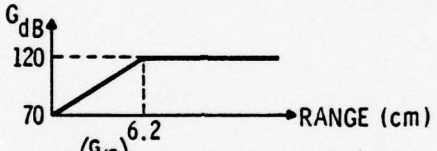

$$y = 10^{\left(\frac{G_{dB}}{20}\right)} \cdot x \; ; \quad y \in [0, 1]$$

SINGLE SLOPE GAIN WITH LOG COMPRESSION:

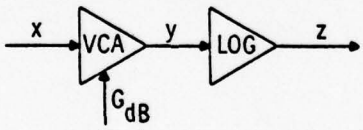

$$y = 10^{\left(\frac{G_{dB}}{20}\right)} \cdot x \quad \text{(see above)}$$

$$z = \frac{1}{2} \text{LOG } y + 1 \; ; \quad z \in [0, 1]$$

Figure 4.22 Compression Algorithm Used for Comparison

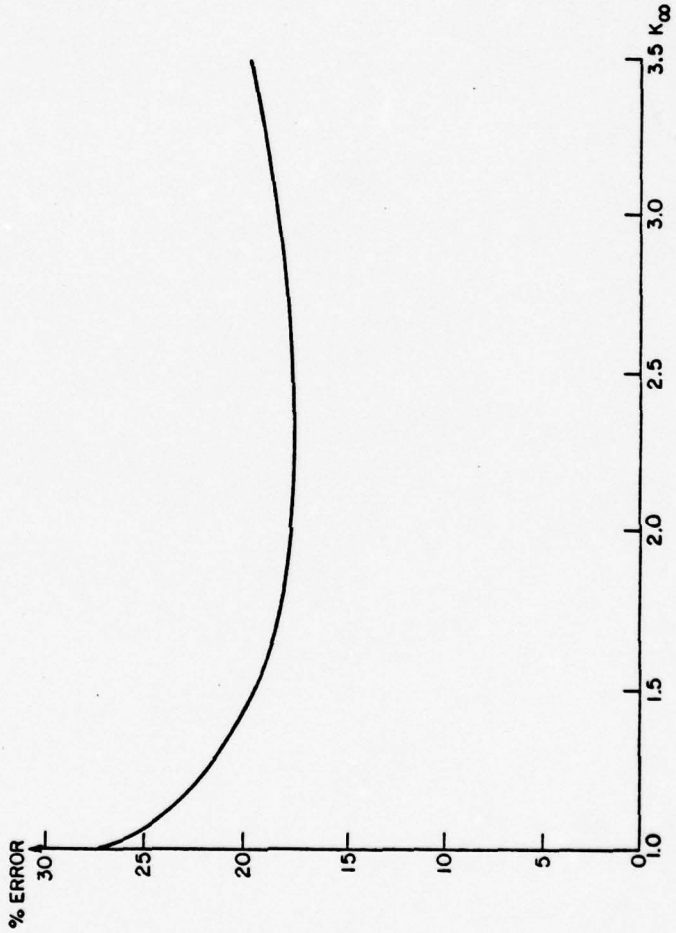

Figure 4.23 Average Percentage Error vs. K_∞

$$E_{Total} \cong E_Q + \int_0^{S_L} p_S(s)ds + \int_0^{S_U} p_S(s)ds \ ,$$

where

E_Q = quantization error,

S_L = low level exclusion level, and

S_U = saturation level.

S_L and S_U are functions of the number of quantization levels and of the inverse nonlinear transformation $T^{-1}(s)$. Since the gain applied is $K_\infty \hat{\sigma}_o$, assuming $\hat{\sigma}_o = \sigma_o$, we have:

$$p_S(s) = K_\infty^2 s \, e^{-K_\infty^2 s^2} \ ,$$

and therefore,

$$E_{Total} \cong E_Q + \left[1 - e^{-s_L^2 K_\infty^2} \right] + e^{-S_u^2 K_\infty^2} \ .$$

The expression $(1-e^{-S_L^2 K_\infty^2})$ increases as K_∞ increases, while $e^{-S_u^2 K_\infty^2}$ decreases as K_∞ increases. Since $S_L >> S_U$, the form of the total error as a function of K_∞ is concave as in Figure 4.23. For K_∞ between 1.75 and 2.75, the total percentage error changes very little. This insensitivity helps the designer in choosing K_∞.

For $K_\infty = 2.25$, the total percentage error for the adaptive dynamic range compression algorithm for stationary targets and for moving targets are presented in Table 4.2.

Table 4.2 Percentage Errors for Different Dynamic Range Compression Algorithm

	STATIONARY TARGET	MOVING TARGET	% CHANGE
LOG COMPRESSION	26.6 dB	36.5 dB	37.2 dB
SINGLE SLOPE	23.7	34.5	45.6
SLOPE W/LOG	16.4	25.7	56.7
ADAPTIVE COMP.	17.6	20.4	15.9

Note that the single slope with logarithmic compression has the lowest percentage error for stationary targets. This is expected because logarithmic compression yields the lowest percentage error no matter what the distribution is. Since the dynamic range compression algorithm is designed for imaging, the logarithm compression approach was not used.

The percentage change from stationary targets to moving targets for the various gain controls are also shown in Table 4.2. Obviously, the dynamic range compression presented has the best performance in a dynamic target environment. Also, note that no operator adjustment is required even for one single scan.

4.2.3.4 Effects of Quantization

An actual implementation of the M-mode adaptive dynamic range compression algorithms will utilize an eight-bit A/D converter for the purpose of estimating the power statistics and will utilize an eight-bit control word to the voltage control amplifier. An examination of what effect this will have on the image will be examined here. Again, the average percentage error is used to evaluate this effect. Theoretically, the quantization effects are minimal. Quantization adds a random error term. For eight-bit quantization, this introduces a noise level 58.9 dB below the signal level. Even if this error is fairly high, the relative insensitivity of the algorithm to K_∞ will not degrade the saturation performance much. The suppression level will suffer slightly due to quantization. For eight-bit quantization, this degradation is negligible. Figure 4.24 shows the average percentage

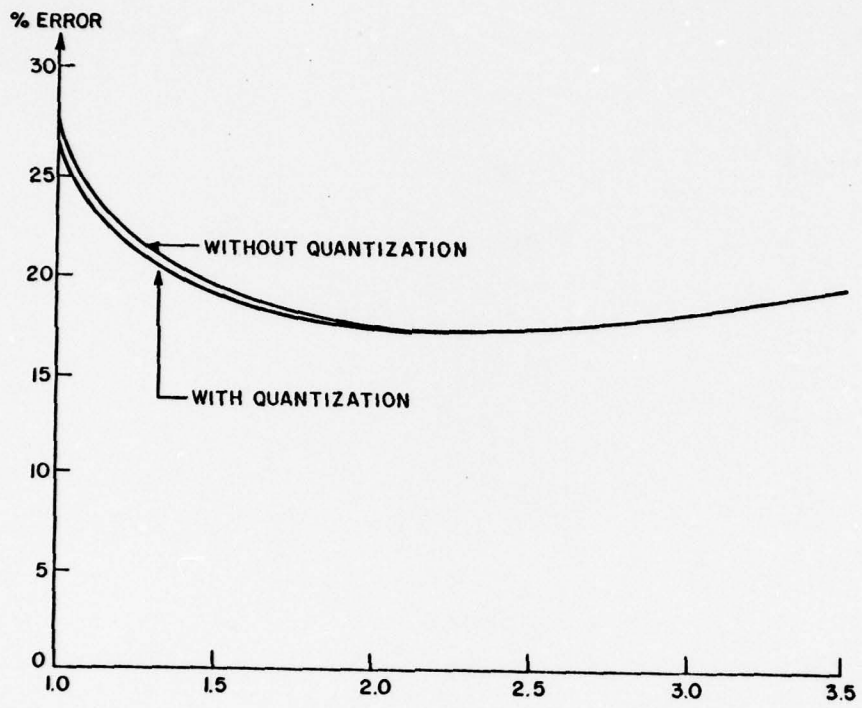

Figure 4.24 Percentage Error With and Without 8-Bit Quantization

error with and without quantization in the power estimate and gain control versus K_∞. Obviously, the effect is negligible.

4.3 Three-Dimensional Sector-Scanned Snapshot Mode Dynamic Range Compression

For multidimensional echocardiography, the dynamic range compression algorithm may be implemented differently from the M-mode technique suggested. One reason is the inherent complexity of multidimensional scanners. The addition of hardware or software to implement the dynamic range compression algorithm is of little impact to the system. Such an example is the three-dimensional sector-scanned snapshot camera suggested by Miller, Lawther and Zelis.[39] The snapshot camera utilizes digital memory for the bulk storage of three-dimensional sector-scanned echocardiographic signal data. Subsequent reconstruction of sector display is controlled by a minicomputer. The addition of control interfaces for voltage control amplifiers and digital look-up tables do not increase the system complexity by a significant amount. The following snapshot mode dynamic range compression algorithm is designed specifically for this echocardiographic system.

4.3.1 Snapshot Mode Implementation

For three-dimensional snapshot, the dynamic range compression algorithm can be applied after data acquisition. Since an eight-bit analog-to-digital converter is used, logarithmic compression and subsequent expansion should yield reasonable data with post scan expansion. With the full reconstructed dynamic range data, one can apply the dynamic

range compression algorithm as suggested in Chapter III. For a large amount of data, the post scan data processing time can be quite long, therefore, an alternative application of the dynamic range compression algorithm with partial hardware implementation is desirable. Figure 4.25 shows a schematic of such a design.

The operational aspects of the snapshot camera allows the possibility for an initial scan to acquire the gain and bias parameters. Then, the actual diagnostic scan can be taken. This single channel realization eliminates the dual channel electronics. Since a high-speed analog-to-digital converter is used in conjunction with a digital memory for the snapshot camera, the dual channel slow-conversion approach for the M-mode imaging systems seems unnecessary.

In Figure 4.25, the receiver consists of a voltage controlled amplifier detector, logarithmic amplifier, eight-bit A/D converter, a programmable table, and waveform generator. The digital memory provides data storage, and the CPU is used to calculate gain and bias. The CPU also controls a grey scale display unit which uses the data from memory. The waveform generator provides a piece-wise linear continuous gain profile (in dB) to the UCA. Sixteen instruction words provide the initial gain and incremental gains as illustrated in Figure 4.26. The piece-wise linear continuous gain profile eliminates the abrupt switching transient as in the M-mode implementation. Also, the manually adjusted piece-wise linear continuous gain profile is used clinically; thus, acceptability of the gain profile by the end user is enhanced.

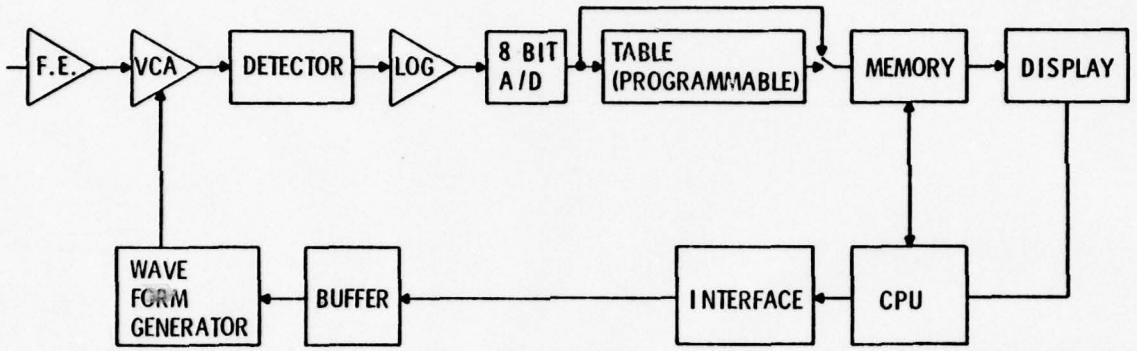

Figure 4.25 3D Snapshot Implementation of Adaptive Dynamic Range Compression Algorithm

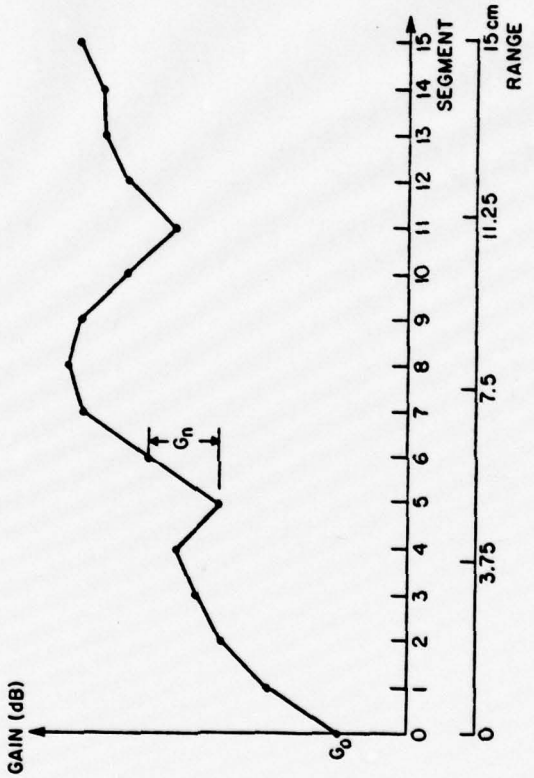

Figure 4.26 Initial Gain G_o and Incremental Gain G_n

The voltage-controlled gain amplifier should be located at the front end of the receiver chain to keep the signal-to-noise ratio of the latter stages high. Since the bias parameter is not critical, the bias parameter can be applied digitally and in real time with a table look-up technique. A programmable table is connected to the eight-bit A/D converter and updated as the range changes. This will dynamically apply the bias versus range profile. The effects of segmenting the bias parameter are minimal. If sixteen segments are used, the first segment is about 6 cm long in range for the near zone. The remaining segments are 0.6 cm. Therefore, the largest error in bias will occur adjacent to the transition zone. This will contribute 10% error to the bias parameter at this maximum error range. Since the bias is a lower limit for blood level only, this 10% error will not affect the suppression function. Of course, at higher ranges, this error is smaller, the minimum being at the maximum range with 4.3%. This programmable table also provides the necessary nonlinear transformation to the log-compressed data to yield a uniform output distribution. Since the transformation is programmable, one can use a different one as desired. This configuration offers tremendous flexibility. A detailed schematic of this programmable table is shown in Figure 4.27. The main function of the table is to form a four-bit word from an eight-bit input. This can be accomplished by using random access memories (RAMs). The eight-bit input forms part of the address to the RAMs. Another four bits forms the address to

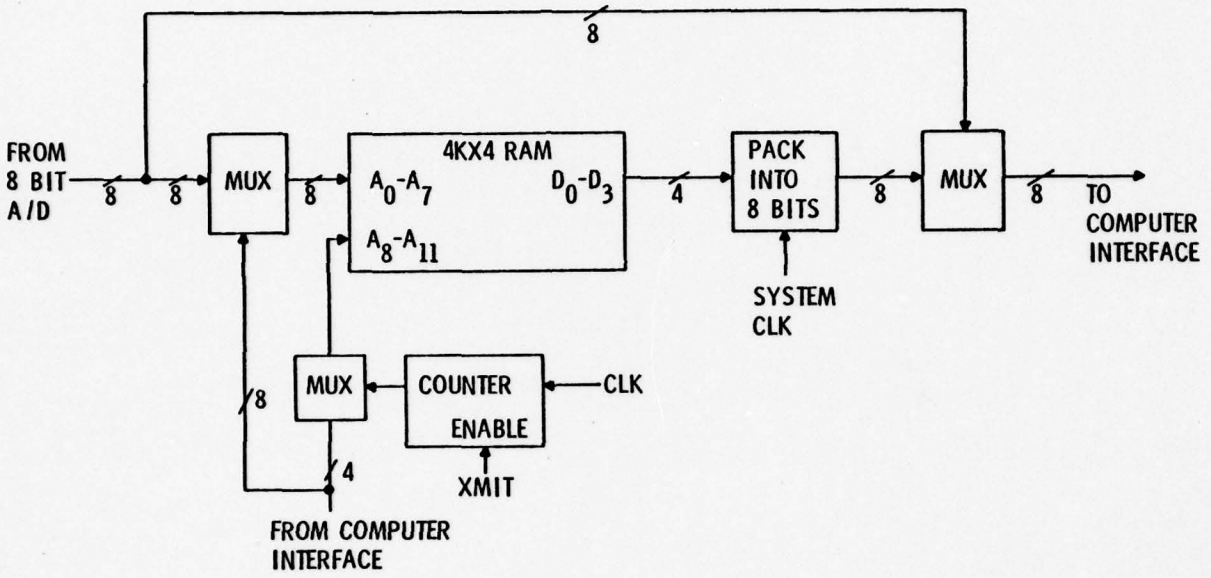

Figure 4.27 Look-up Table Schematic

advance the table as a function of range. A clock and counter can be set to increment range counts at the far zone. The four-bit output words can then be packed into eight bits so that it is compatible with the interface. At each of the sixteen bias range increments, the bias level can occur at any one of the lower levels. Figure 4.28 illustrates the bias level for different segments. For this illustration, 64 levels are suppressed by the bias level; there are 192 levels left over to perform the transformation. Figure 4.29 illustrates the eight-bit input, four-bit output transformation. Under actual operating conditions, since the bias parameter and the gain parameter are uncorrelated for nonblood volumes and correlated for blood volumes, the bias parameters can increase or decrease from one segment to another. Therefore, the remaining range encoding into nonzero symbols also changes. This necessitates a new transformation for that particular segment. Therefore, the sixteen look-up tables vary for each of the bias segment for each statistical window. This implementation of a look-up table enables the real-time application of the algorithm by eliminating the point-by-point computations required.

The application of the above implementation technique consists of the following steps and calculations:

1) Transfer initial gain vector to buffer.

   Let $G = [G_o, G_1, \ldots, G_{15}]^T$,

   where

   G_o = initial gain in dB, the selection of

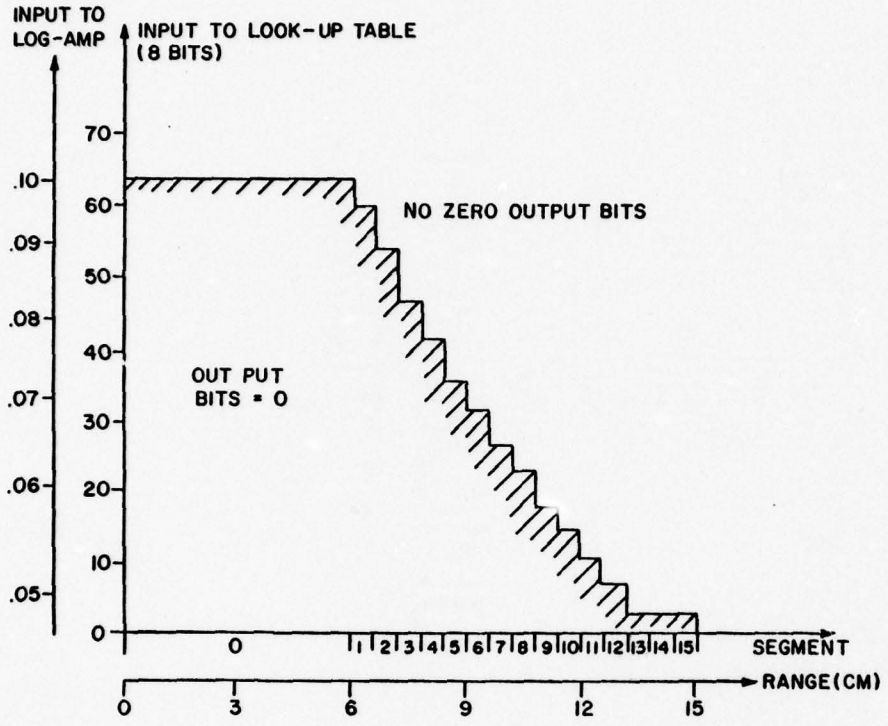

Figure 4.28 Illustration of Look-up Table (for constant power and gain levels)

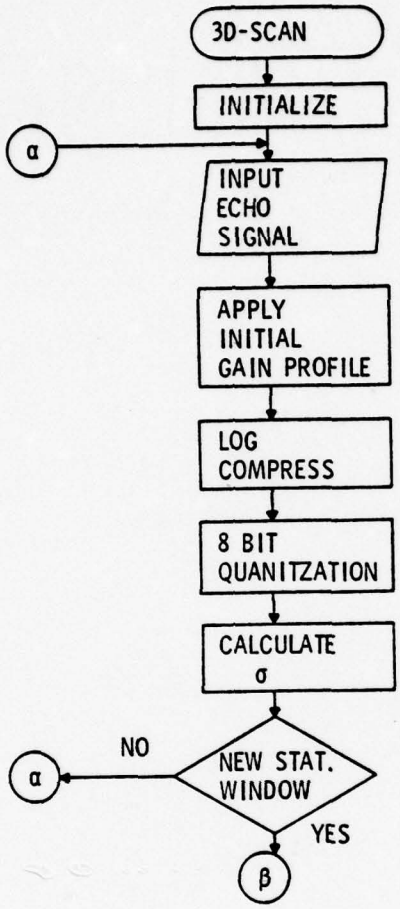

Figure 4.29 Computer Implementation of 3D Snapshot Dynamic Range Compression Algorithm

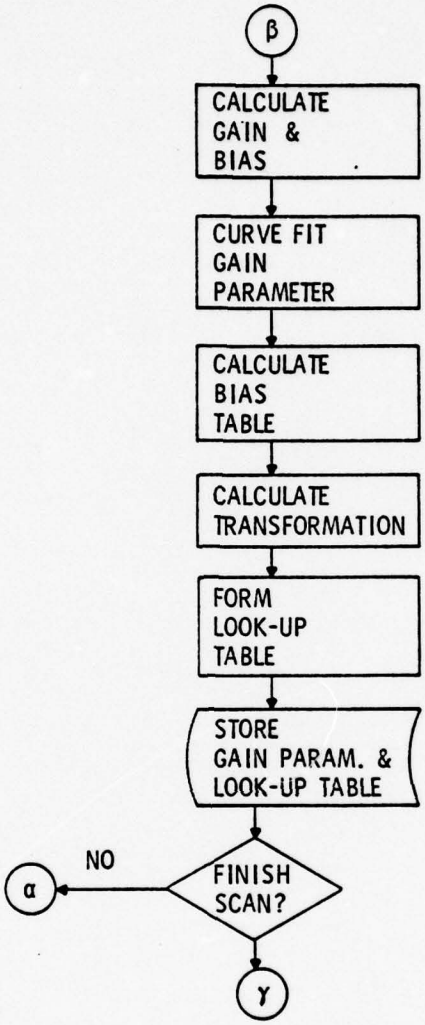

Figure 4.29 Continued

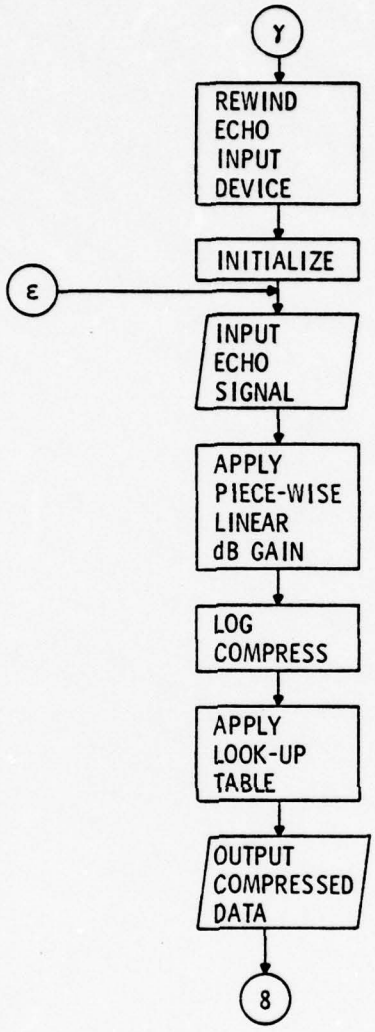

Figure 4.29 Continued

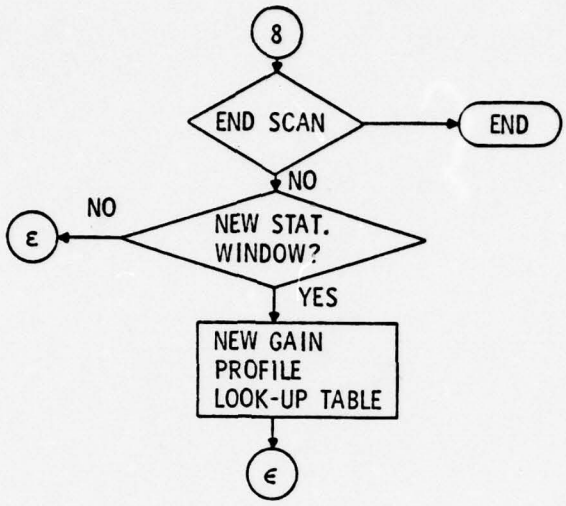

Figure 4.29 Continued

which depends on the approximate initial signal strength.

$G_1, \ldots, G_{15}$ = +2 dB/cm (for example)
= incremental gain in dB,

2 dB/segment is chosen to compensate for some attenuation effects but low enough so that the latter segments are saturation free.

2) Commence gain parameter acquisition scan. The eight-bit log-compressed data for a complete scan are stored in memory for the derivation of gain and bias parameters.

Let $x_{i,j,k} = \log g_i \, s_{ijk}$

where

$x_{i,j,k}$ = log compressed data as a function of range and scan angles (see Table 4.2.2.1)

g_i = initial gain for range i.

$s_{i,j,k}$ = raw echo signal.

3) Derive gain and bias parameters for diagnostic scan. The calculations are as follows:

a) Calculate variance for each statistic using correct window and range. The window refers to box car averages over the two scanning angles

$$\log s_{i,j,k} = x_{i,jk} - \log g_i,$$

$$s^2_{i,jk} = \log^{-1}[2 \log s_{i,j,k}]$$

$$\sigma^2_{i,p,q} = \frac{1}{N_I N_J N_K} \sum_{\text{BOX}} \sum_{\text{CAR}} \sum_{\text{SUM}} s^2 ,$$

$$\sigma_{i,p,q} = \sqrt{\sigma_{i,p,q}} ,$$

where p = index of angle segment over scanning plane θ, and
q = index of angle segment over scanning plane Ø.

Also let

$$\sigma_{min} = \min\{\sigma_{i,p,q}\} ,$$

and

$$I_{min} = \left\{ i \;\middle|\; \min_{i,p,q} (\sigma_{i,p,q}) \right\} .$$

b) Calculate gain segments,

$$K_{i,p,q} = f(K_1, K_\infty, \sigma_{i,p,q}\, \sigma_{min}) ,$$

where

f = nonlinear function to limit signal near the minimum level (see Section 3.2.5).

$$g_{i,p,q} = 1/K_{i,p,q} \cdot \sigma_{i,p,q} ,$$

$$\hat{g}_{i,p,q} = 20 \log g_{i,p,q} ,$$

where $g_{i,p,q}$ = new gain at range i, angle segments p,q, and $\hat{g}_{i,p,q} = g_{i,p,q}$ in dB's.

Fit $\hat{g}$ to piece-wise linear continuous curve by

$$\underset{\sim}{G}_{p,q} = (F^T F)^{-1} F \underset{\sim}{\hat{g}}_{i,p,q} ,$$

where F = f(i) = function to generate piece-wise linear continuous function, and $\underset{\sim}{G}_{p,q}$ = new gain parameters for angle segments p,q.

After all gain parameters are used to solve for the different angles and angle segments, transmit to buffer.

c) Calculate bias parameter

First calculate average gain over segment, (since bias refers to the raw signal and in this implementation the suppression is applied post multiplication, and multiplicative constant must be removed.)

$$\tilde{g}_{n,p,q} = \frac{1}{20} \underset{\sim}{W}_n^T \underset{\sim}{G}_{p,q}$$

where $g_{n,p,q}$ = average gain in dB's over bias segment n, and $\underset{\sim}{W}_n$ = weighting function for bias segment n.

The minimum and the maximum bias parameters can be calculated by,

$$b_{min} = K_b \sigma_{min}$$

$$b_{min} = \begin{cases} \left(\frac{I_{min}}{I_{FF}}\right)^2 b_{min} & I_{min} > I_{FF} \\ b_{min} & I_{min} \leq I_{FF} \end{cases}$$

where K_b = constant dependent on missed target rate, and I_{FF} = far-field range.

Then the segmented and quantized gain applied with the look-up table can be calculated by:

$$B_{o,p,q} = \tilde{g}_{o,p,q} + \log b_{max}$$

$$B_{n,p,q} = g_{n,p,q} + \max\left[b_{min}, \left(\frac{I_n}{I_{FF}}\right)^2 b_{max}\right]$$

for $n = 1,2,\ldots,15$,

where I_n = average range for bias segment n.

The quantized value of $B_{n,p,q}$ (in this case $[0, \frac{1}{256}, \frac{2}{256}, \ldots]$) can then be used to set the look-up table zero output symbols.

d) Calculate breakpoints for look-up table

The nonzero ranges, $B_{n,p,q}$ to 1, should be grouped among fifteen symbols according to the cumulative distribution transformation. Since the cumulative distribution transformation is

$$T(s) = 1 - \frac{N-1}{N} e^{-\ln(N-1)s^2} ,$$

where N = 16.

And the log amplifier transformation is:

$$y = \frac{1}{3} \log x+1 .$$

The breakpoints are:

$$y_i = \frac{1}{3}\log\left[(1-B_{n,p,q})\sqrt{\frac{\ln\frac{N}{N-1}(1-\frac{1}{i})}{-\ln(N-1)}} + B_{n,p,q}\right]+1,$$

where i = 1,2,...,15, and y_i = decision levels for the look-up table transformation.

e) Set look-up table

With $B_{n,p,q}$ and its corresponding y_i, the output symbols can now be set at decision points ($B_{n,p,q}$, y_1, y_2,...,y_{15}) with corresponding symbols (0,1,2,...,15).

4) Commence diagnostic scan

As scanning plane and angle increments, the different gain and bias parameters are applied by the waveform generator and multiplier, and by the RAM look-up table, respectively.

As shown in the above algorithm, the hardware takes over the post processing requirement for the computer. In an actual hardware implementation, the buffers can be eliminated. The same computer memory used for storing the initial data and the final image can be used for storing the gain and bias parameters. The data rate for the final image is reduced to eight-M-bits/sec assuming a 2 MHz sampling rate of the ultrasonic signal. This is well within the one M-words/sec DMA transfer rate of a 16-bit/word minicomputer. Therefore, time can be shared between storing the image data and transferring the gain and bias parameters through the DMA channel of the minicomputer. Furthermore, this technique can easily adapted to real time sector scanning. Since ample data samples are available for each statistic window, these samples can be reduced in the initial scan so that data over time can also be sampled to derive a set of gain and bias parameters over four dimensions.

4.3.2 Results

Figure 4.29 shows the computer algorithm to emulate the three-dimensional sector-scanned snapshot mode adaptive dynamic range compression algorithm as outlined in the last subsection. The program reads in a complete sector scanned snapshot during the first pass and uses it to derive the gain parameters and the look-up tables. During this pass, an initial gain profile and a logarithmic transformation are used to compress the echo data to eight bits, simulating the actual process of the snapshot camer hardware. The statistic window used to derive these parameters is three pings by three pings, corresponding to a three degrees solid angle. After the gain profile and bias parameters are calculated for that statistic window, the gain profile in dB verse range is fitted to a piece-wise linear continuous curve and the bias parameters are used to set up the look-up table. The program is then ready for the second pass. The input device is rewound. As each ping of the three-dimensional sector scan is read in during the second pass, the gain profile is applied and the result is log-compressed and quantized. The eight-bit log-compressed signal is then used in the look-up table to apply the bias and the histogram equalization transformations. The four-bit data is now ready for plotting or other evaluation purposes.

Figure 4.30 shows a typical set of raw and compressed data. Also shown is the saturation level. Although the saturation level does not match the raw data exactly for this ping, it clearly is adequate for tracking the power profile.

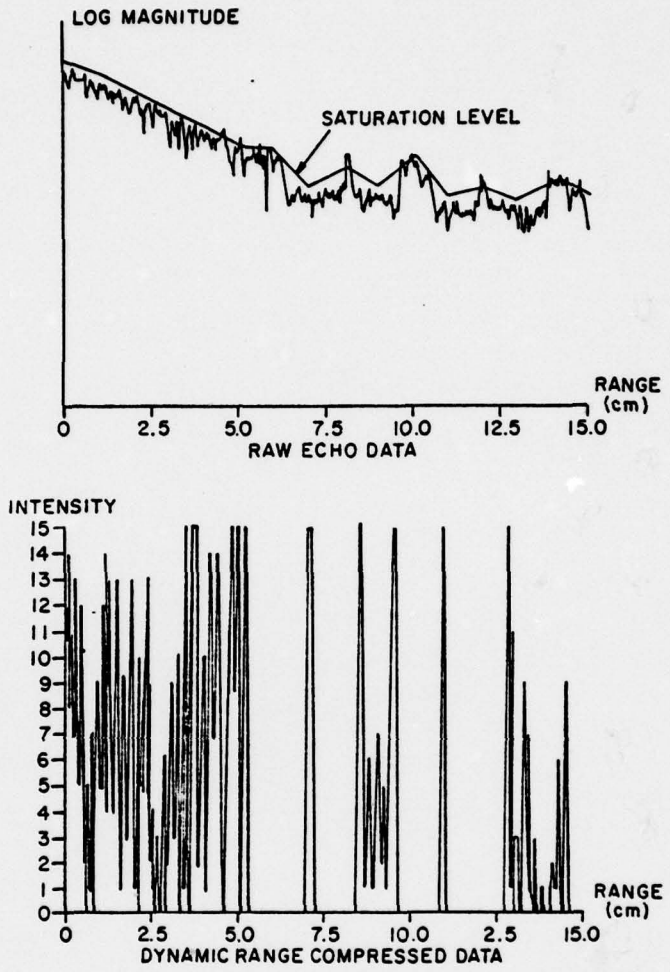

Figure 4.30 Raw and Compressed 3D Snapshot Echo Data

From the adaptive dynamic range compressed graphs, it is clear that the algorithm distinguishes blood volume with a minimum of artifacts and at the same time offers varied intensity levels in arrears with significant returns. This particular implementation is similar to an M-mode technique; therefore, all discussion of the algorithm also applies to this technique.

CHAPTER V

SUMMARY AND CONCLUSIONS

In echocardiography, there are two types of signals present at the receiver. One is from specular returns due to abrupt changes in acoustic impedance; the other is scatterer returns due to heterogeneous tissue layers or blood cells. As an echocardiographic image, the specular returns and the scatterer returns from tissues are of interest. Therefore, for a grey scale display, maximum brightness for the specular reflectors and a grey scale for the tissue scatterers form an acceptable image. In order to generate an image from the wide dynamic range echo data, the image processor must adaptively compensate for the attenuation effects and automatically reject returns from a blood volume. Variable gain and bias parameters are suggested to adaptively normalize the desired echo signals and to adaptively reject the undesired echo signals. Two economically feasible implementation techniques were shown. A model and its simulated echo data were used to evaluate the above techniques for M mode and three-dimensional snapshot echocardiography. Performance for both techniques was found satisfactory; no other adaptive techniques are available.

For future research, many improvements can be made to the echo signal model and adaptive dynamic range compression algorithm. The model developed herein is

primarily for the test of the adaptive algorithm response to different power profiles. But the model has shown promise to simulate echo data if exact cardiac geometry and biological parameters are used as inputs. In-vitro experiments with fairly complicated structures can be performed to verify the echo signal model. This will enhance an understanding of the available single-structure biological parameters. With this verification of model, perhaps an iterative process of regressing the actual echo cardiac signal data to fit a cardiac structure model is feasible. This process is in accordance with the ultimate goal of identifying different cardiac structures automatically. Another way to achieve this goal is through the use of pattern recognition techniques. With the adaptive dynamic range compression technique, full dynamic range echo data can be reconstructed with off-line computers. Since blood volumes have lower amplitude and higher doppler shifts than other cardiac structures in general, pattern recognition techniques can be applied on these two features to extract cardiac chamber geometries. This two-feature pattern recognition technique should offer better performance than the single-feature (level discrimination) technique suggested here.

In summary, the adaptive dynamic range compression algorithm is capable of compressing raw echo data directly to display level dynamic ranges. Also, since the technique

allows the digital storage of echocardiographic data economically and permits the reconstruction of the full dynamic range raw echo data, it opens endless possibilities to process the echo data to suit diagnostic needs.

BIBLIOGRAPHY

1. Andrews, H. C., Tescher, A. G. and R. P. Kruger, "Image Processing by Digital Computer," IEEE Spectrum, Vol. 9, No. 7, July 1972, pp. 20-32.

2. Åsberg, A., "Ultrasonic Cinematography of the Living Heart," Ultrasonics, April 1967.

3. Ballard, D. H., Waag, R. C., and E. S. Angel, "Advanced Ultrasonic Imaging for Clinical Diagnosis," Computer Science, Engineering Research Review, University of Rochester, 1977-1978.

4. Barnes, R. W., Nomeir, A. M., Pardue, G. T., and P. N. Nuss, "An Ultrasound Receiver with Programmable Time Gain Control," J. Clin. Ultrasound, Vol. 3, 1975, pp. 121-124.

5. Bom, N., Roelandt, J., and P. G. Hugenholtz, "Ultrasonic Viewer for Cross-Sectional Analyses of Moving Cardiac Structures," Biomed. Eng., Vol. 6, 1971, pp. 500-508.

6. Burckhardt, C. B., "Speckle in Ultrasound B-Mode Scans," IEEE Trans. on Sonics and Ultrasonics, Vol. SU-25, No. 1 January 1978.

7. DeClercq, A., and M. Maginess, "Adaptive Gain Control for Dynamic Ultrasound Imaging," Ultrasonics Proceedings, IEEE Catalog No. CHO 994-4SU, 1975.

8. Dunn, F., "Ultrasonic Attenuation, Absorption, and Velocity in Tissues and Organs," Proc. of Seminar on Ultrasonics Tissue Characterization held at NBS, Gaithersburg, MD., May 28-30, 1975.

9. Elder, I., and C. H. Hertz, "The Use of the Ultrasonic Reflectoscope for the Continuous Recording of Movements of Heart Walls, Kungl," Fysiog. Sallsk. Lund Forh., Vol. 24, 1954, pp. 1-19.

10. Feigenbaum, H., Echocardiography, Lea and Febiger, Philadelphia, Pa., 1972.

11. Firestone, F. A., "The Supersonic Reflectoscope, an Instrument for Inspecting the Interior of Solid Parts by Means of Sound Wave," J. Acous. Soc. Amer., Vol. 17, 1945, p. 287.

12. Fry, W. J., Leichner, G. H., Oemyama, D., Fry, F. J., and E. K. Fry, "Ultrasonic Visualization System Employing New Scanning and Presentation Methods," J. Acous. Soc. Amer., Vol. 44, No. 5, 1968.

13. Gallager, R. G., Information Theory and Reliable Communication, John Wiley and Sons, 1968.

14. Gersho, A., and D. J. Goodman, "A Training Mode Adaptive Quantizer," IEEE Trans. on Information Theory, Vol. IT-20, No. 6, November 1974.

15. Griffith, J. M., and W. L. Henry, "A Sector Scanner for Real-Time Two-Dimensional Echocardiography," Circulation, Vol. 49, 1974, pp. 1147-1152.

16. Griffith, J. M., and W. L. Henry, "Switched Gain: Simplifies Ultrasonic Measurement of Cardiac Wall Thickness," 27th ACEMB, Marriott Hotel, Philadelphia, PA., October 6-10, 1974.

17. Hall, E. L., "Almost Uniform Distribution for Computer Image Enhancement," IEEE Trans. Computers, Vol. C-23, No. 2, February 1974, pp. 207-208.

18. Hall, E. L. et al., "A Survey of Preprocessing and Feature Extraction Techniques for Radiographic Images," IEEE Trans. Computer, Vol. C-20, No. 9, September 1971, pp. 1032-1044.

19. Hill, C. R., "Frequency and Angular Dependence of Ultrasonic Scattering from Tissue," Proceedings of Seminar on Ultrasonic Tissue Characterization held at NBS, Gaithersburg, MD., May 28-30, 1975.

20. Howry, D. H., and W. R. Bliss, "Ultrasonic Visualization of Soft Tissue Structures of the Body," J. Lab. Clin. Med., Vol. 40, 1952, pp. 579-592.

21. Hubebank, M., "Computer Enhancement of Ultrasound Images," Sc. D. Thesis, MIT, Department of Electrical Engineering, August 1972.

22. Jones, J. P., "Current Problems in Ultrasonic Impectiography," Proceedings of Seminar on Ultrasonic Tissue Characterization held at NBS, Gaithersburg, MD., May 28-30, 1975.

23. Kak, A. C., "Acoustic Impedance Profiling: An Analytical and Physical Model Study," Proceedings of Seminar on Ultrasonic Tissue Characterization held at Gaithersburg, MD., May 28-30, 1975.

24. Keidel, W. D., Uber eine Methode Zur Registriering der Volumanderungen des Herzen am Menschen. 2. Z. Kreisl.-Forsch., Vol 39, 1950, p. 257.

AD-A080 982 PENNSYLVANIA STATE UNIV UNIVERSITY PARK APPLIED RESE--ETC F/G 6/5
ADAPTIVE DYNAMIC RANGE COMPRESSION ALGORITHM FOR ECHOCARDIOGRAP--ETC(U)
MAY 79 E H LAM N00014-79-C-6043
UNCLASSIFIED ARL/PSU/TM-79-138 NL

3 OF 3
AD-
A080982

END
DATE FILMED
2-80
DDC

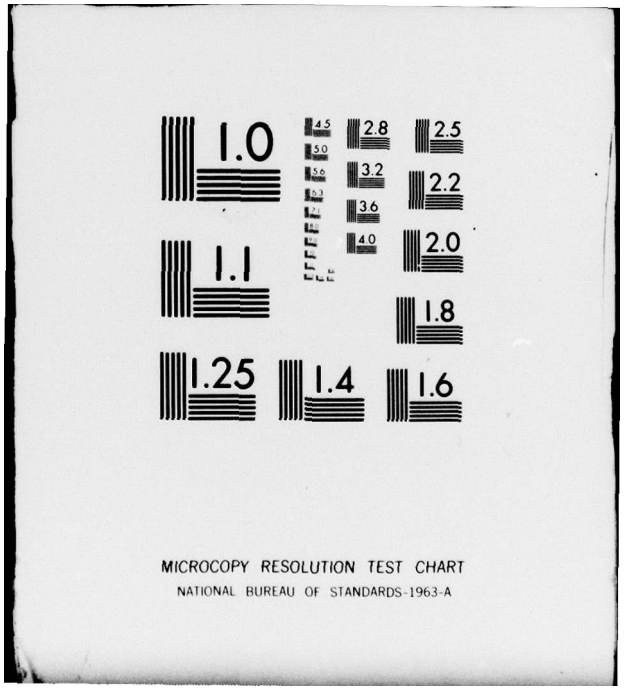
1.0
1.1
1.25
1.4
1.6
1.8
2.0
2.2
2.5
2.8
3.2
3.6
4.0
4.5
5.0
5.6
MICROCOPY RESOLUTION TEST CHART
NATIONAL BUREAU OF STANDARDS-1963-A

25. Kennedy, R. S., Fading Dispersive Communication Channels, Wiley Intersciences, 1969.

26. Kikuchi, Y., Okuyama, D., and M. Tanaka, "Kinetic-Ultrasonatomography of the Heart," Ultrasound, 3 Abstracta, 1st World Congress on Ultrasonic Diagnostics in Medicine, No. 245, Vienna 1969.

27. King, D. L., Editor, Diagnostic Ultrasound, C. V. Mosby Co., 1974.

28. Korpel, A., Whitman, R. E., and M. Ahmed, "Elimination of Spurious Detail in Acoustical Images," Acoustical Holography, Vol. 5, P.S. Green, Editor, Plenum Press, New York 1974, p. 373.

29. Kossoff, G., Garrett, W. J., and G. Radovanovich, "Grey Scale Echography in Obstetrics and Gynecology," Australian Radiology, Vol. 68, March 1974, p. 62.

30. Kossoff, G., Robinson, R. E., and W. J. Garrett, "Ultrasonic Two-Dimensional Visualization for Medical Diagnosis," J. Acous. Soc. Amer., Vol. 44, No. 5, 1968.

31. Lam, E. H. T., and N. B. Miller, "Digital Adaptive TVG Control for Grey Scale Ultrasonic Echocardiography," 94th Meeting, Acous. Soc. Amer., Miami, FL., December 1977, pp. 12-16.

32. Leighton, R. F., Rich, J. M., Pollack, M. E., and P. I. Altieri, "Clinical Application of a Quantitative Analysis of Regional Left Ventricular Wall Motion," Cardiovascular Imaging and Image Processing: Theory and Practice, Harrison, D.C. ed., 1975.

33. Lele, P. P., Mansfield, A. B., Murphy, A. I., Namery, J., and N. Senapati, "Tissue Characterization by Ultrasonic Frequency-Dependent Attenuation and Scattering," Proceedings of Seminar on Ultrasonic Tissue Characterization held at NBS, Gaithersburg, MD., May 28-30, 1975.

34. McDicken, W. N., Evans, D. H., and D. A. R. Robertson, "Automatic Sensitivity Control in Diagnostic Ultrasonics," Ultrasonics, Vol. 12, July 1974, pp. 173-176.

35. McSherry, D. H., "Computer Processing of Diagnostic Ultrasound Data," IEEE Trans. on Sonics and Ultrasonics, Vol. SV-21, No. 2, April 1974.

36. McSherry, D. H., and J. R. Keller, "Ultrasonic Cardiac Imaging and Image Enhancement Techniques," 1974 Ultrasonic Symposium Proceedings, IEEE Catalog No. 74, CHO 896-1SU.

37. Mannos, J. L., and D. J. Sakrison, "The Effects of a Visual Fidelity Criterion on the Encoding of Images," IEEE Trans. on Information Theory, Vol. IT-20, No. 4, July 1974.

38. Marich, K. W. et al., "Real-Time Imaging with a New Ultrasonic Camera: Part 1, In Vitro Experimental Studies on Transmission Imaging of Biological Structure," J. Clin. Ultrasound, Vol. 3, No. 5, March 1975.

39. Miller, N. B., Lawther, J. M., and R. Zelis, "Multi-dimensional Echo Imaging of the Ischemic Heart," Proposal No. 169, The Applied Research Laboratory, 1976.

40. Morse, P. M., and K. V. Ingard, Theoretical Acoustics, McGraw-Hill, 1968.

41. Mussman, H. E., Dutton, R. W., and J. D. Meindl, "A Monolithic Analog Signal Processor for Ultrasonic Imaging Systems," 1975 IEEE International Solid State Circuits Conference.

42. Myrick, R. J., and R. M. Arthur, "Real-Time Digital Echocardiography Using Burst Analog Sampling," IEEE Trans. on Sonics and Ultrasonics, Vol. SU-24, No. 1, January 1977.

43. Oppenheim, A. V., and R. W. Schaffer, Digital Signal Processing, Prentice-Hall, Englewood Cliff, NJ., 1970, pp. 487-500.

44. Oppenheim, A. V., Schaffer, R. W., and T. G. Stockham, "Nonlinear Filtering of Multiplied and Convolved Signals," Proceedings of the IEEE, Vol. 56, No. 8, August 1968.

45. Papoulis, A., Probability, Random Variables and Stochastic Processes, McGraw-Hill, 1965.

46. Pratt, W. K., Digital Image Processing, John Wiley and Sons, 1978, pp. 311-318.

47. Rappaport, S. S., "On Optimum Dynamic Range Centering," Proceedings of the IEEE (Letter), August 1966, pp. 1067-1068.

48. Rappaport, S. S., "Statistically Optimum AGC for Rayleigh-Distributed Signals of Unknown Strength," IEEE Trans. on Information Theory (Correspondence), Vol. IT-1b, May 1970, pp. 351-352.

49. Rappaport, S. S., and C. P. Wang, "Adaptive Gain Control," IEEE Trans. on Information Theory (Correspondence), Vol. IT-17, September 1971, pp. 625-627.

50. Rappaport, S. S., "Gain Control for Diversity Receivers," The Bell System Technical Journal, November 1968, pp. 2015-2027.

51. Rappaport, S. S., "Communication and Radar Receiver Gains for Minimum Average Cost of Excluding Randomly Fluctuating Signals in Random Noise," The Bell System Technical Journal, October 1967, pp. 1753-1773.

52. Rasmussen, D., "Computer Measurement and Representation of the Heart in Two and Three Dimensions," Cardiovascular Imaging and Image Processing: Theory and Practice, Harrison, D. C. ed., 1975.

53. Reid, J. M., "Challenges and Opportunities in Ultrasound," Proceedings of Seminar on Ultrasonic Tissue Characterization held at NBS, Gaithersburg, MD., May 28-30, 1975.

54. Reid, J. M., "The Scattering of Ultrasound by Tissues," Proceedings of Seminar on Ultrasonic Tissue Characterization held at NBS, Gaithersburg, MD., May 28-30, 1975.

55. Robinson, D. E., "Display of Three-Dimensional Ultrasonic Data for Medical Diagnosis," J. Acous. Soc. Amer., Vol. 52, No. 2 (Part 2), 1972.

56. Sanders, W. J., and D. C. Harrison, "Computer Processing of Echocardiographic Images," Cardiovascular Imaging and Image Processing: Theory and Practice, Harrison, D.C. ed., 1975.

57. Shung, K. K., Sigelman, R. A., and J. M. Reid, "The Scattering of Ultrasound by Red Blood Cells," Proceedings of Seminar on Ultrasonic Tissue Characterization held at NBS, Gaithersburg, MD., May 28-30, 1975.

58. Stockham, T. G., Jr., "The Application of Generalized Linearity to Automatic Gain Control," IEEE Trans. on Audio and Electroacoustics, Vol. AU-16, No. 2, June 1978.

59. Tayler, K. J. W., "Digital A-Scan Analysis in the Diagnosis of Chronic Splenic Enlargement," Proceedings of Seminar on Ultrasonic Tissue Characterization held at NBS, Gaithersburg, MD., May 28-30, 1975.

60. Termini, B. A., and Y. C. Lee, Essentials of Echocardiography, Medical Economics Co., NJ., 1976.

61. Thurstone, F. L., and O. T. Von Ramm, "A New Ultrasound Imaging Technique Employing Two-Dimensional Electronic Beam Steering," Acoustical Holography (ed. P. S. Green), Vol. 5, Plenum Press, New York, 1974, pp. 149-159.

62. Van Trees, H. L., Detection, Estimation and Modulation Theory, Part I: Detection, Estimation and Linear Modulation Theory, John Wiley and Sons, 1968.

63. Waag, R. C., and R. Gramiak, "Computer-Controlled Two-Dimensional Cardiac Motion Imaging," 1974 Ultrasonic Symposium Proceedings, IEEE Catalog No. 74, CHO 896-1SU.

64. Waag, R. C., and R. Gramiak, "New Concepts for Acquiring, Processing and Imaging Cardiac Ultrasound Data," Ultrasonics in Medicine, Proceedings of the Second World Congress on Ultrasonics in Medicine, Rotterdam, The Netherlands, June 1973, pp. 4-8.

65. Waag, R. C., Gramiak, R., Woody, L., and G. Günes, "Processing and Display of Cardiac Ultrasound Data," 26th ACEMB, Minneapolis, MN., September 30 - October 4, 1973.

66. Waag, R. C., Gramiak, R., Woody, L., and D. Günes, "Image Processing in Cardiac Ultrasound," 27th ACEMB Philadelphia, PA., October 6-10, 1974.

67. Waag, R. C., Myklebust, J. B., Rhoades, W. L., and Gramiak, R., "Instrumentation for Noninvasive Cardiac Chamber Flow Rate Measurement," 1972 Ultrasonics Symposium, IEEE Catalog No. 72, CHO 708-8SU.

68. Wells, P. N. T., Physical Principles of Ultrasonic Diagnosis, Academic Press, New York, 1969.

69. Wells, P. N. T., "The Receiver in the Pulse-echo System," In Ultrasonics in Medicine, (ed. M. de Vlieger, D. N. White, and V. R. McCready), Excerpta Medica, Amsterdam, pp. 30-36.

70. Wells, P. N. T., Biomedical Ultrasonics, Academic Press, New York, 1977.

APPENDIX A

HUMAN TESTS OF ADAPTIVE TVG USING M-MODE ECHOCARDIOGRAPHY

In this appendix, one-dimensional dynamic range compression of real A-mode echocardiographic data is presented. The data was taken from normal volunteers with a commerical echocardiographic imaging system. The received echo signal was also fed to manually adjust multisegment time varying gain (TVG) controlled amplifiers. This manually dynamic range compressed signal was subsequently recorded on digital magnetic tape for off-line analysis. Since the amplifiers were calibrated and the gain control signal were recorded, an off-line reconstruction of the full dynamic range echo signal was possible. This full dynamic echo data were then compressed with the stated algorithm. Such a technique can be applied to the three-dimensional snapshot camera. But due to the technique presented in Section 4.3. This appendix also includes results from the off-line implementation of the dynamic range compression algorithm operating of real data.

Medical diagnostic pulse-echo instruments produce echo signals with dynamic range of about 100 dB,[69] depending upon the application. Echocardiographic signals, which typically span dynamic ranges of 90 dB, need to be compressed, with minimum resulting image distortion. The requirement on compression of dynamic range is set mostly by display devices, which are limited to less than 15 dB.

Several two dimensional-echocardiographic scanners and experimental results are desired in the literature.[15,61] The transducer apertures typically vary from 10 mm diameter to arrays 12 mm by 24 mm. The reasonant transducer frequency range is primarily from 2.25 to 2.5 MHz. Two- and three-dimensional scanners are being studied, including scanning pistons and a two-dimensional electronically-phased transducer array.

The basic elements of a pulse-echo system were shown in Figure 1.2. Large diameter ranges are the result of ultrasonic absorption,[68] reflection, and wave divergence. Echo power profiles, being dependent on tissue structure, differ with transducer look direction and with the phase of the cardiac cycle. These cannot be compensated by operator manual adjustment in sector-scanning echocardiography. Repeatable results cannot be assured using manual adjustments of time varying gain (TVG). Also, a major workload is involved in control manipulation.[7] These considersations have motivated work on adaptive TVG profiles or AGC (adaptive gain control) for ultrasound imaging. AGC systems for many signal processing applications previously have been developed and studied.[7,12,34,49,50,58] For example, DeClercq and Maginess[7] describe an analog AGC for dynamic ultrasound imaging and discuss the relationship to manual ultrasonic TVG and radio AGC; Stockham describes the application of

homomorphic filtering to AGC;[58] Oppenheim has applied generalized linear filtering techniques to automatic correction of dynamic range limitations in photographic images;[43] and Fry, et al. have applied computer control to the problem of gain adjustment.[12]

The AGC objectives being sought for in sector-scanning echocardiography are grey scale imaging display and avoidance of image artifacts caused by the AGC. Optional ability to reproduce the full dynamic range when desired has been implemented because of research objectives. Digital signal processing is used to permit the study of different processing and display techniques. This AGC approach consists of consecutive functions: reversible signal compression to permit A/D signal conversion; and signal compression to satisfy the restricted limits of display dynamic range.

In this approach, the receiver digitally derives received signal power statistics to control the TVG amplifier, as shown in Figure A.1. The purpose of the TVG is to have constant A/D input level by using known but adaptive gain. The TVG is a piecewise-linear continuous dB curve which is commanded by a digital processor in terms of an initial value and 15 slopes. The maximum range is typically 15 centimeters; hence, a different slope can, in this case, be specified for each centimeter increment of range. The data needed to derive

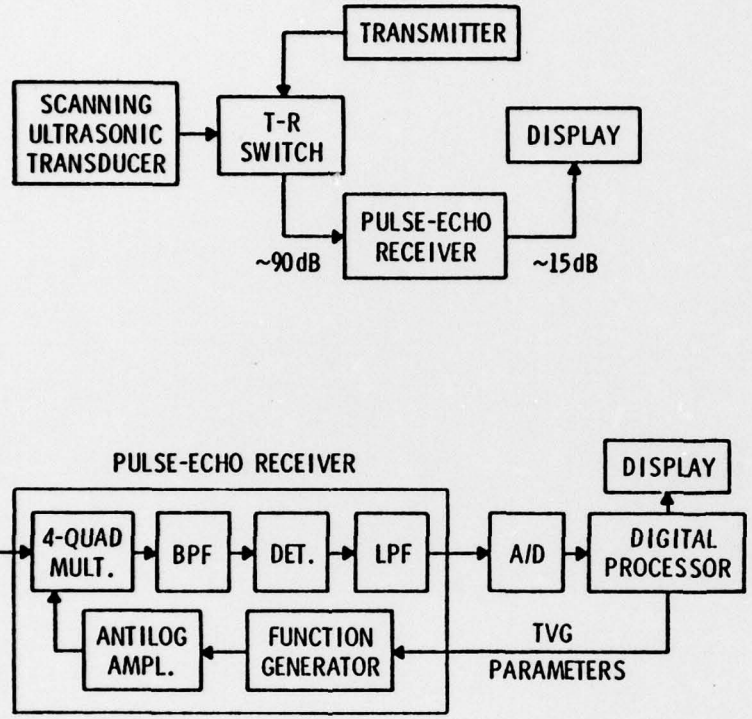

Figure A.1 Adaptive-TVG Pulse Echo Receiver

these TVG parameters is taken during a set-up scan prior to the scans for diagnostic images.

A window is used to cover an increment of range (and also of angle in the scanning echocardiographic systems). Such a window finds use both to calculate the TVG gain profile and to compress the dynamic range of the image for display. Figure A.2 illustrates a two-dimensional image raster that is typical of a scanning echocardiograph. The figure includes a window which in size is θ degrees by m millimeters. To calculate the TVG profile for a two-dimensional image, one can make a choice between different window shapes and signal statistics. The selected statistic in dB units then is used for a least-mean-square curve fit to a piecewise-linear curve. The piecewise-linear curve is readily converted into a TVG command function which controls the TVG receiver gain as shown in Figure A.1. The steps followed in TVG profile generation are:

1. Acquire data with initial gain profile.
2. Combine gain and receiver output to yield echo data.
3. Perform weighted LSF of logarithmic echo data.
4. Convert LSF parameters of gain profile.
5. Acquire data with new gain profile.

After the echo signal from the TVG amplifier output is converted into digital form, the signal can be merged

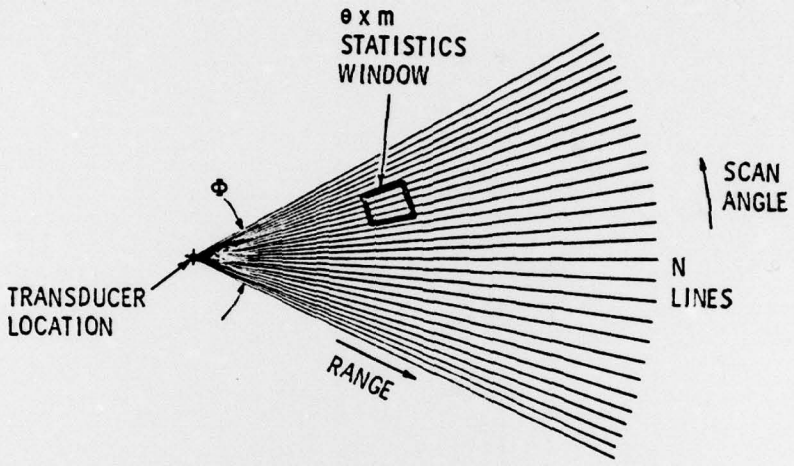

Figure A.2 Echocardiographic Two-Dimensional Scan Raster

with the stored TVG gain commands. This restores the signal samples to the initial dynamic range, unaltered by the TVG gain profile. In an echocardiogram, almost all look directions of interest contain a region of blood, so that some small duration of signal contains only backscattering from blood. The smallest value of the selected signal statistic (e.g., noncausal r.m.s. value taken over the windowed aperture) will occur at such a region. A proportional signal threshold can then be defined at this range; the threshold amplitude, in general, is then scaled according to the square of range, corresponding to the divergence of sound waves. This adjusted threshold technique has been applied to a one-dimensional (range versus amplitude) segment of video heart-echoes in Figure A.3. Here the dynamic range of the signals has been restored, and crosses mark the peak echo-values which exceed the threshold. Processing for display can be seen from Figure A.3 to consist of several steps: signal detection where echoes of significant amplitude are identified, clustering where separate tissue structures are identified, and amplitude compression where each separate tissue structure is scaled so that echoes of different amplitudes within the structure are assigned to appropriate brightness levels, but all amplitudes are visually discernible. Figure A.3 generalizes to a contour map in the case of two-dimensional scanning.

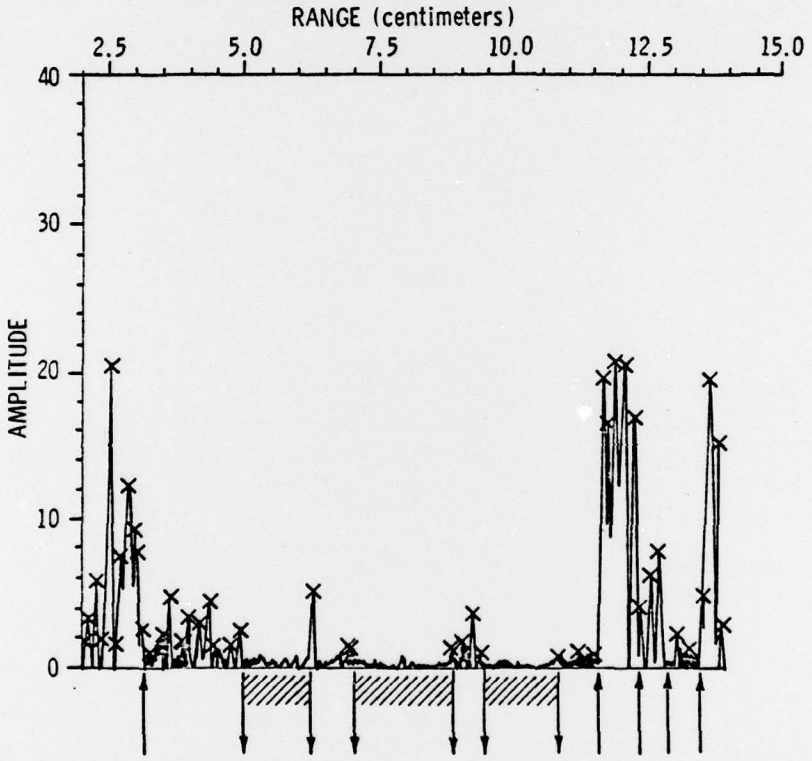

Figure A.3 The Problem of Amplitude Compression for Image Display

The application of adaptive TVG to improve the accuracy of the A/D converter will be illustrated, and an example will be given of an amplitude compression algorithm for image display. These examples will use snapshots of A-mode (amplitude versus range) echocardiographic data. Generalizations to scanning images are straightforward. These demonstration data were taken by recording the transducer output of a commercial M-mode echocardiographic system. The test set-up is shown in Figure A.4. The test data exclude approximately the first 2.5 cm of range; this does not restrict the validity of the TVG and compression algorithm results. This has been checked in subsequent tests. The TVG amplifier is able to adjust over a gain-range greater than 90 dB.

A TVG adaptation algorithm is illustrated in Figure A.5. The merged TVG gain and amplifier output is represented in the upper left-hand curve. This represents the envelope of the RF signal at the TVG amplifier input. The sample signal vector in dB is designated by y. The diagonal weighting matrix W selects the peak values of y. The graph of y and the best mean-square curve fit of a piece-wise linear graph to Wy are shown in the lower left of Figure A.5. The derived gain profile is shown in the upper right, and the lower right shows the TVG amplifier output which results from using this gain profile. The

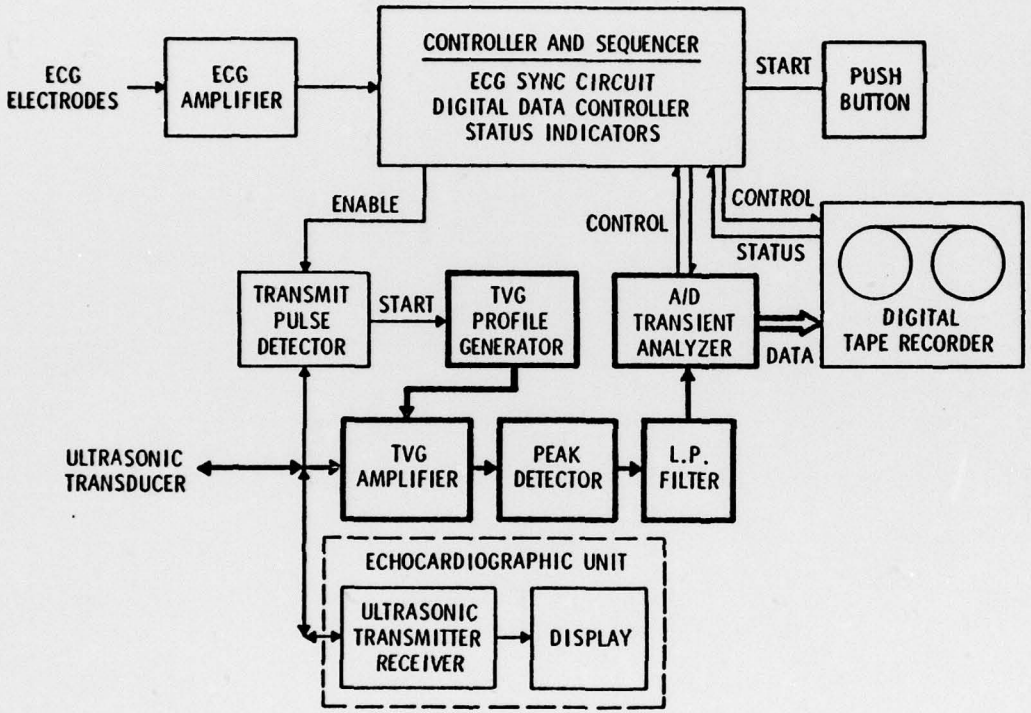

Figure A.4 Echo-Level Recording System

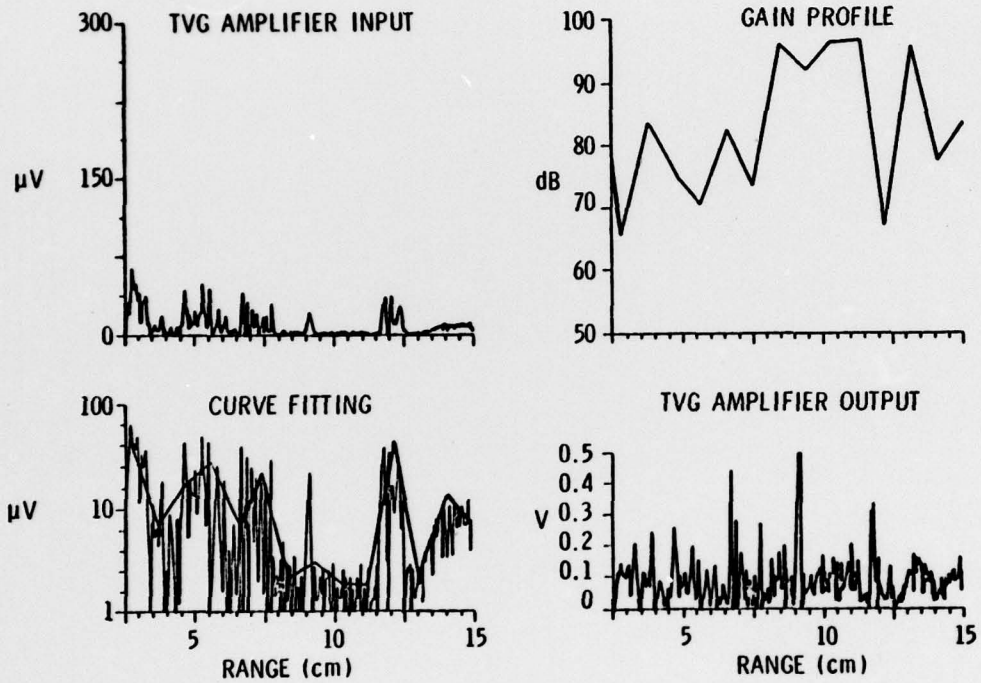

Figure A.5 Generation of TVG Gain Profiles

output has been rendered relatively stationary compared with the input. The equation representing the solution for the parameters a of the mean-square fit is

$$a = (F^T W F)^{-1} F W y \quad ,$$

where F is the matrix such that the sample vector of a piece-wise linear curve y is:

$$y = Fa$$

for a given vector a.

Figure A.6 is a flow diagram of an amplitude compression algorithm used for echo preparation prior to image display. The application of the algorithm is shown for three transducer beam directions in Figures A.7 through A.9. The window size, (2N+1) signal samples, is 5.6 mm in these examples. The window in this algorithm serves to cluster echoes from the same structure, and the r.m.s values taken over the window form the basis for scaling the amplitudes to fit within the display brightness range.

Other amplitude compression and enhancement methods can be used with this system implementation. For example, the clustering illustration of Figure A.3 can be implemented by thresholding on amplitude and identifying

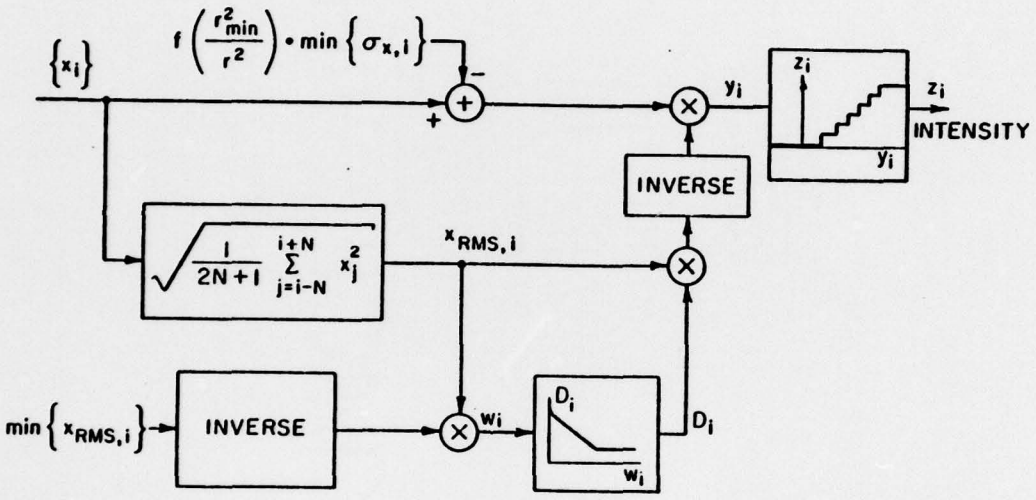

Figure A.6 Display Algorithm

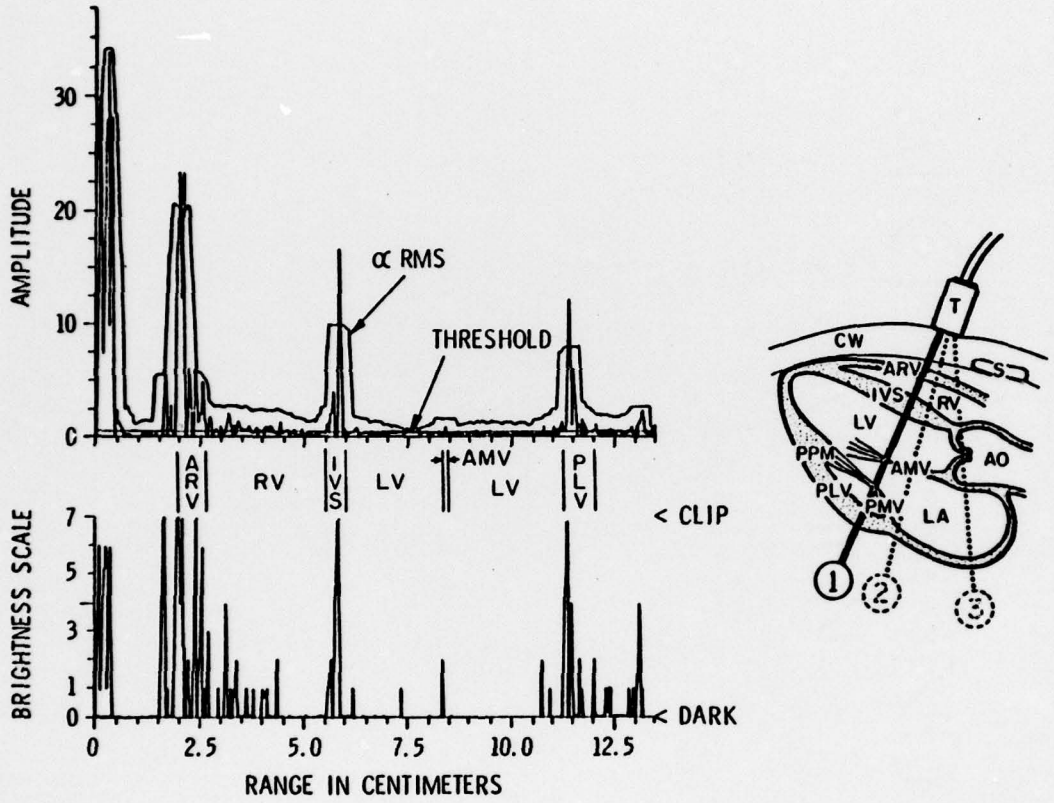

Figure A.7 One-Dimensional Case of Window-Normalizing Algorithm

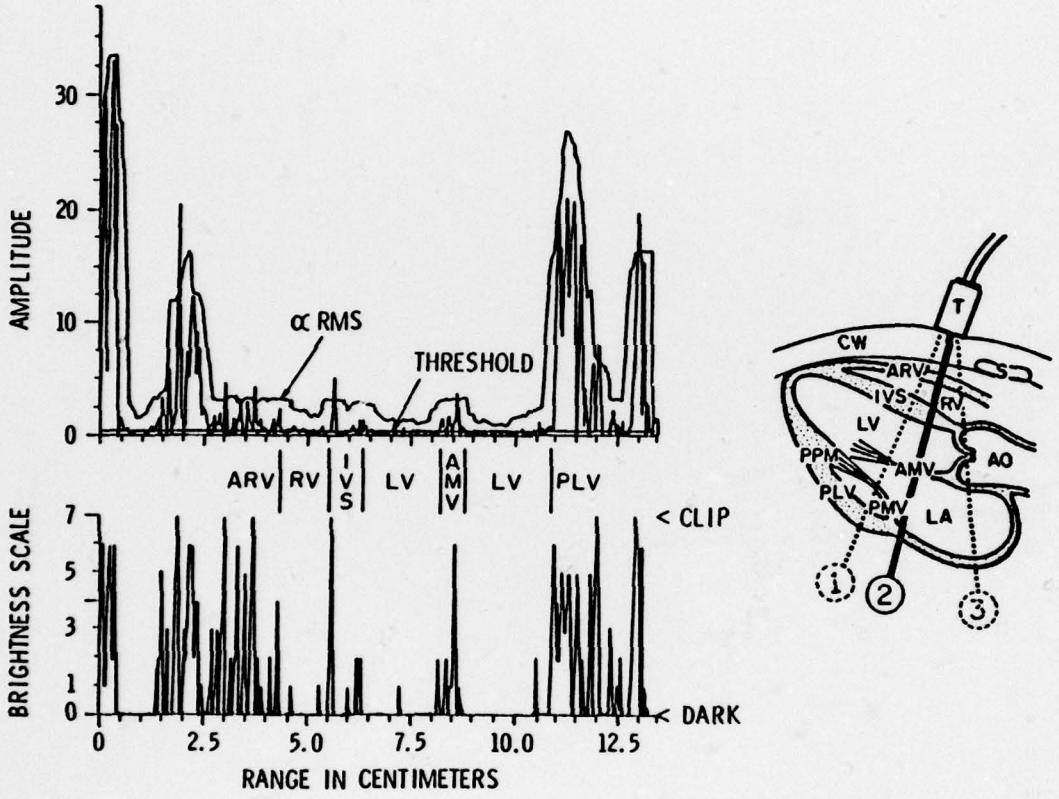

Figure A.8 Two-Dimensional Case of Window-Normalizing Algorithm

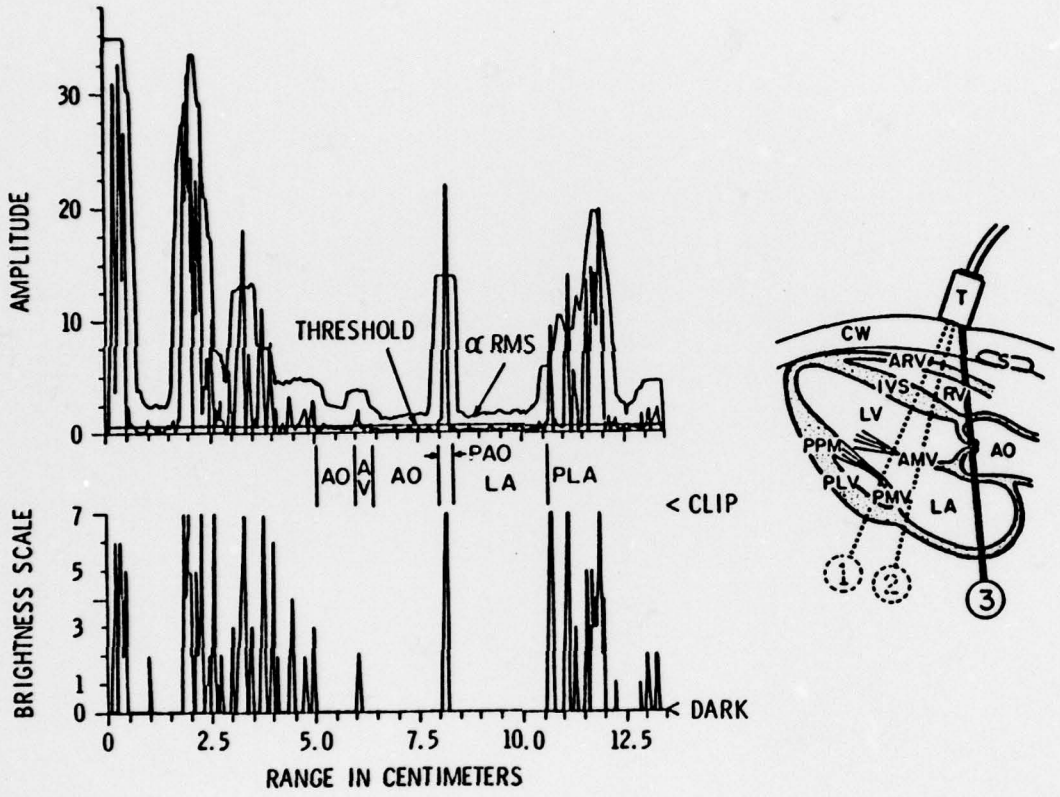

Figure A.9 Three-Dimensional Case of Window-Normalizing Algorithm

peaks, then thresholding successive range intervals to identify clusters, followed by comparing successive amplitudes within a cluster to identify regions for amplitude, or brightness, adjustment.

The design of a system for clinical use will combine the two adaptive steps of TVG signal compression and image grey-scale adjustment into one real-time TVG and thresholding operation after the set-up runs. This will be done within the system organization of Figure A.1 by design changes of the TVG amplifier. The result will be processing with display available to the operator with minimum time delay.

DISTRIBUTION

Commander (NSEA 09G32)
Naval Sea Systems Command
Department of the Navy
Washington, DC 20362 — Copies 1 and 2

Commander (NSEA 0342)
Naval Sea Systems Command
Department of the Navy
Washington, DC 20362 — Copies 3 and 4

Defense Technical Information Center
5010 Duke Street
Cameron Station
Alexandria, VA 22314 — Copies 5 through 16